NORTHWESTERN UNIVERSITY

Equilibrium Phase Behavior of Ionomers

A DISSERTATION

SUBMITTED TO THE GRADUATE SCHOOL

IN PARTIAL FULFILLMENT OF THE REQUIREMENTS

for the degree

DOCTOR OF PHILOSOPHY

Field of Materials Science and Engineering

By

Ha-Kyung Kwon

EVANSTON, ILLINOIS

September 2018

ABSTRACT

Equilibrium Phase Behavior of Ionomers

Ha-Kyung Kwon

Charge-containing polymers have received considerable attention for many decades, as these polymers combine the flexibility of polymer chains with electrochemical properties of the ions to provide a highly tunable, chemically and mechanically versatile class of materials. These materials have found use in energy conversion devices, high-density energy storage devices such as batteries, biomedical applications as drug delivery mechanisms, organic photovoltaic devices, and surface coatings, among many. An effort to fully utilize and optimize these materials has called forth the need to understand the equilibrium phase behavior of charge-containing polymers. However, despite the wealth of theoretical and experimental investigations, a complete and comprehensive understanding of electrostatics in charge-containing polymers remains elusive. This thesis is an attempt to add to the existing literature by considering multi-scale effects of Coulombic interactions. Specifically, we attempt to describe the phase behavior across multiple regimes of dielectric constants observed in experimental systems.

This thesis opens with a backdrop of current research in the field of neutral polymer systems and ionomer systems (Chapter 1). The rest of the thesis is organized into two sections. First, a

theoretical framework for describing multi-scale effects of ionomer blends is developed (Chapter 2). It is found that the ion-ion correlations, incorporated into Flory-Huggins theory via liquid state theory, can qualitatively change the mixing thermodynamics in simple binary blends on ionomers (Chapter 2). The phase diagram is extended to a more complicated ternary ionomer blends, where plasticizer and salt effects are taken into account (Chapter 3). Interfacial adsorption of the minority component is investigated and compared against classical Flory-Huggins type treatment. In Chapter 4, dielectric heterogeneity is taken into account, and we examine multiple regimes of electrostatic interactions, where a different driving force dominates each regime.

In the short second section, an experimental confirmation of theoretical results is attempted by identifying a model experimental system and conducting preliminary investigation on the equilibrium phase behavior at an interface and in the bulk (Chapters 5 and 6).

Acknowledgments

"It was the best of times, it was the worst of times, it was the age of wisdom, it was the age of foolishness, it was the epoch of belief, it was the epoch of incredulity, it was the season of Light, it was the season of Darkness, it was the spring of hope, it was the winter of despair [...]" -Charles Dickens, "A Tale of Two Cities"

Graduate school was, above all, a time of self-discovery. I would not be here without the support of the following people.

First and foremost, I'd like to thank **Monica**, who has been my staunch supporter throughout it all, for her endless support and numerous valuable life lessons, for making sure that I'm not "barking up the wrong tree," for shared tears, and for encouraging me to dream bigger. I am especially thankful for her creativity, passion, and dedication, which pushed me to pursue exciting ideas. I am likewise heavily indebted to **Ken**, for taking me under his wing and "adopting" me into the group, and encouraging me to think broad, think deep, and think outside the box (and in the lab).

My committee members have also made a lasting impact on my growth as a researcher: **Juan**, who always made me feel welcome at any Northwestern-UChicago meetings, and motivated me to become more confident; **Peter**, who taught two of the most fascinating and best taught classes I have ever taken; and **Jos**, whose infinite patience and friendship have been invaluable. I would also like to thank **Rick**, for being a great friend and a mentor, and for inspiring me to challenge myself.

My heartfelt thanks go out to the past and present group members of the Olvera group: **Charles**, who sparked my interest that eventually developed into this thesis; **Vikram**, who taught me the importance of work-life balance through squash; **Ting, Yufei, Josh, Saijie**, for welcoming me into the group; **Victor**, for sage advice on polymers, career, life; **Honghao and**

Dongxu, for first-year camaraderie; **Felipe, Aykut, Trung, Jaime, Meng, Yuba, Baofu**, for career advice; **Martin, Yaohua, Prusty, Chase, Ali, Jeremy, Yange, Hang, Hector**, for being supportive; **Rebecca**, for helping me keep things together; and **Boran**, for always listening, for going for runs with me, for keeping me sane, and for just being a really great friend.

Of course, I am extremely grateful to my adopted group, who always made fun of me for being clumsy, but nevertheless treated me like one of their own: **Elizabeth** and **Josh**, for being a big sibling to me; **Yaoyao**, for being my little "mentor" and a constant inspiration; **David**, whose pranks never failed to make me laugh; **Kazi**, for commiserating with me on tough and finicky moments of graduate school; **Meredith**, for being caring; **Tom** and **Victoria** for being great group members; and **Shawn**, for being my first– and best– friend in graduate school, and for sharing in my miseries and triumphs.

The five years were packed with amazing moments, and for that, my heart goes out to my friends: **Karen**, of the Crew, for being the best person to run, work out, live, and boil brats with, and prominently featuring in all of my Midwestern adventures; **Garrett**, of The Brunch Fund, for being the most patient, caring, and thoughtful friend to Garrett with; **Haemin** and **Youngeun**, who were always in it with me from near and far; **June**, **Matt**, **Eddie**, and **Haji** for our Monthly Star Club; and **Karl, Yue, Say, Charlotte, Vinay, Amit** for growing from bright-eyed first years to forever-jaded fifth years together.

No words can express my gratitude for **Christopher**, who has now supported me through two theses: thank you for sharing in my brightest and darkest moments, and for fighting on my side every step of the way.

I owe the direction of my journey through life to my brother and forever role model **Byung-Seok**, whom I've followed to engineering, to graduate school, and now to the Bay Area. I am especially thankful to him for hours-long phone calls, for always checking up on me to see if I was doing okay, and just for knowing what it's like.

Last not but least, I would like to dedicate this thesis to my parents, **Umma** and **Appa**, who have given me more love, encouragement, and support than I could ever hope to deserve. I hope I have made you proud.

This work was performed under the following financial assistance award 70NANB14H012 from U.S. Department of Commerce, National Institute of Standards and Technology as part of the Center for Hierarchical Materials Design (CHiMaD) and generously funded by Weertman Fellowship.

Table of Contents

List of Tables

List of Figures

CHAPTER 1

Introduction

This chapter covers many aspects of the mixing thermodynamics in polymer systems with and without charge, with the goal of providing a foundation for understanding the subsequent chapters of this thesis. It begins with illustrations of the phase diagrams of polymer blends and block copolymers in the melt and in presence of dilute concentrations of solvent, highlighting the characteristic properties of self-assembled systems and major driving factors affecting these properties. Discussions of charge effects subsequently follow. A brief review of the recent advances in self-assembly of ionomers is presented prior to discussing methods used in the subsequent chapters.

1.1. Background

1.1.1. Phase behavior of binary systems of polymers

Polymer blends are mixtures of at least two or more different types of polymers that have been blended to create a new material with different physical properties. The incompatibility between the different monomers induces a macroscopic separation of the dissimilar components, where each phase is rich in one component.[8] The composition of each phase is determined by the molecular weight of each chain, the Flory-Huggins interaction parameter χ between the immiscible components, and the volume fraction of each component. The mixing thermodynamics are described by Flory-Huggins theory, which gives the Helmholtz free energy of mixing per lattice site:[8]

$$\Delta F_{mix} = \Delta U_{mix} - T\Delta S_{mix} \tag{1.1}$$

$$= k_B T \left[\frac{\phi_A}{N_A} ln\phi_A + \frac{\phi_B}{N_B} \ln \phi_B + \chi_{AB}\phi_A\phi_B \right] \tag{1.2}$$

Here, the first two terms describe the entropic contribution from A and B polymer chains, and χ_{AB} describes the enthalpic interaction between A and B polymers. A positive χ_{AB} opposes mixing, while a negative χ_{AB} lowers the energy of mixing. The phase boundary is determined by the common tangent of the free energy at equilibrium compositions. For neutral symmetric binary polymer blends, this can be found analytically for each value of χN, as shown in the sample in Figure 1.1

A volumetrically symmetric blend macrophase separates above a critical χN of 2. Since χ is a property inherent to the chemistry of each mer, the segregation strength in the blend can be tuned by the degree of polymerization N.

When the two types of polymers are covalently end-linked to each other, diblock copolymers are made. The phase behavior of diblock copolymers are more rich, as immiscibility in these systems can induce a local separation of the dissimilar blocks into ordered nanodomains of various morphologies that are rich in one of the components.[9] The size and morphology of the domains can be controlled by Flory-Huggins interaction parameter between the two constituent blocks (χ), length of each block (N), and volume fraction of each block (ϕ).[9] The classical morphological structures are body-centered cubic array of spheres (S), hexagonally packed cylinders (C), gyroid (G), and lamellae (L), which can be accessed by changing the volume fraction of the diblock copolymer. These morphologies are shown in Figure 1.2.

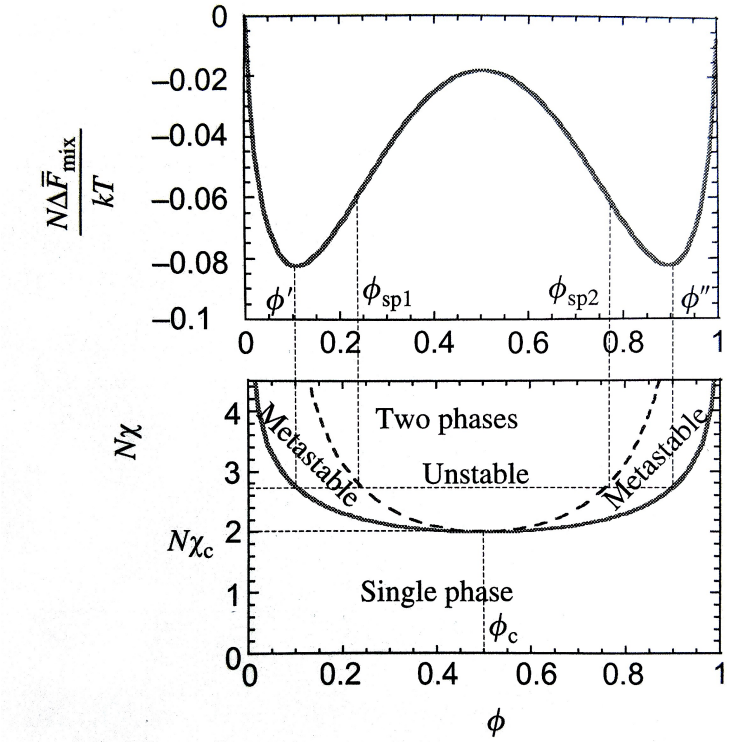

Figure 1.1. Free energy of mixing curve (top) and corresponding phase diagram (bottom) for a symmetric polymer blend with $\chi N = 2.7$. Both binodal (solid curve) and spinodal (dashed curve) are shown on the phase diagram. Image from Rubinstein and Colby.[1]

Similarly to the blend case, a volumetrically symmetric diblock copolymer with segregation strength χN above a critical value ($\chi N = 10.5$) phase separates into ordered domains. For a single system, where χ is fixed, the morphology and size of the domains can be tuned by moving horizontally across the phase diagram (by changing the volume composition of each block) or vertically across the phase diagram (by tuning the degree of polymerization N).

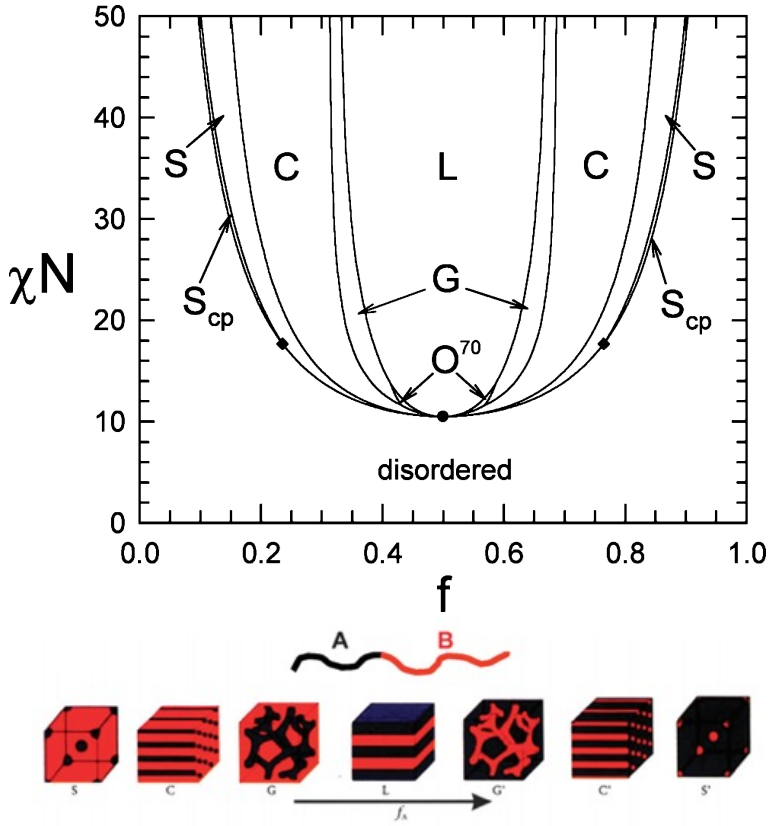

Figure 1.2. SCFT-calculated phase diagram for conformationally symmetric diblock copolymers in the melt, from M. W. Matsen.[2] Corresponding morphologies from Bates and Frederickson.[3]

1.1.2. Phase behavior of ternary systems

Equilibrium behavior of multiple component systems has been extensively studied and documented.[4,10,11] Adding a tertiary component C to a binary system of polymers A and B introduces an additional volume fraction, ϕ_C, and an additional set of interaction parameters, χ_{AC} and χ_{BC}, such that the free energy per site is as follows:[4]

$$\frac{\Delta \mathrm{F}_0}{\mathrm{k}_B T} = \frac{\phi_A \ln \phi_A}{N_A} + \frac{\phi_B \ln \phi_B}{N_B} + \frac{\phi_C \ln \phi_C}{N_C} + \chi_{AB}\phi_A\phi_B + \chi_{BC}\phi_B\phi_C + \chi_{AC}\phi_A\phi_C \tag{1.3}$$

By imposing the condition that the chemical potential of each component I be equal in all phases, $\mu_I = \frac{\partial \Delta F_0}{\partial n_I}$, and that mass is conserved (i.e. that the mean composition of I in the system is equal to the sum of the mean composition of I in each phase multiplied by the volume fraction of the phase), one can solve for equilibrium volume fractions. For symmetric ternary systems, where $\chi_{AB} = \chi_{BC} = \chi_{AC} = \chi$, the equilibrium phases are highly dependent on the value of χ chosen. For $2 \lesssim \chi N < 2.57$, three critical points are found, and three regions of two-phase coexistence between $\alpha + \beta$, $\beta + \gamma$, and $\alpha + \gamma$ emerge (Figure 1.3(a)). When χN is increased to 2.65, three three-phase regions appear (Figure 1.3(b)), each of which is separated from the single phase regions by two-phase regions. As χN is further increased, the two-phase regions separating the three-phase regions from single phase regions overlap and converge, and the three-phase regions grow to be the majority region in the phase diagram where formation of single phases is unstable (Figure 1.3(f)).

Biasing the interaction between the different components $(\chi_{AB} > \chi_{BC} > \chi_{AC})$ can asymmetrically skew the phase diagram. This is especially important, as adding charge can introduce asymmetric interactions into the system. Furthermore, this may serve as a point of comparison for comparing the non-linear electrostatic interactions between ions and charged monomers with the Flory-Huggins type interaction between solvents and neutral monomers.[4]

1.1.3. Interfacial behavior of ternary systems

When one of the components C is a minority component, it can act as an interface modifier to induce mixing in immiscible blends of A and B homopolymers.[5] This is an alternative method to using chemically inhomogeneous $A - B$ copolymers to stabilize the interface between A

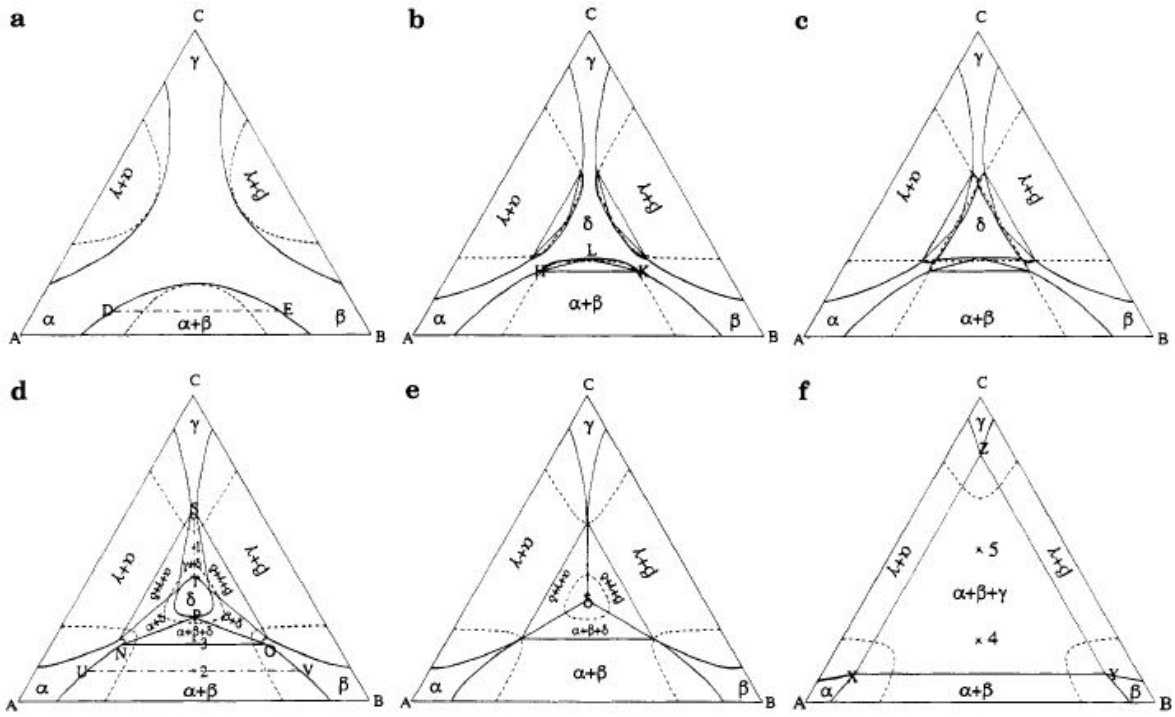

Figure 1.3. The phase diagrams of symmetric ternary systems for $(a)\chi N = 2.4, (b)\chi N = 2.65, (c)\chi N = 8/3, (d)\chi N = 2.7, (e)\chi N = 2.7456$, and $(f)\chi N = 3.0$. The symbols (—) and (-.-) correspond to the spinodal curves and tie lines, respectively.[4]

and B polymers,[12] and instead uses a homogeneous component, C, with tunable selectivities χ_{AC}, χ_{BC}.[5]

When the minority component C is non-selective, and has no interactions with A or B components ($\chi_{AC} = \chi_{BC} = 0$),[13] component C aggregates at the interface between α and β phases to decrease contact between A and B, and subsequently broadens the interface.

If C is non-selective but has non-zero interactions with A and B components, $\chi_{AC} = \chi_{BC} = \eta\chi_{AB}$ where $\eta \neq 0$, the adsorption behavior depends on the boundary conditions. If the system is in a two-phase coexistence of α and β where increasing the concentration of C, ϕ_C, leads to a critical point, as in Figure 1.4 (b), then there is a maximum in adsorption per interfacial thickness Γ_C, at a certain $\phi_C^{maximum} < \phi_C^{crit}$, shown in Figure 1.4 (c). At $\phi_C > \phi_C^{maximum}$, the

minority component is decreasingly adsorbed, until the system moves from a two-phase coexistence to a mixed state. If the system is in a two-phase coexistence of α and β but increasing ϕ_C leads to a three-phase coexistence, such as in Figure 1.3 (d), then there is adsorption at every interface, where the adsorbed species is the minority component in the two interfacing phases. This means that there is an adsorption of A, B, and C at $B-C$, $A-C$, and $A-B$ interfaces, respectively.

When C is a selective minority component, where $\chi_{AC} = \eta\chi_{AB}$ and $\chi_{BC} = \epsilon\chi_{AB}$, the equilibrium volume fraction of C is not equal in α and β phases. Consider the cases in which $\eta = 0$. The volume fraction profile for a ternary system, where $\chi_{AB}N = 2.7$ and $\epsilon = 0.2$, is shown in Figure 1.5(a). C preferentially mixes into the A phase, and thus we find a higher volume fraction of C in the A-rich phase. We still find adsorption of C at the interface. The adsorption of C is at a minimum when $\epsilon = 1$, where the system is effectively a binary blend with $\phi_1 = \phi_B$ and $\phi_2 = \phi_A + \phi_C$. For $\epsilon \geq 1$, the repulsion between B and C is too big, and as a result, there is no adsorption of C at the interface. The maximum adsorption of C is found at $\epsilon = 0$, which reduces to the non-selective case. Adsorption behavior in systems of $\phi_C << \phi_A = \phi_B$ can be summarized using Γ_C, which quantifies adsorption of C per interfacial thickness, η, and ϵ, as shown in Figure 1.6. Γ_C is symmetric about the line $\eta = \epsilon$. As $\eta = \epsilon$ increases, Γ_C increases. When $\epsilon(\eta)$ is fixed, Γ_C peaks at $\eta = \epsilon$, as shown in Figure 1.6 (b). Understanding the factors that affect adsorption of the minority component is critical to understanding the interfacial behavior of ionomers, especially when the minority component is an ion. This wealth of literature on the interface of neutral blends serves as a good foundation for comparison with interfacial properties of ionomers, where electrostatic interactions between the charged monomer and mobile ions will affect the selectivity of the minority component.

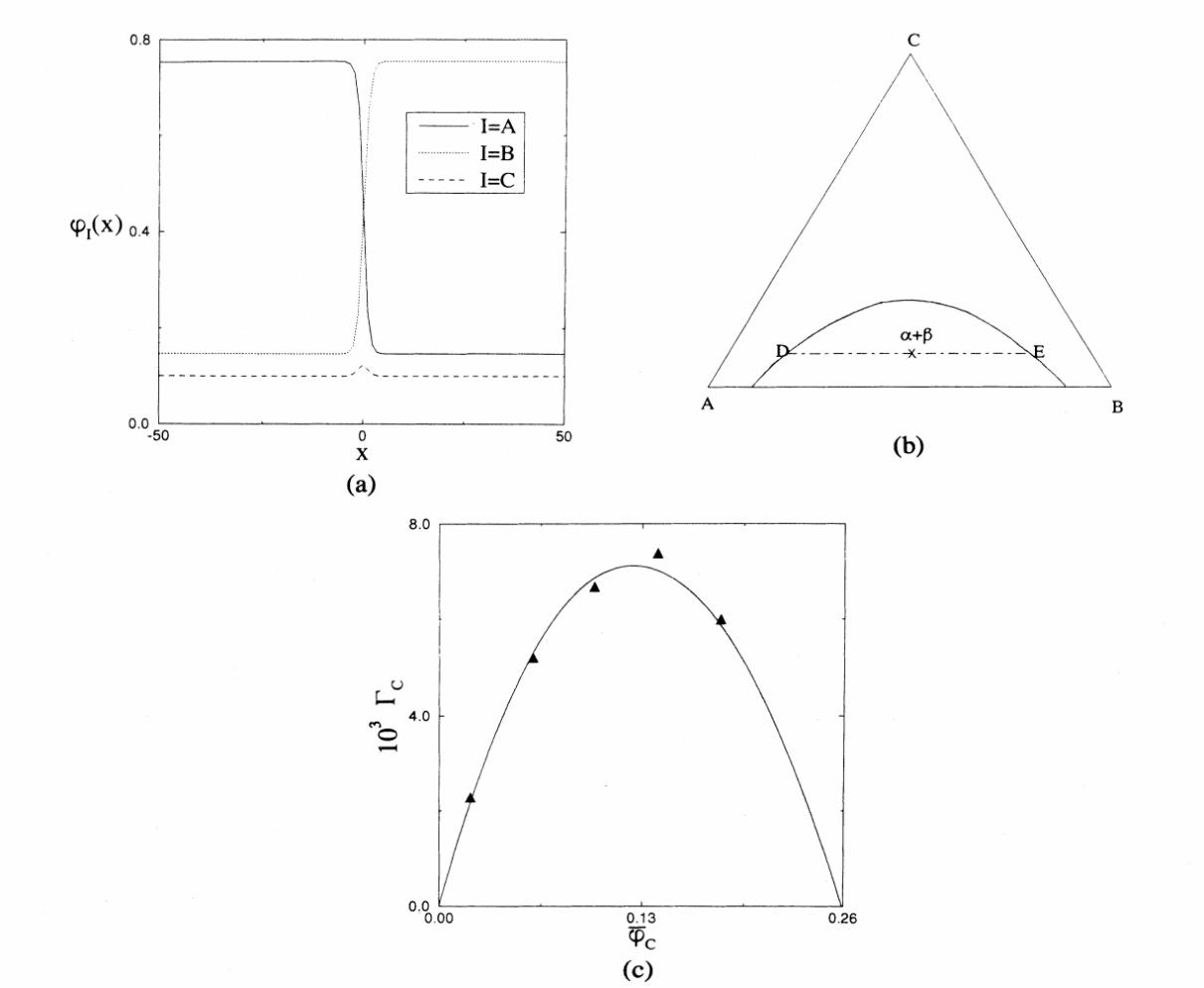

Figure 1.4. (a) The steady state composition profile of a nonselective C system $\chi_{AC} = \chi_{BC} = 0$ with mean compositions (0.45, 0.45, 0.1) for $\chi_{AB}N = 2.7$, shown as (x) in the phase diagram (b), in which the equilibrium compositions in the tie line(——.——), D = (0.754, 0.146, 0.1) for α, and E = (0.146, 0.754, 0.1) for β, respectively. (c) Plot of Γ_C, defined to be the adsorption of C per interfacial thickness in the α and β interfaces, vs. ϕ_C in systems with $\phi_A = \phi_B$.[5]

1.1.4. Phase behavior of ionomers

When one of the constituents within a system has charged monomers along the backbone, the ionic interactions can dramatically change the phase behavior of polymer blends and block copolymers, altering the miscibility and nanostructure formation within the system.[14,15] The

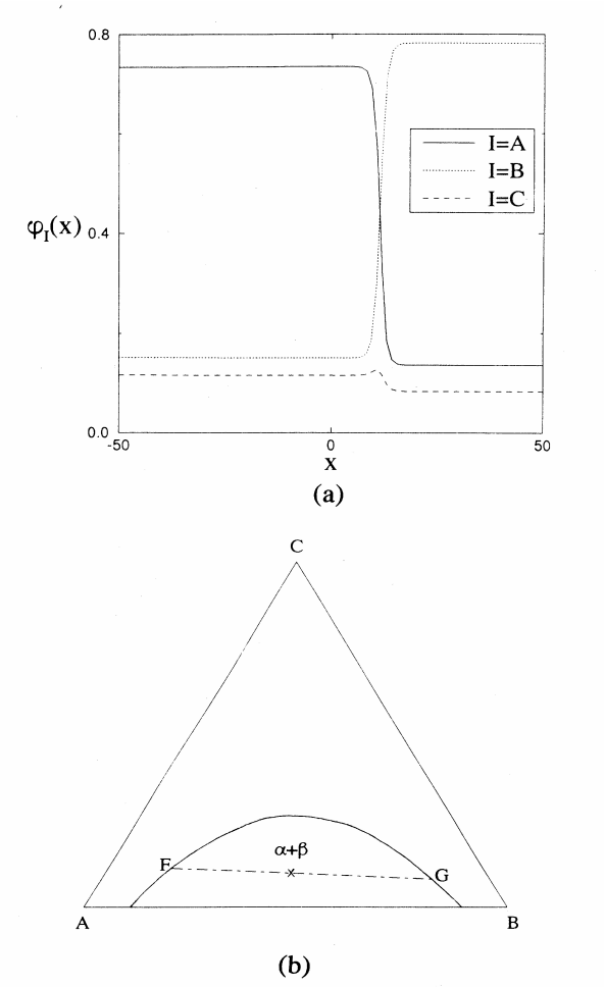

Figure 1.5. The steady state composition profile of a selective C system ($\chi_{AC} = 0, \chi_{BC} = 0.2\chi_{AB}$) with mean compositions (0.45, 0.45, 0.1) for $\chi_{AB}N = 2.7$, shown as (x) in the phase diagram (b), in which the equilibrium compositions in the tie line (—-.—-), F = (0.734, 0.151, 0.115) for α and G = (0.135, 0.782, 0.083) for β, respectively.[5]

changes in the equilibrium morphology has remarkable consequences in the dynamic response of the system, i.e. ion transport through the material.[16] There has been considerable effort in studying the effects of charge on the bulk phase behavior of polymeric materials, with the goal of creating a predictive method for charge-containing polymers that can accurately capture the multi-scale effects of Coulombic interactions on the morphology and miscibility of polymers.

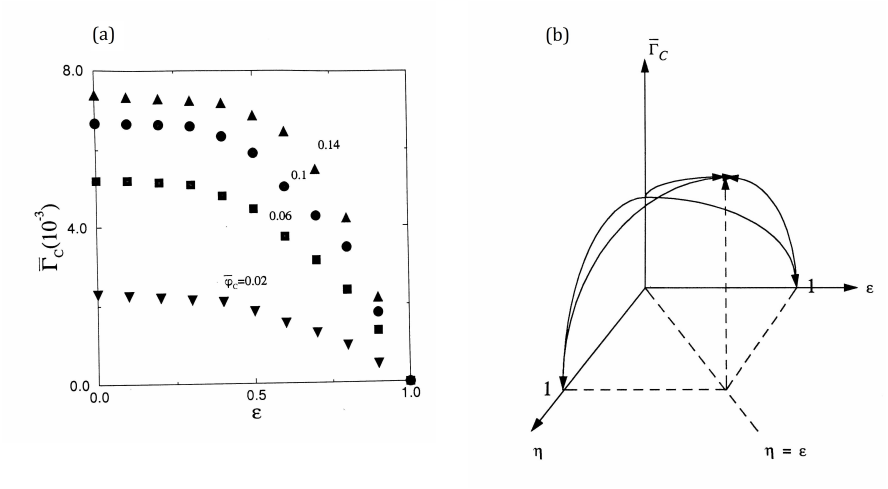

Figure 1.6. (a) Plot of Γ_C, adsorption of C per interfacial thickness, vs. ϵ varying ϕ_C in systems with $\phi_A = \phi_B$. Here, $\chi_{AC} = 0, \chi_{BC} = \epsilon\chi_{AB}$ for $\chi_{AB}N = 2.7$. (b) Plot of Γ_C as a function of η and ϵ.[5,6]

However, developing a comprehensive model that can cover all charge-containing systems has been a challenge, due to the multiple effects that arise, such as strong coupling between the ions,[17,18] self-energy related to solvation of ions,[19–23] polarizability of the media, translational entropy of ions, and effect of the valency of ions.[24,25] In this thesis, we employ and improve upon a theoretical model based on liquid state theory by solving the Ornstein-Zernike equation[26,27] with a closure that was developed in the Olvera de la Cruz group.[28] This theory allows us to consider explicitly the ionic correlations separately from Flory-Huggins effects, instead of wrapping the ionic interactions in an effective χ-parameter.

This theory differs from classical mean field theory for polymers based on Debye-Hückel electrostatics, such as Voorn-Overbeek theory.[29] Mean-field electrostatics smear out the local coupling between ions, instead treating them as "mean-field" effects. While these theories can successfully describe experimental results of charge-polymer systems such as coacervates,[30,31] the applicability is limited to systems with weak individual couplings between ions, such as

those in the coacervate phases. However, such mean field theories may be less useful if ionic couplings play a more dominant role, for example in ionomer blends, where dielectric screening is much weaker than in water, or in polymerized ionic liquids.[32,33] For this reason, we limit our study to ionomers, which are characterized by a small degree of charge (lower than 15%) and a low dielectric constant (ϵ_r). In these systems, the coupling between charge components is significant, unlike polyelectrolytes which are characterized by a high fraction of charge and a near complete dissociation of charge due to weak ionic coupling.

1.1.5. Liquid state theory and appropriate closures

To fully understand the phase behavior of ionomers, multi-scale effects of local charge ordering and large-scale chain conformation must be simultaneously captured using multi-scale hybrid theory.[18,28,34] This theory builds upon classical Flory-Huggins theory, which characterizes interaction between polymers using Flory-Huggins interaction parameter χ.[8,35,36] The interaction between charges is described using a standard electrostatic parameter $\Gamma = \frac{e^2}{8\pi\epsilon_0\epsilon_r k_B T a}$, which quantifies the strength of ionic coupling.[37,38] Here, a is the radius of a spherical charge, ϵ_0 the vacuum permittivity, and ϵ_r the relative dielectric constant of the background. Γ is equal to Bjerrum length normalized by the closest distance between the two charges, $2a$, and signifies the energy (in kT) required to separate two attracted charges.[7,37] When ϵ_r is low, the charges are highly coupled, and do not move freely through the medium. This coupling between the two charges can be described by a high Γ. When ϵ_r is high, the charges are mobile, and the weak coupling is described by a low Γ. For a specific value of Γ, we can calculate the additional contribution to free energy from ionic correlations. This free energy is a function of the charge density, ρ. The ionic correlations are then linked to the classical Flory-Huggins theory

by setting the charge density ρ equal to the density of charged monomers, $f_q\phi_A$, where A is the charged component and f_q the fraction of charge along the backbone of A.

To determine the excess free energy contribution from ionic correlations, Ornstein-Zernike equation is used:[26,27]

$$\hat{h_{ik}} = \hat{c}_{ik} + \sum l\rho_l \hat{c}_{il}\hat{h}_{lk} \tag{1.4}$$

where $h_{ik}(r)$ and $c_{ik}(r)$ are total and direct correlation functions, respectively, and carets correspond to Fourier-transformed values of the functions. The total and direct correlation functions are unknown, and therefore need a closure. Solving for these correlation functions allows us to calculate the distribution of ions, and subsequently the resulting free energy. The exact closure relation for the Ornstein-Zernike equation can be derived by comparing the cluster expansion in terms of Mayer functions with that of the total correlation h_{ik}:[27]

$$c_{ik} = h_{ik} - \ln(h_{ik} + 1) - \beta u_{ik} + d_{ik} \tag{1.5}$$

where u_{ik} is the pair potential between charges i and k, and d_{ik} is the bridge function.

Many approximations of this closure relation have been discussed, including the Mean Spherical Approximation (MSA) and Hyper-Netted Chain (HNC) closures.[39,40] The HNC approximation ignores the bridge function, while MSA ignores all but the pair potential. The HNC thereby can accurately describe long-range interactions, and produces results that are consistent with non-linear Debye-Hückel electrostatics, but may not always converge. Approaches based on the mean spherical approximation (MSA) capture effects due to ion size to a certain extent,

except that the electrostatic correlations in the MSA are effectively of the (linearized) mean field type. This means that the correlations between the ions are underestimated .

This thesis employs Debye-Hückel extended MSA closure (DHEMSA):[28]

$$c_{ik} = h_{ik} - \ln(h_{ik} + 1) - \beta u_{ik} \tag{1.6}$$

where u_{ik} is the pair potential between charges i and k.

The use of DHEMSA closure combines non-linearized electrostatic correlations and hard-core interactions, effectively capturing ion-ion correlations that arise at moderate densities and high ionic coupling strengths. In constructing this closure, the exact total correlation function h_{ik} in equation 1.5 with the potential mean force with a hard sphere (HS) correction:[28,41]

$$ln(g_{ik}^{DHHS}) = \phi_{ik} - \beta\omega_{ik}^{HS} \tag{1.7}$$

While errors are found at short distances and high densities, DHEMSA closure allows for a numerically efficient calculation of distributions, as it does not follow the iterative process employed by HNC but instead makes an educated guess about the correlation functions.

For thermodynamic analysis of blends discussed in this thesis, the free energy can be calculated by a thermodynamic integration:

$$f_{exc} = \frac{\rho^2}{2} \int_0^1 d\lambda \int dr dr' g_{\lambda,ik}(r, r') u_{ik}(r, r') \tag{1.8}$$

The total free energy of mixing based on Flory-Huggins theory[8] with the contribution from ionic correlations and Born solvation is used to probe the thermodynamics of mixing in this

thesis. This yields a picture of charge-containing polymers that considers both local structure (through ionic correlations) and the large-scale inhomogeneities (from Flory-Huggins interaction).

For the calculation of local structures within block copolymers and distribution of solvent across interfaces, a combination of liquid state theories and self-consistent field theories (LS-SCFT) is used. In this formulation, the chemical potential from the free energy, $\mu_{corr} = \frac{\partial f_{exc}}{\partial \rho}$ is used. This formulation is briefly described in the following section and in detail in Chapter 3.

LS-SCFT is a numerical execution of the coupling between polymeric interactions and ionic correlations. SCFT is a mean-field method, where the distribution of polymer chains gives rise to a mean field, which then acts on the polymer chains to determine their new distribution.[42] LS-SCFT follows the same algorithm, but utilizes LS to calculate an additional contribution to the mean field from ionic correlations. The volume fraction profile of polymer chains is determined iteratively until the distribution of polymers converges with the mean field generated.

This iterative technique determines the volume fraction of polymer ϕ found at a spatial point x by solving the modified diffusion equation:

$$\frac{\partial q(x,s)}{\partial s} = \left(\frac{b^2}{6}\nabla^2 - \omega(x,s)\right) q(x,s) \tag{1.9}$$

Here, $q(x,s)$ is the distribution function and is related to the probability that polymer chain segment s is located at a particular position x in space. $\omega(x,s)$ is the mean field, and is a function of both the local chain composition and the composition of the surrounding environment, and b is the statistical length.[43,44]

Ionic correlations are included into the SCFT iteration as an excess contribution to the chemical potential μ_x at each grid point x, whose value over the set of grid points form a field, ω, that

is included into the SCFT calculation. In this model, the additional contribution only adds to the field acting upon the charged component A: $f_q(\ln\rho+2\mu_{corr})$, where ρ is the charge density. $\ln\rho$ accounts for the entropy of the mobile counterions, and μ_{corr} comes from LS theory.[43] Initial condition $q(x,0)=1$ is used. Periodic boundary conditions are assumed for the nanophases formed by copolymers. For blends of polymers, finite differences method is employed,[45] where the boundary conditions correspond to the bulk volume fraction and chemical potential values. Using these initial and boundary conditions, the field ω is generated from a starting distribution of polymer chains. The additional contribution μ_{corr} to the total field ω is calculated at each spatial lattice point, as μ_{corr} depends on the volume fraction ϕ at the point. From the field, $q(x,s)$ is calculated, and the corresponding volume fractions ϕ are determined. The new distribution generates a new field, ω, and this process is repeated iteratively until the volume fractions converge.

1.2. Motivation

High density energy materials, such as rechargeable lithium-ion (Li-ion) batteries and polymer electrolyte membrane fuel cells (PEMFC), have become critical to today's society, from use in cars and microchips to space and military applications.[46,47] These applications are operated in high temperature and pressure environments, and thus require thermally robust and non-volatile materials that can withstand a wide range of temperatures and pressures. Charge-containing polymers have been identified as suitable candidate materials for high density energy devices, as they combine the low volatility and high flexibility of polymers with ion-selective conductivity of the charge-carrying backbone.[16,48,49] Specifically, copolymers have received wide attention, as they can microphase separate into nanostructures that combine desirable properties of the

constituent blocks.[50–52] For neutral copolymers, the size and shape of the nanostructures can be tuned by a careful selection of molecular parameters such as Flory-Huggins interaction between the dissimilar blocks, χ, chain length, N, and composition of the copolymer. Using charged constituents in a copolymer has been shown to be a powerful way to control microphase separation of the copolymer, by introducing electrostatic variables such as charge, relative dielectric constant, and ionic correlations.[14,18,53]

The efficiency of these devices relies on the fast and selective transport of ions across the polymer material. In a copolymer, where the immiscible blocks microphase separate to form nanodomains, the size, shape, and continuity of the nanostructures can therefore facilitate efficient transport of ions across the electrolyte.[54–56] The difference in dielectric constants of the nanodomains formed can result in aggregation of mobile ions at the interface,[57] which can affect the transport of ions. In addition, in an immiscible multicomponent blend, adsorption of one of the components can lead to broadening of the interface, which can affect the mechanical behavior and miscibility of the blend.[5]

The miscibility and morphology is determined by the equilibrium phase behavior of these polymers. In order to design polymeric materials with desired properties, we need a comprehensive understanding of the phase behavior of ion-containing polymers. Experiments have shown that block ionomers and ionomer blends exhibit equilibrium behaviors cannot be explained by classical Flory-Huggins theory used for their neutral counterparts.[14,58] Previous models have relied on Poisson-Boltzmann theory or Donnan theory to incorporate electrostatic effects into polymer phase behavior.[53,59] However, these models are only valid for a specific range of polyelectrolyte systems that exhibit increased miscibility upon addition of charge, and cannot account for the reduced miscibility and vastly different nanostructure morphologies found in

other experimental systems.[14,58] Recent theories identify Born energy and ionic correlations as important electrostatic effects in determining phase behavior.[18,60] Specifically, in ionomer melts, where the dielectric constant is relatively low,[18] ionic correlations play an especially dominant role in influencing phase behavior. The multi-scale hybrid model developed by Sing *et al.* simultaneously captures ionic correlations between charged components (1 nm) and interaction between polymer chains (10-100 nm).[17,18,34] by combining liquid state (LS) and self-consistent field theories (SCFT). LS-SCFT is the first theory to accurately describe the enhanced phase separation observed in experimental systems of charge-neutral diblock copolymers and blends and has the potential to be a helpful tool for obtaining a complete and detailed picture of the phase behavior of ionomers. Furthermore, this model can serve as a useful starting point for the behavior of biological phenomena such as complexation.[18,31,43,61,62] In this thesis, we build upon the liquid state theory to study the thermodynamics of binary and ternary ionomer blends with dielectric mismatch $\Delta\epsilon_r$. We extend our investigation to experimental systems of polystyrene-*b*-poly(2-vinylpyridine) in order to confirm theoretical findings.

CHAPTER 2

Thermodynamics of binary ionomer blends

2.1. Abstract

Advanced materials for energy storage and process technology are globally in high demand. Promising components for such materials are polymer blends and copolymers, because of their ability to self-assemble into nanostructured materials that combine desirable material properties, such as high mechanical stability with ion-selective conductivity. It remains a challenge to predict the nanoscale structure in charged polymers, because of intricate ionic correlations that can influence the structure at many length scales. Here we present a free energy analysis of charged polymer blends with electrolytes of the primitive model, by combining a Flory-Huggins-type theory with liquid state methods, relying on the Ornstein-Zernike equation. We find that different mechanisms, driven by entropy and electrostatics, can stimulate or repress phase separation in blends. These mechanisms can enable the existence of a triple point, where three phases can coexist in an effective two-component blend. We analyze the influence of chain length and electrostatic coupling strength, set by the ion type and dielectric properties of the polymer, on the coexistence lines and nanoscale structure within the blend. Our predictions may add resolution to the perspective on multi-phase coexistence in blends of charged polymers, and the formation of nanoscale structure in ionic gels and ionomers such as Nafion. Reproduced with permission

from Ha-Kyung Kwon, Jos W. Zwanikken, Kenneth R. Shull, Monica Olvera de la Cruz, "Theoretical analysis of multiple phase coexistence in polyelectrolyte blends," *Macromolecules*, **2015**, *48* (16), 6008-6015.

2.2. Introduction

There has been a strong demand for advanced materials that are able to sustain a high energy and power density.[48] Explorations are currently performed to combine these properties in soft materials, to enable these materials to be elastic and to respond mechanically on electric stimuli.[63,64] Polymers have the potential to realize these intentions, because of their highly versatile and tunable properties. Copolymers have the ability to spontaneously self-assemble into materials with distinct nanostructures that combine different physical properties into a single material.[50] These properties are highly tunable by tailoring the chemical and physical properties of the backbone and side groups. In particular, polymer charge was recently identified as a versatile tuning parameter that can drastically change structure and functionality at multiple length scales.[18] Predictive methods could accelerate the search for polymeric materials with desirable properties, but the incorporation of charge has challenged numerical and theoretical research, because of the multi-scale effects of Coulomb interactions. When scattering experiments cannot offer direct information about the microscopic structure, a comparison with high-resolution theoretical predictions can provide strong indications,[65] as demonstrated by Schmidt-Rohr *et al.*[66] who investigated the morphology of nano-channels in the ionomer Nafion.[54] Motivated by these intentions, we develop a predictive method for charged polymer blends that is able to investigate the multi-scale effects of Coulomb interactions and yields detailed structural information at the nanoscale. We base our method on classical Flory-Huggins theory and solve the

Ornstein-Zernike equation[26,27] with an accurate closure equation[28] to calculate the ionic effects. Inspired by the ability of Flory-Huggins theory[8,35,36] to capture the critical behavior of neutral polymer blends by a single parameter χ, we use a second parameter Γ to determine the full effect of ionic correlations that result from excluded volume and charge. The Γ parameter is a standard electrostatic coupling parameter[37,38] and measures the bare Coulomb energy that is required to separate two ions at contact, divided by the thermal energy kT ($\Gamma \approx 1$ for monovalent ions in water, and $\Gamma \gtrsim 10$ in a blend with relative dielectric permittivity $\epsilon \lesssim 15$). We present the phase diagrams of model polymer blends that include charges, and study the critical behavior as a function of the χ parameter, the electrostatic coupling parameter Γ, the length N of the neutral polymer, and charge fraction of the charged polymer f_q. The contribution to the free energy that contains the Γ-parameter is more complicated than that of the χ-parameter and depends intricately on the polymer volume fraction ϕ, the charge fraction of the polymer backbone f_q, and the Γ-parameter, and needs to be calculated via the Ornstein-Zernike equation[26,27] and appropriate closure.[28] We explicitly consider the ionic correlations separately and do not attempt to wrap the ionic correlations in an effective χ-parameter. This enables us to distinguish the nontrivial ionic effects from the more well known behavior of neutral polymers. The effects of ion self-energy[19–22] can effectively rescale the χ-parameter[18] and for this reason will not be mentioned explicitly, although they may be important in determining the magnitude of χ. From the free energy analysis, we can isolate the effects of ion charge, ion size, and dielectric constant quantitatively.

The theory advances beyond existing methods at several points. Classical mean field theory for polymers based on Debye-Hückel electrostatics, such as Voorn-Overbeek theory,[29] has recently shown to be successful in describing experimental results on complex coacervates in the

extensive work of Spruijt *et al.*[62,67,68] and Qin *et al.*[30,31] Voorn-Overbeek theory ignores ion size and electrostatic cohesion (the ion activity coefficient), and may therefore work if the individual couplings between the ions are weak, as is the case for coacervate phases. However, such mean field theories may be less useful if ionic couplings play a more dominant role, for example in polymer blends, where dielectric screening is much weaker than in water, or in polymer-ionic liquids.[32,33] Approaches based on the mean spherical approximation (MSA) capture effects due to ion size to a certain extent, except that the electrostatic correlations in the MSA are effectively of the (linearized) mean field type. This means that the correlations between the ions are underestimated (up to several kT's per ion, as we will show). Our results confirm the conclusions from Monte Carlo simulations[69,70] that the critical volume fraction can be reduced by increasing the polymer chain length, but only down to a certain finite asymptote. This result contrasts with classical Flory-Huggins theory where the critical volume fraction approaches one as the chain length is reduced. The theory relates the underlying electrostatic origin for the finite asymptote to the critical behavior in primitive model electrolytes.[71,72] However, we show here that the discussion of a single critical point is not sufficient. Sing *et al.*[18,73] identified two opposing ionic effects that can either repress or stimulate phase separation, one driven by the ion entropy and the other by electrostatic cohesion. Here we confirm these results by a full free energy analysis, and extensively explore parameter space to obtain a complete picture of the criticality of the model system. We demonstrate that the two opposing tendencies can actually give rise to two critical points, and enable the existence of a triple point in a binary polymer blend. The ionic structure within the three coexisting phases differs clearly, the dilute phase showing strong ion pairing, the dense phase a more liquid-like ordering of charges, and the intermediate phase containing finite ion clusters. Triple points are typically found for parameters that correspond

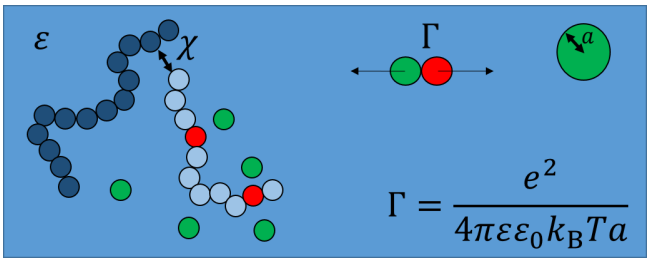

Figure 2.1. Schematic of the model system. The polymer chains of type A and B are described by a Flory-Huggins theory with interaction parameter χ, whereas the negative charges on the backbone of polymer A (red) and the positive charges of the counterions are described by a liquid-state theory of the primitive model, with coupling parameter Γ which characterizes the required energy to separate two charges at contact distance $2a$, normalized by the thermal energy kT.

to model ionomers (low charge fraction and longer chain lengths). With a minimal, quantitative model we capture the complex phenomenology in polymer blends caused by ion charge and size, and present simple explanations of the underlying mechanisms, together with guidelines to estimate the phase behavior.

2.3. Theoretical formulation of multiscale hybrid theory

We base our model system on the classical Flory-Huggins model[8,35,36] for neutral polymers that characterizes the polymer chains by a number N_i of monomers per chain of type i, a volume fraction ϕ_i, and an interaction parameter χ_{ij} between polymers of type i and j. Simple as the model may seem, it describes accurately the critical behavior of neutral polymer blends[74] once the appropriate χ-parameter is found. We connect this well-known model to another extensively studied model, known as the primitive model of electrolytes. Charges of the primitive model have a hard core of radius $a_\pm$ and a charge $\pm q_\pm e$ (e is the elementary charge), and interact in a structureless dielectric background with homogeneous dielectric constant ϵ relative to the vacuum permittivity ϵ_0.

In a symmetric mixture where $a_\pm = a$ and $q_\pm = 1$ one can define a single parameter $\Gamma \equiv (qe)^2/8\pi\epsilon\epsilon_0 kTa$ that represents the required energy to separate two opposite charges at contact, divided by the thermal energy kT.[37] Criticality of the primitive model has been studied extensively, e.g. with the Monte Carlo simulations by Luijten *et al.*,[71] showing that a high Γ of ≈ 22 is required for critical behavior, appearing at relatively low concentrations of charges (packing fractions of the order of a percent). We combine the two model systems by coupling the volume fraction of polymers ϕ to a volume fraction of charges $f_q\phi$ tuned by the fraction f_q of charged monomers on the backbone. This implies the assumption that the average net charge is constant zero (local charge neutrality), but not that the conditional averages are zero, i.e. the pair correlation functions will be explicitly calculated. We calculate the pair correlation functions by solving the Ornstein-Zernike equation:[26,27]

$$h(r) = c(r) + f_q\phi\, c * h, \tag{2.1}$$

($*$ is a convolution) with the so-called Debye-Hückel extended MSA closure (DHEMSA)[28] for a given composition $f_q\phi$ of charges,

$$c = \tilde{h} - \ln(\tilde{h} + 1) - u/kT, \tag{2.2}$$

where u is the pair potential between the charges, c is the direct correlation function, and $\tilde{h}$ is an estimation for the total correlation function h made by nonlinear Debye-Hückel theory, hence the rather cumbersome name for the closure (DHEMSA). In its algebraic form, the closure resembles the so-called Hyper-Netted Chain (HNC), and the results are in fact very close to those of the HNC, except that it shows a better mathematical stability and, in contrast to the HNC, converges in the critical regime.[28] From the pair correlation functions we can calculate

electrostatic contributions to the free energy directly by means of a thermodynamic integration. A general form of the total free energy density would look like:

$$f_{\rm tot}(\{\phi_i\},\{N_i\},\{\chi_{ij}\},\{a_i\},\{f_{qi}\},\{\Gamma_{ij}\}) = \\ f_{\rm FH}(\{\phi_i\},\{N_i\},\{\chi_{ij}\}) + f_{\rm PM}(\{\phi_i\},\{a_i\},\{f_{qi}\},\{\Gamma_{ij}\}), \tag{2.3}$$

where the subscript FH refers to Flory-Huggins, and PM to the primitive model of electrolytes. We focus here on symmetric binary electrolytes, such that we can drop many indices, and define a single χ, a, f_q, and Γ, and two polymer types A and B of which A is negatively charged. The PM contribution includes the entropy of the positive charges that represent the counterions, and ignores that of the negative charges that are bound to the backbone of polymer A. A graphic representation of the system is shown in figure 3.1.

We investigate criticality of a model system with total free energy

$$\begin{aligned} f_{\rm tot} &= \frac{\phi}{N_A}\ln\phi + \frac{(1-\phi)}{N_B}\ln(1-\phi) + \phi(1-\phi)\chi \\ &+ f_q\phi\ln\phi + f_{\rm exc}(f_q\phi,\Gamma) \end{aligned} \tag{2.4}$$

by evaluation of the inflection points (spinodals) and common tangents (binodals). The first three terms derive from a Flory-Huggins[8,35,36] theory, with interaction parameter χ, volume fraction ϕ of polymer A and volume fraction $1-\phi$ of polymer B. Unless otherwise indicated, the number of monomers per chain in A and B polymer is the same (N_A = N_B = N). The Flory-Huggins free energy, $f_{\rm FH}$, increases with χN, and promotes phase separation of the polymers. The fourth and fifth terms describe the electrostatic effects, and include the counterion entropy (which suppresses phase separation) and excess free energy due to ionic correlations

(which favor phase separation), calculated from the Ornstein-Zernike equation with DHEMSA closure. Both terms depend on the volume fraction of the charged polymer and the fraction f_q of monomers that are charged. The last term also depends on the electrostatic coupling parameter Γ. These contributions are shown in figure 2.2, including a common tangent construction, the method we use to find coexistent volume fractions from the total free energy. The total free energy density f_{tot} is divided into three contributions, that isolate the Flory-Huggins part f_{FH}, the counterion entropy $f_{\mathrm{PM-id}}$, and the ionic correlations $f_{\mathrm{PM-exc}}$. To find the coexistence volume fractions, method of common tangent is used. Two volume fractions coexist if the chemical potential of the two components, A and B, are equal in all phases. We search for all pairs of coexistent volume fractions (ϕ_1, ϕ_2) for which

$$\left.\frac{\partial f_{\mathrm{tot}}}{\partial \phi}\right|_{\phi=\phi_1} = \left.\frac{\partial f_{\mathrm{tot}}}{\partial \phi}\right|_{\phi=\phi_2} \tag{2.5}$$

and

$$\left.\left(f_{\mathrm{tot}} - \phi\frac{\partial f_{\mathrm{tot}}}{\partial \phi}\right)\right|_{\phi=\phi_1} = \left.\left(f_{\mathrm{tot}} - \phi\frac{\partial f_{\mathrm{tot}}}{\partial \phi}\right)\right|_{\phi=\phi_2}. \tag{2.6}$$

Equations (2.5) and (2.6) are the necessary conditions for thermal equilibrium. Depending on the form of the free energy curve, it is possible to find multiple coexisting volume fractions.

2.4. Results and discussion

2.4.1. Emergence of a eutectic-like triple point

The phase behavior of the blend can be understood as a competition between three mechanisms. The first relates to the χ-parameter, which describes the repulsion between the polymers and

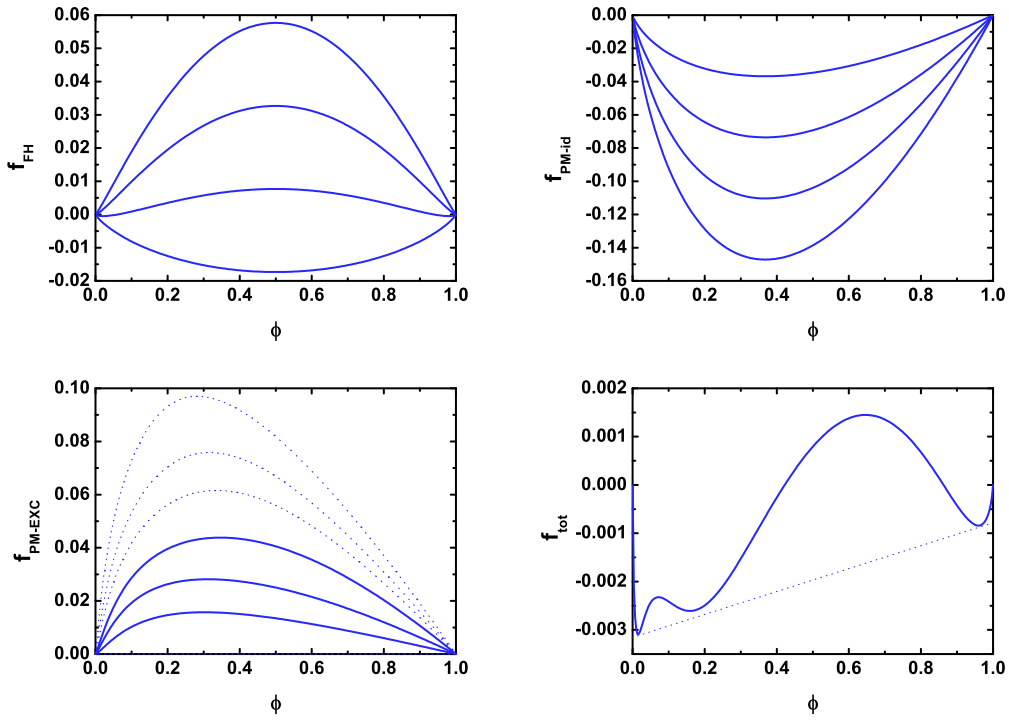

Figure 2.2. A breakdown of total free energy into f_{FH}, $f_{\mathrm{PM-id}}$, and $f_{\mathrm{PM-exc}}$. f_{FH} increases with χ, and $f_{\mathrm{PM-id}}$ decreases with f_q. $f_{\mathrm{PM-exc}}$ increases with Γ (solid lines), but the location of the maximum shifts to a higher ϕ_A with an increase in Γ. $f_{\mathrm{PM-exc}}$ further increases with f_q (dashed lines) and the location of the maximum shifts back to a lower ϕ_A.

promotes separation of the blend. The second mechanism is driven by the entropy of the counterion and the polymer chains, which suppresses phase separation; the third originates from ionic correlations, which represent the tendency of ions to segregate into ordered structures. In systems with relatively little coupling between the ions ($\Gamma \lesssim 10$), the system is dominated by the entropy of the counterions and the polymer chains, and tends away from phase separation. Therefore, in low Γ conditions, higher values of χ are needed to induce separation of the mixture, leading to a high $\chi N_{\mathrm{critical}}$, especially compared to the critical value for a neutral polymer blend, $\chi N_{\mathrm{critical}} = 2$. This results in an initial suppression of phase separation for the lower

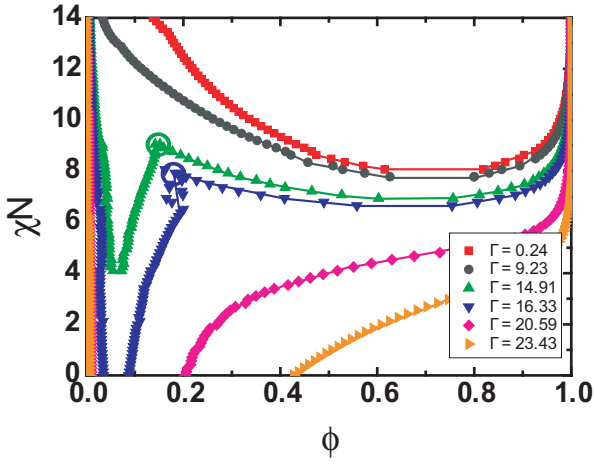

Figure 2.3. The effect of Γ on the phase diagram of polyelectrolyte blends. Lines have been drawn to guide the eye. Hollow circles indicate triple point, where three phases can coexist.

values of Γ. However, as the coupling strength Γ increases, the attractions between the ions become stronger, and this can eventually drive the blend to phase separate even in the absence of χ interaction. This effect results in enhanced phase separation, and shifts the phase boundary down to lower χN values. This effect is shown in figure 2.3, for $\Gamma > 14.91$. It is important to note that the deviation of the charged blend from the phase behavior of neutral polymer blends is significant at low volume fractions of the charged polymer, ϕ.

When the driving force for phase separation (ionic correlations and Flory-Huggins interaction) are comparable in magnitude to those favoring mixing (from chain and counterion entropy), we observe a multi-curvature phase boundary, where a miscible region is found adjacent to two distinct regions of coexistence at a constant χN. This is shown in figure 2.3 at $\Gamma = 14.91$ and 16.33. The difference in the symmetry of f_{FH} (which is symmetric for a symmetric blend) and f_{PM} (which is highly asymmetric, and largely influences the charge-dilute regions) leads to the rise of two distinct phase-separated regions, driven to phase separation by each of the two

driving forces: ionic correlations in low ϕ, and Flory-Huggins interaction in high ϕ. The driving force away from phase separation, the counterion entropy, is also asymmetric, and counteracts Flory-Huggins interaction and ionic correlations across all phase space. When this driving force is greater than the terms tending toward phase separation, a miscible region, found below the hollow circle in fig 2.3 is found, splitting the phase diagram into two branches, corresponding to two distinct phase behaviors. The splitting of the phase diagram into multiple regions of coexistence results in two critical points that correspond to qualitatively different phase transitions. These competing effects contribute to subtle minima in the total free energy of the system, which can be difficult to calculate using numerical methods. Especially near the triple point, this causes numerical noise in the phase diagram, as can be seen in figure 2.3.

Figure 2.4 zooms in on the transition around the triple point. At $\chi N = 6.5$, there is an immiscible region at lower concentrations driven by ionic correlations. The system shows two disjoint immiscible regions for $\chi N = 7$, one driven by ionic correlations, and one by the Flory interaction. There is a triple point for $7 < \chi N < 8.5$ and above that point, the system has two coexisting volume fractions that are dilute and dense in polymer A, driven by a combination of ionic correlations and the Flory-Huggins interaction. While the ionic structure within these three phases has not been studied extensively, it can be estimated from the pair correlation functions that the ions are ordered in a liquid-like fashion in ion-dense phase, form small clusters in ion-intermediate phase, and form pairs in ion-dilute phase. The radial distribution functions that correspond to these three regimes are shown in figure 2.5. Figure 2.5 shows three radial distribution functions for phases that are dilute, intermediate and dense in charge. The corresponding points in the phase diagram are denoted with a cross, and the estimated spatial ordering of charges is shown in a cartoon, based on the radial distribution functions.

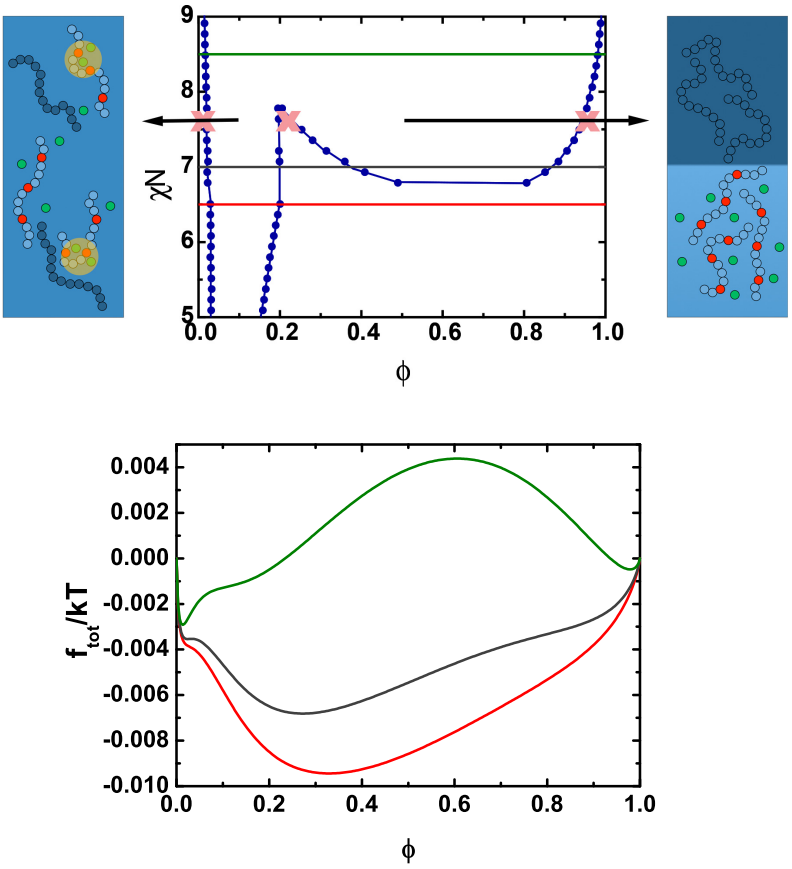

Figure 2.4. Phase diagram for a symmetric polyelectrolyte blend with N = 40, $f_q = 0.2$, and $5 < \chi N < 9$, with f_{tot} corresponding to $\chi N = 8.5, 7, 6.5$. The ionic structure in the phases at the points denoted with a cross is shown in figure 2.5.

2.4.2. Effect of polymer chain length

The phase behavior of polyelectrolyte blends can be tuned by changing the parameters that determine the contribution of each term to the total free energy. In order to further explore the phase behavior, we investigate the effect of the neutral polymer chain length, N_{B}, and the fraction of the charged backbone on the charged polymer, f_q, at chosen Γ values of 9.23, 16.33, and 23.43, which correspond to relative dielectric constants of 12, 6.8, and 4.7, for charges of radius 0.3 nm. The phase behavior of the system at $\Gamma = 16.33$ is of particular interest, as

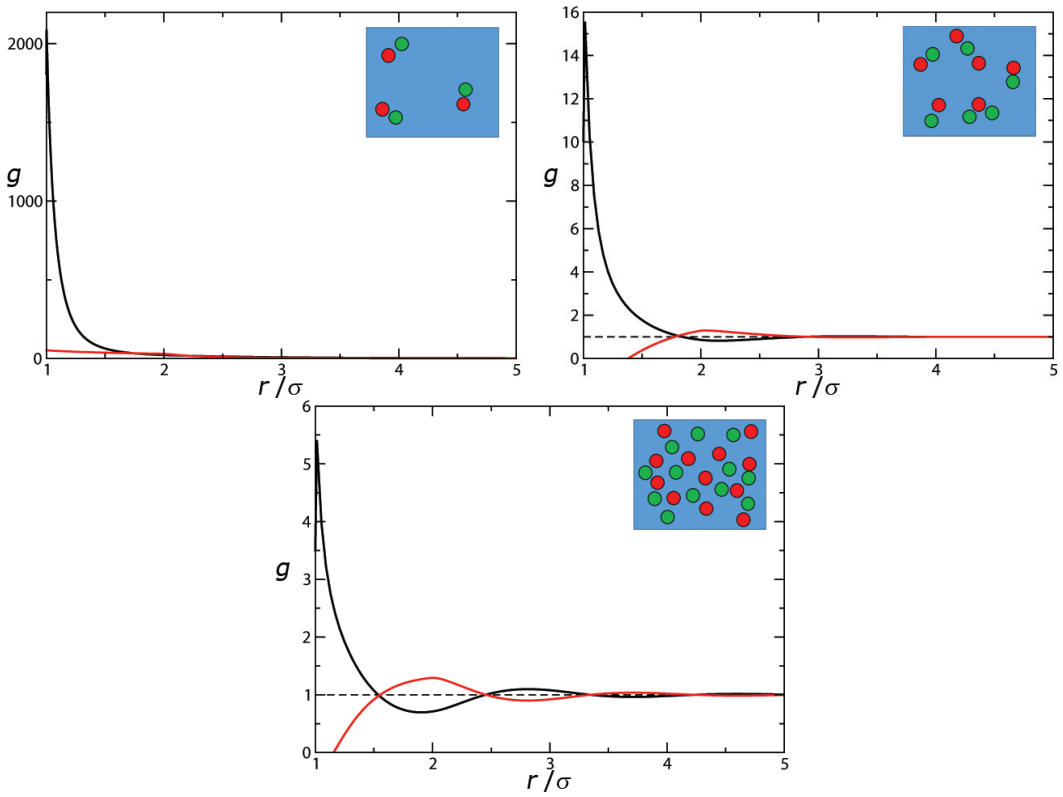

Figure 2.5. The radial distribution functions of the ions of coexisting phases close to the triple point, corresponding to the points in figure 2.4 denoted with a cross. The insets show cartoons of the estimated morphologies. The strong peak of the $g(r)$ of the dilute phase hints at pair formation. The second oscillation at the intermediate density hints at a significant fraction of triplets and larger clusters. The oscillations in the $g(r)$ of the dense phase are caused by a liquid-like order of charges.

the corresponding $\epsilon_r = 6.8$ is comparable to that of Nafion, which has ϵ_r between 4 and 20,[75] and can provide valuable insight into the behavior of experimentally available and physically relevant systems for fuel cell applications. It is expected that the change in f_q affects both the entropic contribution from counterions and the excess free energy contribution due to ionic correlations, while N_{B} only affects the Flory contribution to the total free energy. To quantify the changes in phase behavior of the blend, we look at the movement of the phase boundary with

the change in parameter, as well as the movement of the critical point, which is the lowest χN at which phase separation occurs, and where $\partial^3 f/\partial\phi^3 = 0$. The critical point can be understood to indicate a phase transition between mixed and separated states.

The phase boundaries for $N_{\mathrm{B}} = 4, 10, 40, 80, 800$ are plotted for $\Gamma = 9.23, 16.33, 23.43$ in figure 2.6. As N_{B} increases, phase separation is enhanced and the phase boundaries shift to a lower χN for all values of Γ. This is consistent with the results we expect from the Flory-Huggins free energy expression. An increase in N_{B} decreases entropy of the chains, and thus the system has a lower energy barrier against phase separation. While it is unsurprising that an increase in N_{B} enhances phase separation, it is interesting to note that the shift of the phase boundaries, specifically in their shapes and the location of the critical points, is qualitatively different in each of the three Γ cases.

The movement of the phase boundary is quantified by the movement in the location of the critical point, ϕ_{crit}. For $\Gamma = 9.23$, the critical point moves to a higher volume fraction as N_{B} increases, while for $\Gamma = 16.33$, we see multiple critical points, at low ϕ and high ϕ, the first of which does not shift with with chain length and the other which moves to a higher volume fraction. This is also seen in figure 2.7, where the location of the critical point is plotted against Γ, for all values of Γ between 0.23 and 23.43. At $\Gamma < 12$, ϕ_{crit} increases from 0.5 to 0.9 as N_{B} increase from 4 to 800. At $\Gamma > 12$, multiple critical points develop for longer chain lengths $N_{\mathrm{B}} = 40, 80, 800$, but only the critical point located at $\phi > 0.5$ increases with chain length. The critical point located at $\phi < 0.2$ does not change with change in N_{B}. The third set of critical points plotted in figure 2.7, located between $0.3 < \phi < 0.5$ for $\Gamma > 12$ and $N_{\mathrm{B}} = 40, 80, 800$ (in hatched lines), corresponds to the location of the triple point, where the blend undergoes

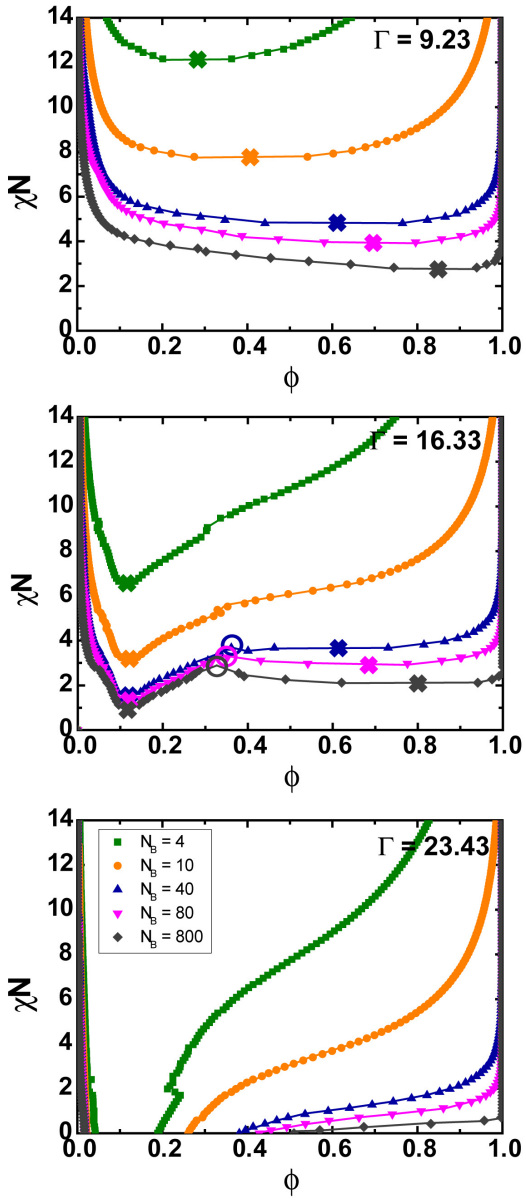

Figure 2.6. Phase diagrams for an asymmetric blend, where the charged component is fixed at $N_A = 40$ and $f_q = 0.1$, and the neutral component B has variable chain length $N_B = 4, 10, 40, 80, 800$. Phase diagrams are shown for three values of Γ, for 9.23 (top), 16.33 (middle), and 23.43 (bottom). As N_B increases, the phase boundary shifts to a lower χN in all cases of Γ, indicating enhanced phase separation. Hollow circles indicate triple point; stars indicate critical points.

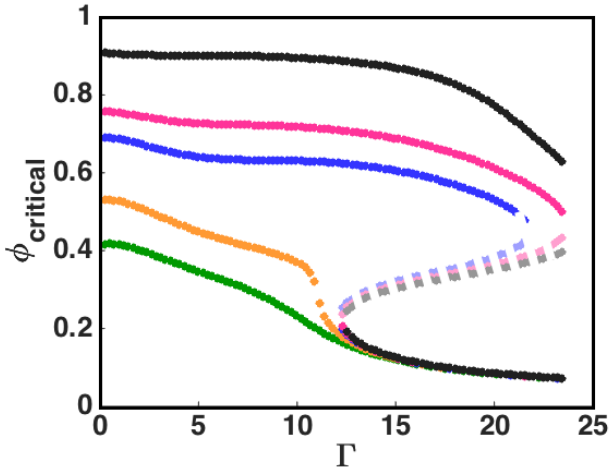

Figure 2.7. The location of the critical point at Γ, where chain length N_B changes from 4 (in green) to 800 (in black). Legend is same as in figure 2.6. At very small values of Γ, the location of the critical point moves to higher ϕ_A with increasing N_B. At high values of Γ, a second critical point develops at low ϕ_A, which does not move with N_B.

a eutectic-like transition from a mixture of ionic phases (having different morphologies of ion clusters) to equilibrium between two polymer phases.

From the movement of the multiple critical points in figure 2.8, we can identify the nature of the phase transition. Critical points of χ-induced phase transitions move to higher ϕ as the chain length of the uncharged component increases, while the location of the critical points corresponding to Γ-induced phase transitions does not depend on the chain length. This confirms the findings from Monte Carlo simulations, combining neutral polymer behavior with the conclusions drawn from primitive model electrolytes.[69] This is because the magnitude of Flory contribution to the total free energy can be tuned by the chain length, while the excess free energy contribution is independent of N_{B}. Furthermore, we can tune the phase transitions in both low ϕ and high ϕ regions using the parameters we have at hand.

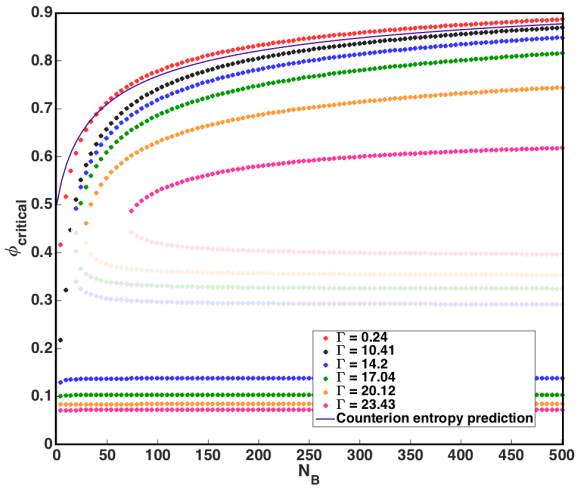

Figure 2.8. Location of the critical point against the neutral component chain length, N_B, at selected values of Γ. Plotted in solid is the predicted movement of the critical point with N_B if only counterion entropy is accounted for.

2.4.3. Effect of charge fraction

As previously shown, charge fraction f_q can be used to tune the magnitude of ionic effects in the model, to highlight the correlations between the charged monomers and the counterions. By increasing the fraction of charged backbone, we also increase the amount of counterions present in the blend, magnifying the contributions to total free energy from ionic correlations and counterion entropy. Here, we show the changes in the phase boundary of symmetric polyelectrolyte blends (where $N = 40$) in three ionic environments: $\Gamma = 9.23$, which corresponds to a weakly coupled system; $\Gamma = 16.33$, which corresponds to moderately coupled system, such as Nafion; and $\Gamma = 23.43$, where the oppositely charged ions are strongly attracted to each other.

When the ions are relatively weakly correlated, for $\Gamma = 9.23$, increasing f_q has negligible effects on the ionic correlations, while drastically increasing the counterion entropy. The added

entropy suppresses phase separation, shifting the phase boundary to a higher χN. As previously noted, this effect is especially significant in charge-dilute systems, where confinement of charges can have large entropic penalties. At $\Gamma = 23.43$, where the ions are strongly correlated, the system is found to be strongly segregated at all values of f_q, even when the interactions between the polymers promote mixing ($\chi < 0$). As f_q increases, the entropic effects push the phase boundary to a higher χN in the high ϕ region, where the entropic effects push the phase boundary to a higher χN, suppressing phase separation. In the low ϕ region, the increase in f_q broadens the Γ-induced phase boundary, indicating a stronger segregation occurring at higher values of f_q. This is due to the competition between the counterion entropy and ionic correlations in the low ϕ region. In systems with moderate coupling, where $\Gamma = 16.33$, we observe the same effect in high ϕ regions, but an opposite effect in the low ϕ region.

The deviation of the charged blend from the phase behavior of neutral polymer blends is significant at low volume fractions of the charged polymer, ϕ. This is because the difference in f_{PM} of the phase-separated state and the mixed state is especially large for a system dilute in the charged component, where the ions become much more ordered in the phase-separated, charge-dense states, compared to the mixed state, where the ions are spread far apart. As the system transitions from a mixture dilute in A to segregated regions rich in the charged polymer A, the change in the free energy is larger than that of a system that transitions from a mixture already dense in A to segregated regions, also dense in A.

In charge-rich systems, where A is the majority component, phase behavior is determined by the competition between Flory interaction, which does not depend on f_q, and counterion entropy, which increases with f_q. Therefore, phase separation is suppressed in charge-rich

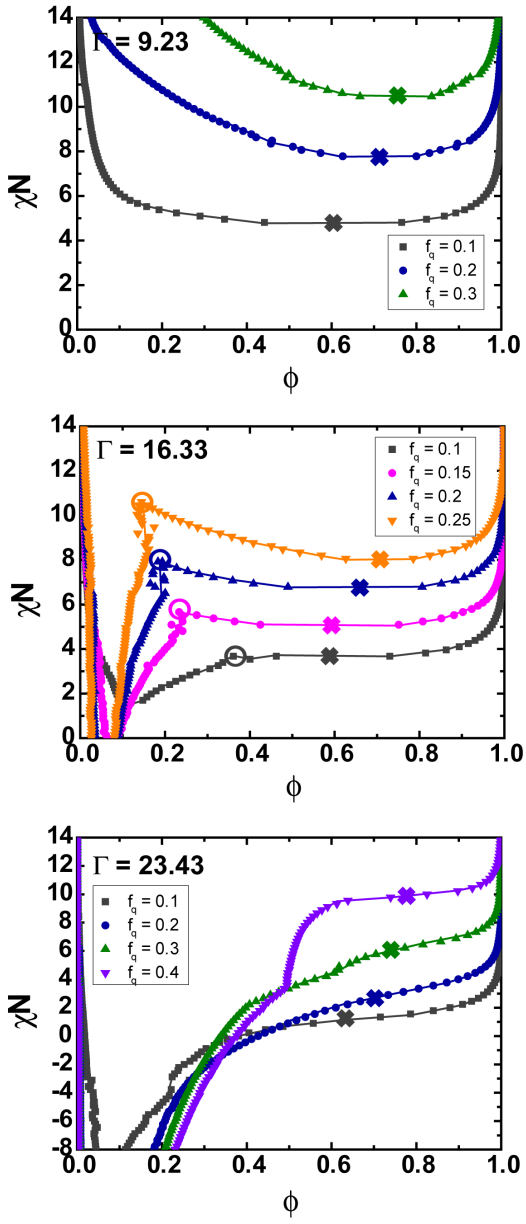

Figure 2.9. Phase diagrams for a symmetric blend of $N = 40$, where the charge fraction f_q on the charged component A is varied from 0.1 to 0.4 at $\Gamma = 9.23$ (top), 16.33 (middle), and 23.43 (bottom). Phase boundaries shift with change in f_q, but the shift depends on the value of Γ. For $\Gamma = 9.23$, the shift is to a higher χN, but for $\Gamma = 16.33$ and 23.43, the phase boundary shifts both to a higher χN and to a lower χN in different regions of the phase diagram. Hollow circles indicate triple point; stars indicate critical points.

systems. However, in charge-dilute systems, where the neutral polymer B is the majority component, both ionic correlations and counterion entropy contribute significantly to the total free energy. Ionic correlations can overcome counterion entropy to induce phase separation; however, the effects of ionic correlation become more limited and confined to the low ϕ region as f_q increases, as can be seen in figure 2.9 by the narrowing of the Γ-induced phase boundary.

We consider a solvent-free model system, comparable to blends[24,74,76–78] and copolymers[52] consisting of charged and neutral polymer chains. The effective dielectric constant in the Γ parameter could account for the polarizability of a structureless solvent, but this approach may be largely insufficient to describe the influence of for example water. Our findings may not be applicable to aqueous systems in the first place because of the weak ionic couplings in water. The high dielectric constant of water mitigates the Coulombic interaction, such that the Γ values are reduced to a value of order 1 if the water content is significant.[54,63,66] We expect that ion hydration can be captured to a certain extent by choosing an appropriate ion radius, and that hydrophobic interactions can effectively rescale the χ parameter, or influence the dissociation rate of the polymer backbone. These effects may be captured in more complicated models that necessarily need more parameters, e.g. to model the dissociation rate constants. The phenomena that we present here require a sufficient ionic coupling, and would therefore not be expected in aqueous systems, but rather in the low dielectric environment of solvent-free polymers.[24,52,74,76–78]

2.4.4. The relevance of ionic correlations

The electrostatic part of the free energy expression relies on an approximation in the construction of the closure (the DHEMSA). By elaborate testing we found excellent agreements between

the results of the DHEMSA and molecular dynamics simulations[28] of the primitive model, and expect the results to be close to exact in a large part of parameter space. It is possible that larger deviations occur in the critical regime, which is difficult to verify with both theoretical and simulation methods, but we expect the order of magnitude to be much more accurate than the MSA as can be concluded from figure 2.10. We show here the excess chemical potential (in excess over the ideal) as a function of ion volume fraction ϕ_{ion} (of one of the two ion types). The curves depend on the coupling parameter Γ, but appear to be invariant of ion radius a, if the system is symmetric ($a_{\pm} = a$). The MSA strongly underestimates the excess contribution, especially at low volume fractions, and is at least a factor 2 smaller than the DHEMSA results at higher volume fractions. The DHEMSA predicts excess chemical potentials of $-10\ kT$ per particle for a coupling strength of $\Gamma = 22$ (which corresponds to monovalent ions of radius 0.1 nm in a dielectric environment of relative permittivity $\epsilon \approx 13$), compared to less than -5 kT according to MSA predictions. We conclude from the comparison that the MSA strongly underestimates electrostatic correlations, and that MSA-based methods, for that reason, may miss aspects of ionic criticality.

2.5. Conclusion

We investigate the phase behavior of a model polyelectrolyte blend, and find that ionic effects can strongly change the classical Flory-Huggins picture. The asymmetric effects of ionic correlations appear strongly dependent on the volume fraction of the charged polymer and the coupling strength Γ set by the dielectric properties of the polymer blend, and can therefore not be wrapped in an effective, composition independent χ parameter. The ionic cohesion can be strong enough to cause the two polymer components to segregate, even when $\chi = 0$.

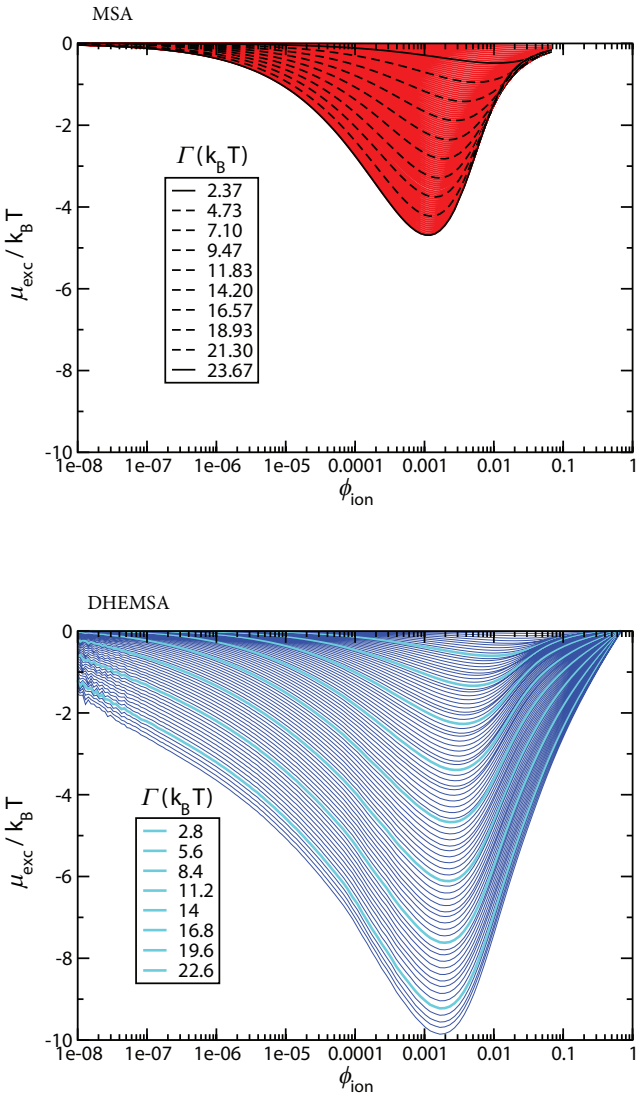

Figure 2.10. Excess chemical potential as a function of ion packing fraction, calculated with the MSA closure (upper figure) and the DHEMSA closure (lower figure), for many values of the coupling parameter Γ. The MSA suggests almost ideal gas behavior at low volume fractions, and the values of $\mu_{\rm exc}$ are at least a factor of 2 smaller than the DHEMSA results, up to orders of magnitude at low volume fractions.

We observe a triple point in the phase diagram at intermediate coupling strengths, where Γ and χ are both relevant parameters, and an appropriate f_q, the fraction of charged monomers on the polymer backbone. The three coexistent phases have three qualitatively distinct radial distribution functions, which hints at different ionic ordering into pairs, clusters, or dense liquid-like order. The analysis provides an understanding of the competing effects that dictate phase behavior of a polyelectrolyte blend, which can be tuned to induce phase behavior that is more conducive to desirable materials properties.

CHAPTER 3

Interfacial segregation of salts in ternary ionomer blends

3.1. Abstract

Solid Polymer Electrolytes (SPEs) consisting of ternary blends of charged polymer, neutral polymer, and plasticizer or salt have received much interest for their low volatility and high flexibility of polymers with ion-selective conductivity of the charge-carrying backbone. It has been shown that in these polyelectrolyte blends, where the dielectric constant is relatively low, ionic correlations can significantly influence the miscibility, inducing phase separation even at negative values of χN. Here we present a comprehensive study of phase behavior and interfacial segregation upon the addition of a tertiary component in blends of charged and neutral homopolymers. Using a hybrid of self-consistent field and liquid state theories (LS-SCFT), we investigate the bulk miscibility and the distribution of ions across the interface, looking at interfacial adsorption and selectivity of the minority component. We demonstrate that the competition between ionic correlations and ion entropy induces complex charge-dependent selectivity that can be tuned by the value of Γ, the ionic correlation strength. We show that charge interactions can have a pronounced effect on the interfacial width and tension, especially at low χN. This work appears in: Ha-Kyung Kwon, Victor A Pryamitsyn, Jos W Zwanikken, Kenneth R Shull, Monica Olvera De La Cruz, "Solubility and interfacial segregation of salts in ternary polyelectrolyte blends," *Soft Matter*, **2017**, *13* (28), 4830-4840.

3.2. Introduction

Solid Polymer Electrolytes (SPEs) have been extensively investigated for their excellent electrochemical and mechanical properties for potential use as rechargeable lithium ion batteries, organic solar cells, display windows, and sensors.[79–83] In order to improve the mechanical integrity and the performance of SPEs, the addition of a third component–in the form of small molecule plasticizers, room temperature ionic liquids (RTIL), and other polymers–has been extensively studied.[84–91]

Blending polymers is an easy and economical alternative method for obtaining materials with targeted properties. In addition, blends can serve as contemporary model systems to investigate thermal, chemical, physical, and electrochemical responses of mixtures of polymers. Although there have been molecular dynamics simulations and experimental studies of ternary polymer blends and their bulk and dynamic properties,[84,89,91–94] there is a limited understanding of the charge effects on the phase behavior of these mixtures, e.g. the effect of ionic correlations on the miscibility and selectivity of the tertiary component. Furthermore, the effects of adding a tertiary component to the interfacial properties of the blend have not been extensively studied. These effects are especially important to consider in SPEs, where the ionic correlation strength is large enough to drastically alter the phase behavior and dynamics of charge in charged binary blends and block copolymers.[7,14,18,73] Many theoretical models for bulk phase behavior of charged block copolymers and coacervate complex systems have been developed.[22,30,95,96] Here, we employ the multi-scale hybrid method which incorporates ionic correlations that can lead to local charge ordering. This effect is significant in polyelectrolytes with dielectric constant $\epsilon_r < 8$. In this theory, we expand upon the Flory-Huggins theory[8,36] using a theoretical framework previously reported[28] to describe the effects of ionic correlations that arise from

excluded volume and multi-scale Coulombic interaction. The strength of ionic correlations is quantified using ionic correlation strength $\Gamma = \frac{q_+ q_- e^2}{8\pi\epsilon_r\epsilon_0 kTa}$, which is the bare Coulomb energy (in kT) that is required to separate the two attracted ions of radius a at contact. This quantity can also be described as $\Gamma = l_B/(2a)$, or the Bjerrum length normalized by the distance between the two ions.[37,38] $\Gamma \approx 1$ for monovalent ions in water, and $\Gamma > 10$ for polymers with $\epsilon_r < 8$. Ionic effects are calculated at a specified ionic correlation strength Γ by solving the Ornstein-Zernike equation[26,27] with an accurate closure equation.[28] This approach has predicted that a non-trivial, complex critical behavior emerges from the competition of ion entropy and ionic correlations, leading to triple points and partial miscibility in a binary blend.[7] In solvent-containing blends, works by Khoklov and Nyrkova *et al* have shown that microphase separation can also occur in these systems.[?,?]

Here, we present a systematic study of ternary blends containing multiple charged components, and study the phase behavior and interfacial segregation as a function of Γ, charge fraction f_q, and $\chi_{AB}N$. This study models the phase behavior and interfacial segregation of polyelectrolyte blends upon the addition of a tertiary component (plasticizers, ILs, polymers, and salt). By using a full free energy analysis, we can explore the parameter space to obtain a complete picture of the phase behavior in charged ternary blends. We begin by analyzing a simple case, where the tertiary component is a neutral, non-selective solvent, and show that the phase behavior deviates significantly from the solvent dilution effect due to the ionic effects in the charged polymer.[97,98] We then demonstrate that adding salts of varying ionic strength can alter the miscibility of the blend due to the competition between ion entropy, ionic correlations, and $\chi_{AB}N$. Using 1-D self-consistent field theory (SCFT), we show that the deviation from

Flory-Huggins theory is due to Γ- and $f_{q,A}$- dependent segregation of the tertiary component, which can be tuned independently to induce desired phase selectivity.

3.3. Theoretical approach

In this study, we consider a ternary blend of components A, B, and C in a homogeneous dielectric medium ϵ_r, where polymer A, with degree of polymerization N_A, is partially negatively charged with charge fraction $f_{q,A}$ along its backbone; polymer B is neutral, and has degree of polymerization of N_B; and C is the tertiary component with $N_C = 1$, whose charge can be tuned by the parameter $f_{q,C}$. In the first case, C is a neutral solvent, where $f_{q,C} = 0$. In the second case, where the tertiary component is a negatively charged, monovalent salt with counterions, $f_{q,C} = 1$. The polymeric interactions are described by Flory-Huggins interaction parameters χ_{AB}, χ_{BC}, and χ_{AC}, and are set independently to tune the selectivity of the tertiary component. The electrostatic interactions are characterized by Γ and the concentration of total negative charge in the system, $f_{q,A}\phi_A + f_{q,C}\phi_C$ where $f_{q,C} = 0$ for a neutral solvent and $f_{q,C} = 1$ for salt. The system contains counterions to achieve electroneutrality. This model system is shown in Figure 3.1.

3.3.1. Flory-Huggins and liquid state theories

The total free energy of the blend is written such that it includes contributions from the Flory-Huggins terms, f_{FH}, and from the primitive model (f_{PM-id}, f_{PM-exc}). The translational entropy of the counterions is described by f_{PM-id}, while the contribution from ionic correlations, f_{PM-exc}, is calculated using the Debye-Hückel Extended Mean Spherical Approximation (DHEMSA) closure on the Ornstein-Zernike equation, shown below:[?,7,18,28]

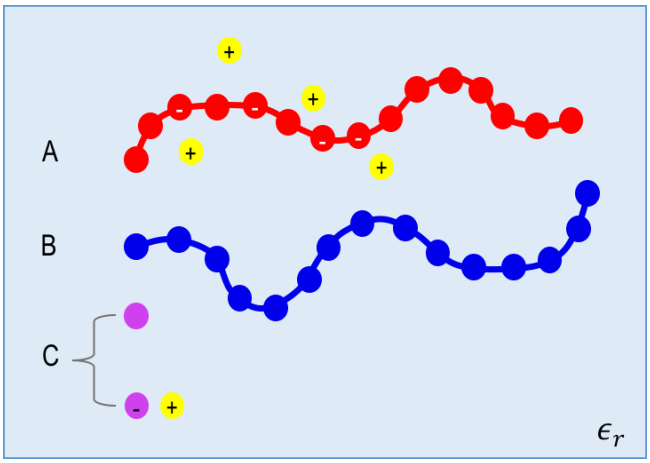

Figure 3.1. Schematic of the model system. Polymer chains of type A and B are described by Flory-Huggins interaction parameter χ_{AB}. $\chi_{AC} = \chi_{BC}$ unless otherwise indicated. The polymers are in a homogeneous dielectric environment with a corresponding ϵ_r, which gives rise to the ionic correlation strength Γ between ions and the counterions.

$$\hat{h}_{ik} = \hat{c}_{ik} + \sum_l \rho_l \hat{c}_{il} \hat{h}_{lk} \tag{3.1}$$

$$c_{ik} = \tilde{h_{ik}} - ln(\tilde{h_{ik}} + 1) - \beta u_{ik} \tag{3.2}$$

where $\hat{c}$ and $\hat{h}$ denote Fourier transforms of the direct and total correlation functions.

The liquid state approach allows for the consideration of charge ordering that is expected for sufficiently high densities and ionic correlation strengths (Γ), which are neglected in the mean-field approach of non-linear Debye-Hückel theory. While DHEMSA closure closely resembles the hyper-netted chain (HNC) closure in its treatment of non-linear long-range electrostatics and short range repulsions, the algorithm has a superior convergence, and enables an efficient

calculation of the pair correlation functions over a large parameter range of the liquid state, by an informed guess of $h(r)$ instead of an iterative calculation approach used in HNC.[28]

With this contribution, the total free energy can be written as:

$$f_{tot}(\phi_k, N_k, \chi_{kl}, f_{q,k}, a_m, \Gamma_{mn}) = f_{FH}(\phi_k, N_k, \chi_{kl}) + f_{PM}(\phi_k, f_{q,k}, a_m, \Gamma_{mn}) \tag{3.3}$$

where indices k and l refer to different polymeric components (A, B, C), and m and n refer to ionic components ($+, -$). Here, a_m is the ion size, which is assumed to be equivalent for anions and cations in this particular study. In addition, it is assumed that all ions are monovalent, and that the anions on the polymer backbone are indistinguishable from dissociated salt anions. All cations are likewise assumed to be indistinguishable. The counterions to the charged backbone and salt anions are likewise indistinguishable. This simplification reduces all charge interactions to one that can be described using a single ion size and Γ, and the indices are subsequently dropped to give a free energy expression more specific to our system:

$$f_{tot} = \frac{\phi_A ln\phi_A}{N_A} + \frac{\phi_B ln\phi_B}{N_B} + \frac{\phi_C ln\phi_C}{N_C} \tag{3.4}$$

$$+ (f_{q,A}\phi_A + f_{q,C}\phi_C) ln(f_{q,A}\phi_A + f_{q,C}\phi_C) + f_{exc}(f_{q,A}\phi_A + f_{q,C}\phi_C, \Gamma) \tag{3.5}$$

Here, $f_{q,A}\phi_A + f_{q,C}\phi_C$ represents the total amount of negative charge; to achieve electroneutrality, the same concentration of counterions is added. $f_{q,A}$ is typically varied between 0.01 and 0.1. $f_{q,C}$ is chosen to be 0 for the neutral solvent case, and 1 for the added salt case. $f_{exc}(f_{q,A}\phi_A + f_{q,C}\phi_C, \Gamma)$ describes the excess energy due to ionic correlations, which favor

phase separation as the total charge concentration $f_{q,A}\phi_A + f_{q,C}\phi_C$ and ionic correlation strength Γ are increased.[7]

While a three-component blend can form four different phases α, β, γ, and δ,[4] we only consider the α-β coexistence in this work by neglecting all Flory terms except for χ_{AB}. In the α-β coexistence, phase separation is driven by the interaction between A and B monomers. The coexistence line (or the phase boundary) is calculated by equating the chemical potential of each component in α (A-rich) and β (B-rich) phases. The chemical potential of each component k, μ_k, is found using the following formula:[12,99]

$$\mu_k = \frac{\partial f_{tot}}{\partial \phi_k} + f_{tot} - \sum\nolimits_k \phi_k \frac{\partial f_{tot}}{\partial \phi_k} \tag{3.6}$$

Here, k can be A, B, or C. Derivatives with respect to a particular ϕ_k are to be taken with other volume fractions held constant. We assume that χ_{AB}, χ_{BC}, χ_{AC} are independent of volume fraction.[12]

This gives us μ_k:

$$\mu_A = \mu_{FH,A} + f_{q,A} ln(f_{q,A}\phi_A + f_{q,C}\phi_C) + f_{q,A} - f_{q,A}\phi_A - f_{q,C}\phi_C + \mu_{LS,A} \tag{3.7}$$

$$\mu_B = \mu_{FH,B} - f_{q,A}\phi_A - f_{q,C}\phi_C + \mu_{LS,B} \tag{3.8}$$

$$\mu_C = \mu_{FH,C} + f_{q,C} ln(f_{q,A}\phi_A + f_{q,C}\phi_C) + f_{q,C} - f_{q,A}\phi_A - f_{q,C}\phi_C + \mu_{LS,C} \tag{3.9}$$

where

$$\mu_{LS,k} = \frac{\partial f_{exc}}{\partial \phi_k} + f_{exc} - \sum\nolimits_k \phi_k \frac{\partial f_{exc}}{\partial \phi_k} \tag{3.10}$$

and

$$\mu_{FH,k} = \frac{ln\phi_k + 1}{N_k} - \sum_k \frac{\phi_k}{N_k} - \frac{1}{2}\sum_{o\neq p}(\phi_o - g_{o,k})\chi_{op}(\phi_p - g_{p,k}) \tag{3.11}$$

Here, $g_{o,k} = 1$ if $o = k$, and $g_{o,k} = 0$ if $o \neq k$.

We then solve for equilibrium compositions whose chemical potential in the two phases are equal; furthermore, the volume fractions all have to add up to 1 to satisfy the incompressibility condition.

$$\mu_A^\alpha = \mu_A^\beta \tag{3.12}$$

$$\mu_B^\alpha = \mu_B^\beta \tag{3.13}$$

$$\mu_C^\alpha = \mu_C^\beta \tag{3.14}$$

$$\phi_A^\alpha + \phi_B^\alpha + \phi_C^\alpha = \phi_A^\beta + \phi_B^\beta + \phi_C^\beta = 1 \tag{3.15}$$

3.3.2. 1-D Self-Consistent Field Theory (SCFT)

Once the equilibrium compositions are obtained, we use 1D self-consistent field theory (SCFT) to find the distribution of the three components across the $\alpha - \beta$ interface using a discrete representation of the modified diffusion equation introduced by Edwards:[44]

$$\frac{\partial q(r,n)}{\partial n} = \frac{a^2}{6}\left(\frac{\partial^2 q(r,n)}{\partial r^2}\right) - \omega(r,n)q(r,n) \tag{3.16}$$

The variables r and n are continuous forms of discrete variables i and j used in this work, where i denotes discrete distance variable and j denotes the index of the repeat unit along a

chain.[99] The width of each layer i corresponds to a, the statistical segment length of one repeat unit, which is defined so that R_g, the radius of gyration of a chain, is equal to $(N_A/6a)^{1/2}$. The mean field $\omega(i,j)$ is a function of the composition along the chain, $g(j)$, and the surrounding composition in the layer i, $\phi(i)$. Since all polymers are homopolymers and the composition does not vary along the chain, $\omega(i,j)$ can be written as a function of only i.

$$\omega_k(i) = \omega_{p,k}(i) + \omega_{ext,k}(i) - k_B T \sum\nolimits_k \frac{\phi_k(i)}{N_k} - \Delta\omega(i) \tag{3.17}$$

The first term, $\omega_{p,k}(i)$ comes from enthalpic contributions characterized by Flory-Huggins parameters $\chi_{AB}, \chi_{BC}, \chi_{AC}$.

$$\omega_{p,A}(i) = \phi_B(i)(1-\phi_A(i))\chi_{AB} - \phi_B(i)\phi_C(i)\chi_{BC} + \phi_C(i)(1-\phi_A(i))\chi_{AC} \tag{3.18}$$

$$\omega_{p,B}(i) = \phi_A(i)(1-\phi_B(i))\chi_{AB} - \phi_A(i)\phi_C(i)\chi_{AC} + \phi_C(i)(1-\phi_B(i))\chi_{BC} \tag{3.19}$$

$$\omega_{p,C}(i) = \phi_A(i)(1-\phi_C(i))\chi_{AC} - \phi_A(i)\phi_B(i)\chi_{AB} + \phi_B(i)(1-\phi_C(i))\chi_{BC} \tag{3.20}$$

The second term, $\omega_{ext,k}(i)$, comes from electrostatic contributions characterized by Γ, $f_{q,A}$, and$f_{q,C}$. This term can be calculated from the chemical potential μ_k:

$$\omega_{ext,k}(i) = \mu_k(i) - \mu_{FH,k}(i) \tag{3.21}$$

The third term in equation 3.17 is the entropic contribution from the three components. The last term, $\Delta\omega(i)$, comes from the incompressibility constraint, where ζ in equation 3.22 is inversely

proportional to the bulk incompressibility of the system.

$$\frac{\Delta\omega(i)}{k_BT} = \zeta(1 - \sum\nolimits_k \phi_k(i)) \tag{3.22}$$

In the presence of a field, the probability distribution functions $q_k(i,j)$ can be obtained using recursion relationships that arise from the connectivity of the chains:

$$q_k(i,j) = \lambda_{-1}1q_k(i-1,j-1) + \lambda_0 q_k(i,j-1) + \tag{3.23}$$

$$\lambda_{+1}q_k(i+1,j-1)exp(-\omega_k(i)/k_BT) \tag{3.24}$$

where the $\lambda_{-1}, \lambda_0, \lambda_{+1}$ are transition probabilities specific to the geometry of the system.[12,99] For homopolymers, only one $q_k(i,j)$ is needed, as the composition profiles from the two ends of a single chain are indistinguishable.

Volume fraction profiles $\phi_A(i), \phi_B(i), \phi_C(i)$ are obtained by summing the probability distribution functions $q_k(i,j)$ from both ends:

$$\phi_k(i) = \frac{1}{N_k} exp(\mu_{bulk,k}/k_BT - 1) \sum_{j=1}^{N_k} q_k(i,j)q_k(i,N_k,j) \tag{3.25}$$

The new field is generated by the calculated volume fraction profile $\phi_k(i)$. The resulting probability distribution function and volume fraction profiles are iteratively and self-consistently solved with the boundary condition where the volume fraction profile at each end ($i = 0, i = i_{\max}$) corresponds to the bulk phase volume fraction and chemical potential $\mu_{bulk,k}$ calculated from the phase diagram.

The interfacial tension is obtained by summing $\Delta\omega$ over all of the lattice layers:[100]

$$\gamma = \sum_i L(i)\omega(i) \tag{3.26}$$

where $L(i)$ is the number of lattice sites in layer i.

3.4. Results and discussion

3.4.1. Phase diagram of solvent-containing blends

First, we examine a ternary blend containing a neutral solvent C ($f_{q,C} = 0$). This system is representative of a polymer blend where a plasticizer is added to suppress crystallization and increase processability.[84–86,88,90] In cases where the solvent is selective for one of the two polymeric components ($\chi_{AC} \neq \chi_{BC}$), the selectivity may complicate the blend miscibility and the resulting phase behavior.[4] Here, we assume non-selective behavior for the solvent ($\chi_{AC} = \chi_{BC} = 0$), in an attempt to decouple effects that arise from ionic correlations from Flory-Huggins type solvent selectivity. These conditions may be difficult to access in experimental conditions, but may be important in understanding the underlying physics. Our system consists of charged polymer A, neutral polymer B, with a neutral, non-selective solvent C where $\chi_{AC} = \chi_{BC} = 0$. For this set of calculations, $N_A = N_B = 40$, $0.01 < f_{q,A} < 0.1$, $\chi_{AB}N = 3$, and $14.44 < \Gamma < 23.43$ unless otherwise specified. These parameters correspond to ionomers with relative dielectric constants ϵ_r of approximately $3 - 5$.[7] At these values of Γ and $\chi_{AB}N$, the magnitude of Flory-Huggins interactions and ionic correlations are comparable, leading to multiple critical phenomena.[7] Parameters Γ, $f_{q,A}$, and χ_{AB} are changed systematically in Figure 3.2 to demonstrate the effect of these parameters on the α-β phase boundary; α phase is rich in

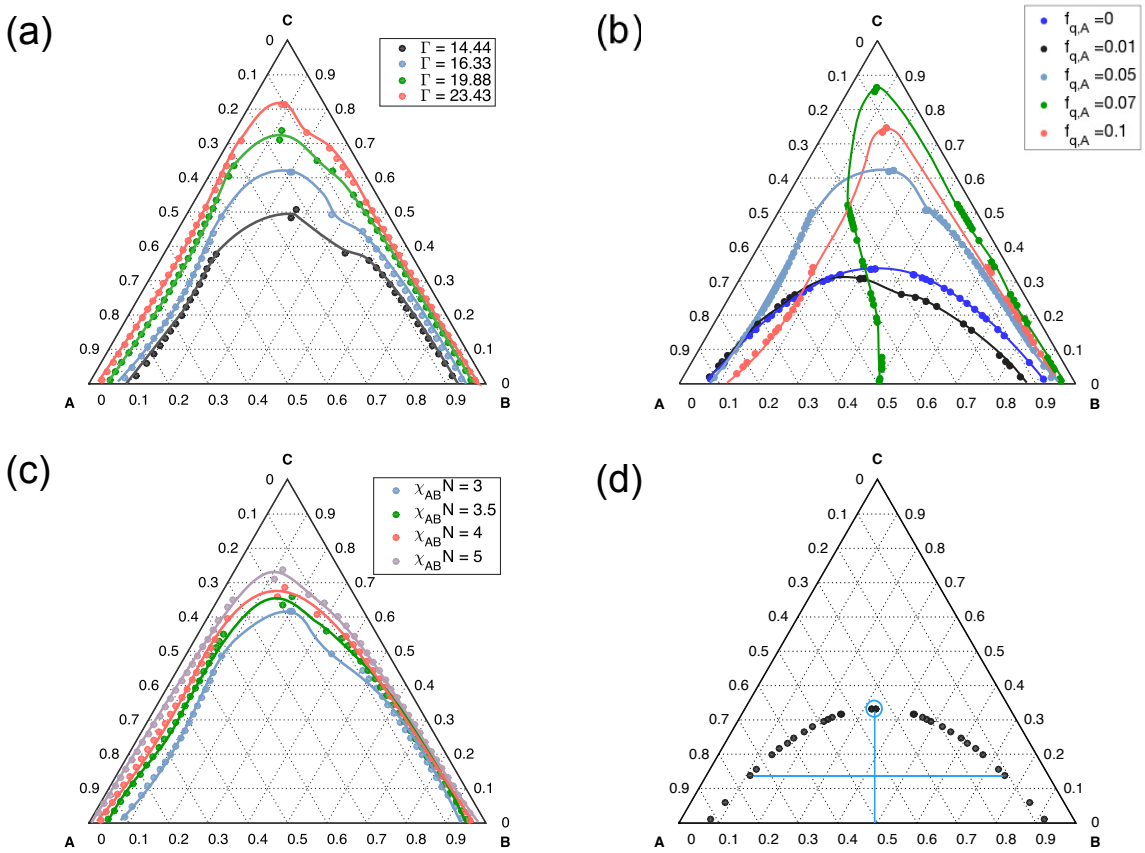

Figure 3.2. The effect of changing Γ (a), $f_{q,A}$ (b) and $\chi_{AB}N$ (c) on the $\alpha - \beta$ phase boundary in a ternary blend of charged polymer A, neutral polymer B, and solvent C. The neutral boundary is shown in (d), with blue lines marking the breadth of the phase boundary and height of the phase boundary to assess miscibility and selectivity. Critical point is marked with a blue circle. While the parameter of interest is varied, all others are held constant at $\Gamma = 16.33$, $f_{q,A} = 0.05$, $\chi_{AB}N = 3$, and $\chi_{BC} = \chi_{AC} = 0$. Lines have been drawn in to guide the eye.

charged polymer A and is the charge-dense phase, while β phase is rich in neutral polymer B and can be described as the charge-dilute phase.

We have shown in a previous study of binary blends that the Γ-dependent phase behavior is due to the competition between the translational entropy of the counterions and the ionic correlations between the oppositely charged components. At sufficiently high values of Γ, ionic

correlations dominate and phase separation is enhanced in the charge-dilute "chimney" region, while phase separation is experimentally shown to be suppressed outside the chimney region, where the volume fraction of the charged polymer is relatively high.[7,101] The effect of Γ on the miscibility of ternary blends mirrors our findings in the binary blend case. The phase boundary shows broadening along the $A-B$ axis at all concentrations of solvent, indicating a decreased miscibility between A and B. The critical point moves to a higher concentration with increase in Γ, further confirming the decreased miscibility between A and B. At $\Gamma = 23.43$, 80 volume percent of solvent is required to solubilize the $A-B$ blend. The location of the phase boundary at the A-B axis ($\phi_C = 0$) is in agreement with the composition of the phase-separated mixture in binary blends of A and B.[7]

With the introduction of strong ionic correlations, the phase boundary becomes asymmetrically skewed, as shown in Figure 3.2(a). The movement of the critical point indicates that criticality is reached at more dilute concentrations of the charged polymer A with increasing Γ. This asymmetry is highlighted in Figures 3.2(b) and (c), where Γ is held constant and $f_{q,A}$ and $\chi_{AB}N$ are varied, respectively. The critical point is at $\phi_A = 0.4$ at $f_{q,A} = 0.01$, and moves to $\phi_A = 0.08$ at $f_{q,A} = 0.1$. Furthermore, an increase in $f_{q,A}$ moves the critical point to a higher concentration of C ($\phi_C = 0.3$ at $f_{q,A} = 0.01, \phi_C = 0.84$ at $f_{q,A} = 0.1$) and narrows the phase boundary along the $A-B$ axis. The movement of the critical point to a higher ϕ_C indicates decreased miscibility between A and B, while the narrowing of the phase boundary shows that the blend is less strongly segregated. This partial mixing is reminiscent of the chimney observed in the charged binary blend, where the free energy change for forming ionic phases from a dilutely charged system is much more favorable than forming the same phases from a densely charged

system.[7,18] In addition, a greater deviation from symmetricity at higher $f_{q,A}$ can be attributed to asymmetry that arises from charge effects.

On the other hand, changing $\chi_{AB}N$ has little effect on the asymmetry of the phase boundary, as seen in Figure 3.2(c). Increasing the value of $\chi_{AB}N$ results in a slight broadening of the phase boundary, accompanied by the movement of the critical point to a higher ϕ_C. These changes are expected from an increase in χ_{AB}, which decreases the miscibility between A and B.

3.4.2. Interfacial adsorption of solvent

To further investigate the implications of the asymmetry of the phase boundary, 1-D SCFT is used to plot the equilibrium volume fraction distribution of the three components across the $\alpha-\beta$ interface for concentrated solutions ($\phi_C = 0.05$). A representative plot is shown in Figure 3.3(a), where the inset shows a zoomed-in distribution profile of solvent. For clarity, only the distribution of the minority component (the solvent) is shown in subsequent plots.

We show that the inclusion of ionic correlations in a charged blend leads to ionically induced selectivity in a "non-selective" ($\chi_{AC} = \chi_{BC} = 0$) solvent, as seen in Figure 3.3(b). Unlike selectivity tuned by Flory-Huggins parameters, where the selectivity of the solvent is fixed by the composition-independent values χ_{AC} and χ_{BC}, selectivity induced by ionic correlations is dependent on charge parameters such as total charge concentration and ionic correlation strength Γ.

The ionically induced solvent selectivity is due to the competition between translational entropy of the counterions and ionic correlations. Entropic effects dominate at relatively low values of Γ, while ionic correlations favor ordering of charges at high values of Γ. This is quantitatively shown in Figure 3.3(b). At $\Gamma = 14.44$, the solvent shows a slight preference for

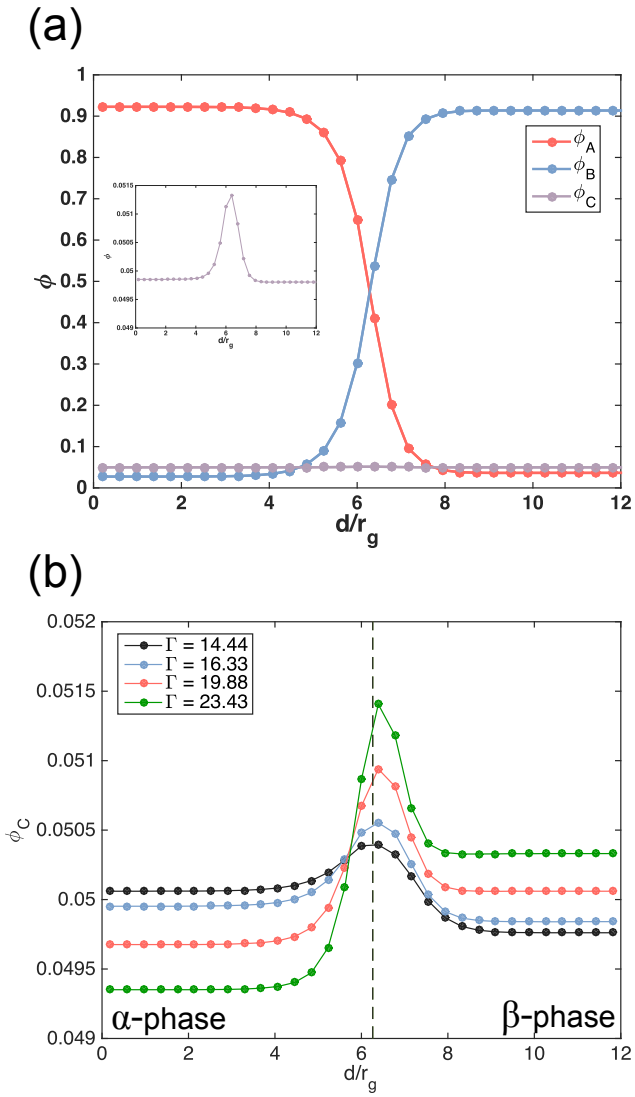

Figure 3.3. A representative plot of A, B, C distribution profile across α-β interface at $\Gamma = 14.44, f_{q,A} = 0.05, \chi_{AB}N = 4$ (a). Inset shows a zoomed-in profile of C across the interface. The distribution of C is plotted with increasing Γ at $f_{q,A} = 0.05, \chi_{AB}N = 3, \phi_C = 0.05$ (b). Increased adsorption is observed with increasing Γ, with the selectivity switching at $16.33 < \Gamma < 19.88$.

the α-phase. The amount of solvent in this phase is 0.0501, compared to $\phi_C^\beta \approxeq 0.04975$. At this relatively low value of Γ, the system moves to maximize the entropy of the counterions. As the counterions are confined to the charge-dense phase, entropy is maximized by swelling the

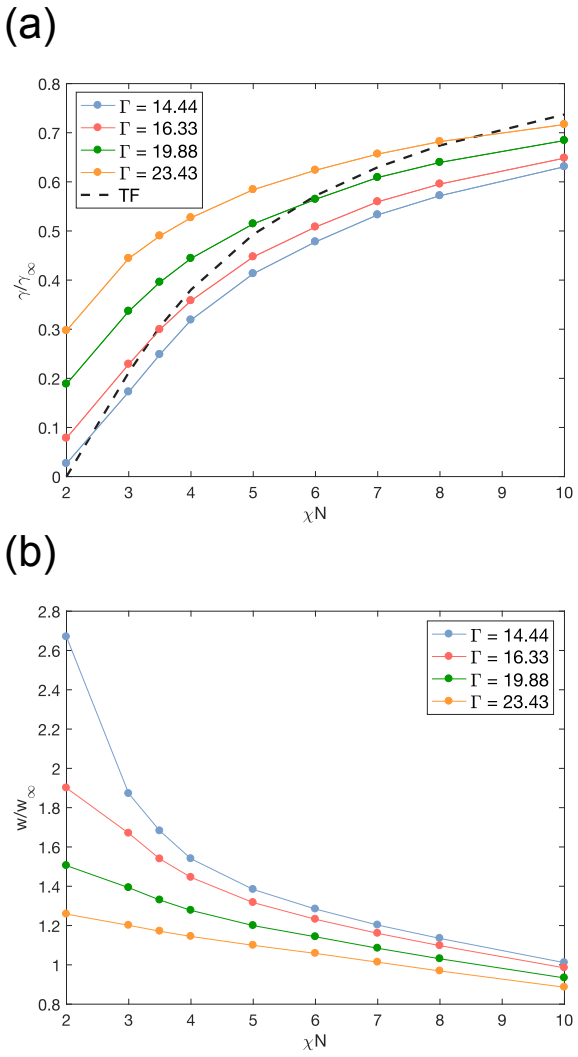

Figure 3.4. The normalized interfacial energy γ/γ_∞ (a) and normalized interfacial width (b) for varying values of Γ. The dashed line represents Tang and Freed predictions for the normalized interfacial energy. Here, $\phi_C = 0.05$.

charge-dense phase with solvent. This effect is relatively small, however, as indicated by the difference between the two bulk phase solvent concentrations ($\frac{|\phi_C^\alpha - \phi_C^\beta|}{\phi_{C,avg}} \approxeq 0.007$).

When Γ is further increased, the selectivity decreases ($\frac{|\phi_C^\alpha - \phi_C^\beta|}{\phi_{C,avg}} \approxeq 0.002$ at $\Gamma = 16.33$) and switches when $\Gamma > 16.33$. For $\Gamma \geq 19.88$, the solvent strongly prefers the β-phase. This is due to ionic correlations, which favor ordering of charges. In a phase-separated blend, this is

achieved by the expulsion of solvent from the charge-dense phase. At $\Gamma = 23.43$, the selectivity ($\frac{|\phi_C^{\alpha} - \phi_C^{\beta}|}{\phi_{C,avg}}$) can be as large as 0.019, which is almost a three-fold increase from the selectivity at $\Gamma = 14.33$.

Previous studies have shown that a non-selective solvent adsorbs at the interface between two majority components to minimize interfacial tension.[5] This adsorption is observed in blends studied in this work, as shown in Figure 3.3(b). The increase in adsorption with an increase in Γ is consistent with decreased miscibility observed in bulk phase behavior in Figure 3.2, and indicates that a strong correlation between the charged backbone and the counterions increases effective repulsion between the A and B components.

The normalized interfacial tension γ/γ_∞ is plotted as a function of $1/\chi N$ for varying values of Γ in Figure 3.4(a) for a ternary blend where $N_A = N_B = 40$, $f_{q,A} = 0.05$. It is known that for a symmetric immiscible neutral blend, the critical point is at $\chi N = 2$. The interfacial energy at $\chi N = 2$ therefore vanishes for neutral blends. At $\chi N = \infty$, the interfacial tension for neutral blends can be analytically calculated by $\gamma_\infty = a\rho_0 k_B T(\chi/6)^{1/2}$.[102] The variance of γ for a charged blend between $\chi N = 2$ and $\chi N = \infty$ is shown in Figure 3.4(a). The dashed line is the approximate form suggested by Tang and Freed[103] for neutral binary blends:

$$\gamma/\gamma_\infty = \left\{1 - \frac{1.8}{\chi N} - \frac{0.4}{(\chi N)^2}\right\}^{3/2} \tag{3.27}$$

It is important to note, however, that no simple free energy function exists in the regime, and that this estimate of the interfacial tension is the simplest form that gives consistent results for $\chi N \cong 2$ and $\gamma/\gamma_\infty = 1$ at $\chi N = \infty$.

First and foremost, we note that the normalized interfacial tensions of the ternary blends are consistently lower than the estimates of Tang and Freed.[103] This can be attributed to the fact that Tang and Freed's estimate was for binary blends; the addition of a tertiary component lowers the interfacial tension across all Γ and χN values. Secondly, we note that a higher value of Γ is correlated with a higher normalized interfacial tension, with $\Gamma \geq 19.88$ giving higher normalized interfacial tension than estimated, and $\Gamma \leq 16.33$ predicting lower interfacial tension than estimated from the Tang and Freed estimate. At lower χN the differences in interfacial tensions calculated for various values of Γ become more highlighted; we expect that the interfacial tensions for $\Gamma \geq 19.88$ do not vanish at $\chi N = 2$, as expected for neutral blends. The trends in interfacial tension can be explained via competition between translation entropy of counterions and effects from ionic correlations. Lower interfacial tensions compared to a neutral blend can be attributed to an entropic-driven tendency toward miscibility, while higher interfacial tensions at large values of Γ can be attributed to decreased miscibility due to ionic correlations. This effect is particularly pronounced at lower χN,where ionic effects become more significant. For larger Γ, we have previously shown that ionic interactions of this magnitude results in a notable suppression of the critical point to $\chi N < 0$, which is reflected in the finite value of γ/γ_∞ at $\chi N = 2$ for larger values of Γ.

The increase in interfacial tension with Γ is correlated with the decrease in interfacial width, as shown in Figure 3.4(b). The interfacial width is normalized by the width of the interface at infinite molecular weight:[104]

$$w_\infty = \frac{2a}{\sqrt{6\chi}} \tag{3.28}$$

where a is the average segment length.

The interfacial width is found by fitting the volume fraction profile to the equation:

$$\phi_k(x) = \phi_{k,L} + 0.5(\phi_{k,L} - \phi_{k,R}) \left\{ 1 + tanh\left(\frac{2(x - x_0)}{w} \right) \right\} \tag{3.29}$$

where x_0 is the location of the interface, $\phi_{k,L}\phi_{k,R}$ are bulk values of component k on either side of the interface, w is the width in terms of a, the width of one lattice layer.

As expected from the trends in the interfacial tension, we see that the interfacial width decreases with increasing Γ. High Γ increases the effective repulsion between A and B components, leading to an enhanced separation and a sharper interface. The effect of Γ on the interfacial width is pronounced at low χN, where the Flory interactions are relatively small in magnitude.

3.4.3. Phase diagram of salt-containing blends

In order to more closely resemble experimental systems which are currently being studied in the field, non-selective, neutral solvent is replaced with monovalent salt ions in this section. The resulting bulk and interfacial behavior is described in a similar fashion as above. Salt ion pairs of symmetric valency and size are added to the blend of charged polymer A and neutral polymer B. Polymer A, degree of polymerization of N_A, is negatively charged along its backbone with charge fraction of $f_{q,A}$. Polymer B has degree of polymerization of N_B and is uncharged. The tertiary component C, of $N_C = 1$, is fully charged ($f_{q,C} = 1$). For simplicity, it is assumed that $\chi_{AC} = \chi_{BC} = 0$. Furthermore, the salt anions are indistinguishable from charged monomer along the backbone, and all positively charged counterions are indistinguishable. This enables the use of a single Γ to capture all electrostatic interactions. System parameters such as Γ, $f_{q,A}$, and $\chi_{AB}N$ are systematically varied in Figure 3.5.

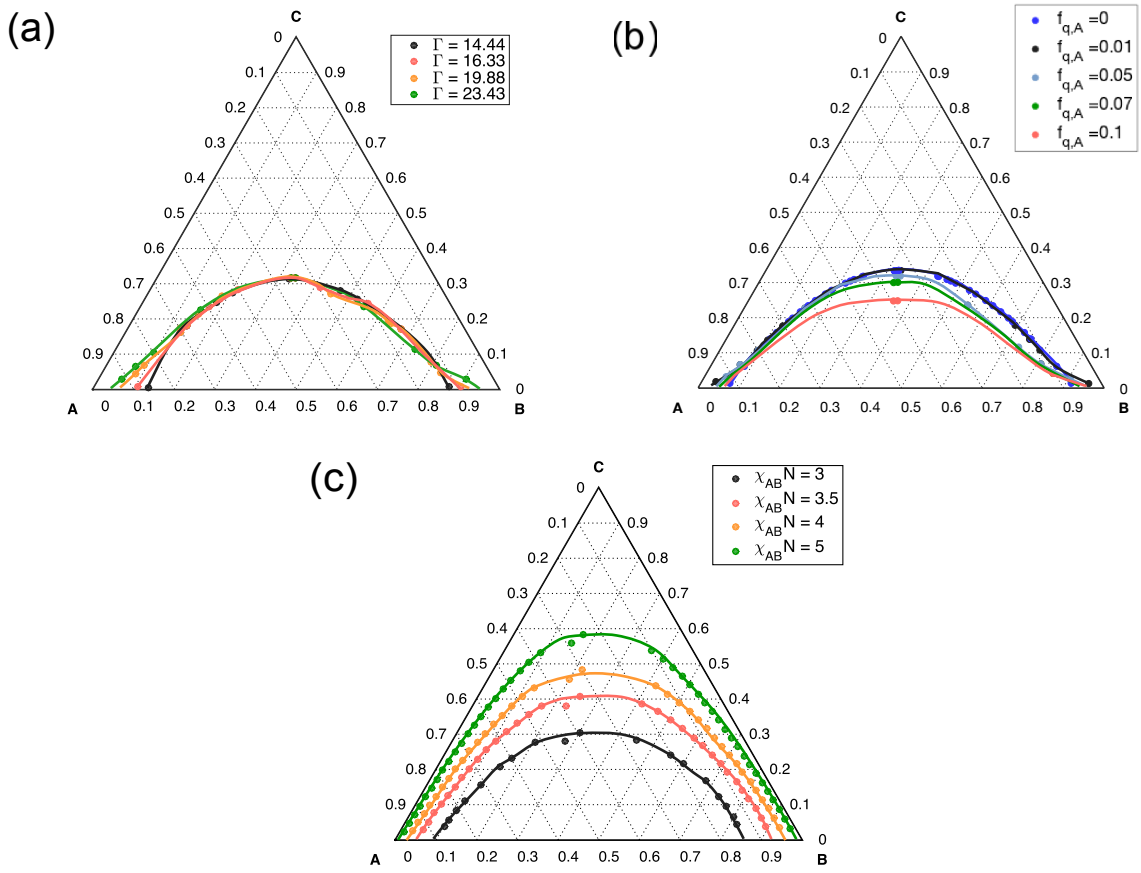

Figure 3.5. The effect of changing Γ (a), $f_{q,A}$ (b), and $\chi_{AB}N$ (c) on the $\alpha - \beta$ phase boundary in a ternary blend of charged polymer A, neutral polymer B, and salt C. While the parameter of interest is varied, all others are held constant at $\Gamma = 16.33$, $f_{q,A} = 0.05$, $f_{q,C} = 1$, $\chi_{AB}N = 3$, and $\chi_{BC} = \chi_{AC} = 0$. Lines have been drawn in to guide the eye.

As shown in Figure 3.5(a), the $\alpha - \beta$ phase boundary is only sensitive to Γ at low concentrations of salt ($\phi_C < 0.1$). This concentration of salt corresponds to approximately 930 mM, which can be two orders of magnitude greater than the concentration of charged monomers on a weakly charged polymer ($f_{q,A} = 0.01$). The backbone needs to have a higher charge fraction ($f_{q,A} > 0.1$) in order for the salt to charged monomer molar ratio to be less than 10. For the range of $f_{q,A}$ investigated in this study, the salt to monomer ratio is very high, at

$\phi_C = 0.05(470mM)$. Therefore, it is not surprising that electrostatic effects are negligible for a majority of the range of ϕ_C investigated in this study. For $\phi_C > 0.01$, the high concentration of salt effectively screens out all electrostatic interactions, and the phase boundaries all collapse onto the neutral phase boundary, as shown in Figure 3.5(a). These phase boundaries appear symmetric, as expected for neutral blends. At low salt concentrations ($\phi_C < 0.01$), the phase boundaries show a Γ-dependent deviation from neutral phase behavior. As Γ increases, the breadth of the phase boundary increases, indicating a stronger segregation. This is consistent with Γ-enhanced phase separation observed in binary and ternary blends.[7] However, the location of the critical point does not change with increasing Γ, indicating that we have a Flory-Huggins type criticality, rather than one induced by ionic correlations.

The phase boundary shows a slight dependence on the fraction of charged monomers, $f_{q,A}$, which is dissimilar to the trend observed in the neutral solvent case (Figure 3.5(b)). For neutral solvents, an increase in $f_{q,A}$ led to an increased height and decreased breadth of the phase boundary. In salt-containing blends, an increase in $f_{q,A}$ leads to a decreased height and decreased breadth (at higher ϕ_C) of the phase boundary. A decreased height indicates increased miscibility between A and B components, as well as a high solvation of salt ions by A. This value can vary from $\phi_C = 0.33$ for $f_{q,A} = 0.01$ to $\phi_C = 0.25$ for $f_{q,A} = 0.1$, showing a 24 percent decrease in the concentration of C required to solubilize the blend. The increased miscibility can be attributed to the concentration of counterions that rises as $f_{q,A}$ is increased.

The free energy change due to counterion entropy is proportional to the total concentration of charge, $f_{q,A}\phi_A + \phi_C$. For neutral solvent-containing blends, this prefactor is equal to $f_{q,A}\phi_A$, which is always less than 0.1. In such a case, the free energy contribution from the translational

entropy of the counterions is relatively small compared to the contribution from ionic correlations. However, for salt-containing blends, this prefactor can be larger than 0.3 for $f_{q,A} = 0.01$. In salt-containing blends, therefore, the entropy of the counterions dominates. A small increase in $f_{q,A}$, which increases the prefactor, can lead to substantial increase in the miscibility of the blend due to entropic effects. It is worth noting that the phase boundary becomes increasingly asymmetric with $f_{q,A}$, demonstrating an increased tendency to form β-phases with a higher concentration of A. This is a stark contrast from the phases obtained in Figure 3.2(b), where both α- and β-phases had dilute concentrations of A, consistent with the formation of ionically driven phases. Here, by increasing $f_{q,A}$, we reverse the formation of these ionic phases.

As can be expected with neutral phase boundaries, we see an increase in the breadth and height of the phase boundary with increasing $\chi_{AB}N$ (Figure 3.5(c)). The phase boundary of salt-containing blends shows the strongest dependence on $\chi_{AB}N$, which is consistent with their behavior as neutral blends from screened out electrostatic interactions.

It is important to note that an examination of only the $\alpha - \beta$ phase boundary is not sufficient to capture the complete phase behavior of salt-containing blends. The formation of a salt precipitate phase is beyond the scope of this work, but will be addressed in a more comprehensive investigation of all possible phases in salt-containing polyelectrolyte blends.

3.4.4. Interfacial segregation of salts

The volume fraction profile of the minority component ($\phi_C = 0.05$) across the $\alpha - \beta$ interface is plotted in figure 3.6(a) using 1-D SCFT. We study blends with dilute concentrations of salt ($\phi_C = 0.05$), where the blend is macro-phase separated into α- and β- phases. Here, we show that ionic correlations can induce selectivity of the salt. Furthermore, we have identified ionic

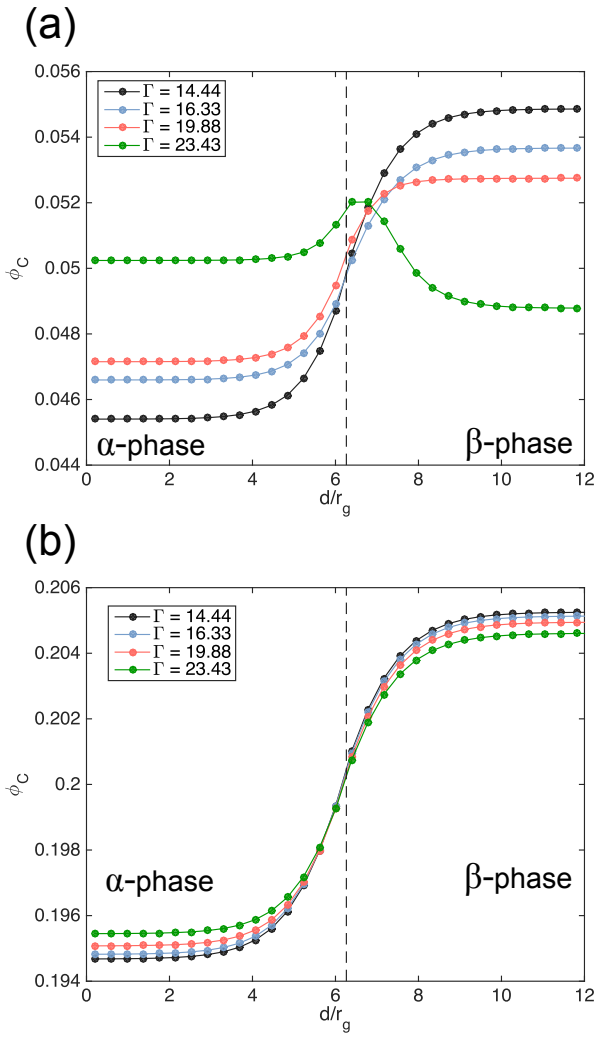

Figure 3.6. Distribution profile of salt C across $\alpha - \beta$ interface at $\phi_C = 0.05$ (a) and $\phi_C = 0.2$ (b), with $f_{q,A} = 0.05$, $f_{q,C} = 1, \chi_{AB}N = 3$. Selectivity switching is observed in (a). (b) exhibits selectivity for β-phase across all values of Γ.

correlation strengths for which salt ions prefer the charge-dilute phase. The underlying physical mechanisms are equal to the neutral solvent case: at low values of Γ, entropic effects dominate, while the behavior at high values of Γ is driven by ionic correlations. However, there are a few points of departure in the degree of selectivity, the direction of selectivity, and the degree of adsorption at the interface.

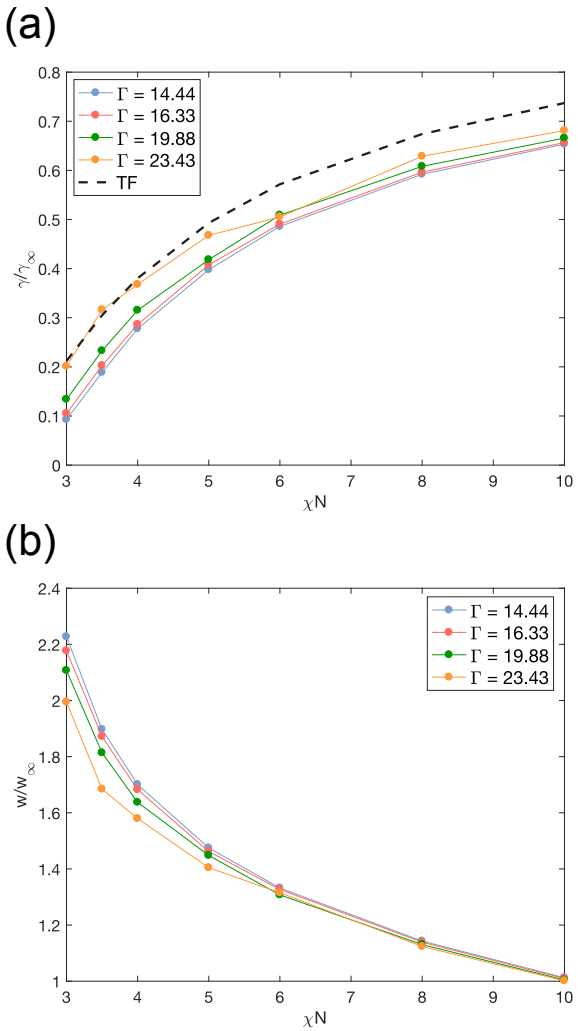

Figure 3.7. The normalized interfacial energy,γ/γ_∞(a) and normalized interfacial width (b) for varying values of Γ. The dashed line represents Tang and Freed predictions for the normalized interfacial energy. Here, $\phi_C = 0.05$.

At low values of Γ, the system tends toward maximizing counterion entropy. This is quantitatively shown in Figure 3.6(a). At $\Gamma = 14.44$, the salt strongly prefers the charge-dilute β-phase, with $\frac{|\phi_C^\alpha - \phi_C^\beta|}{\phi_{C,avg}} \approxeq 0.186$. This selectivity is a 26-fold increase compared to the selectivity of a neutral solvent at the same value of Γ. The increased selectivity is perhaps expected from what our primitive understanding of electrostatic interactions. A salt pair, which carries

charge, is expected to interact more strongly with the charged monomer on the backbone than does a neutral solvent. However, this expectation would lead us to presume that the salt should always reside in the charge-dense α-phase. In fact, we show here that while the degree of selectivity decreases with increasing Γ, the salt is overwhelmingly selective for the charge-dilute β-phase at $\Gamma < 23.43$. In a salt-containing blend, where the salt pair is allowed to between charge-dense and charge-dilute phases, counterion entropy is maximized when the salt resides away from the charge-dense phase. The swelling of salt into the charge-dilute phase allows for charge to be distributed across both phases, increasing the translational entropy of the counterions. When Γ is increased, the selectivity drops ($\frac{|\phi_C^\alpha - \phi_C^\beta|}{\phi_{C,avg}} \approxeq 0.154$ at $\Gamma = 16.33$; $\frac{|\phi_C^\alpha - \phi_C^\beta|}{\phi_{C,avg}} \approxeq 0.12$ at $\Gamma = 19.88$;) until it switches for $\Gamma = 23.43$. At this value, the salt pair is slightly selective for the charge-dense α-phase. The ionic correlations dominate, and the salt ions are brought into the α-phase to achieve charge ordering. The decrease in selectivity can be attributed to the high concentration of counterions which, as outlined above, decreases the effective strength of ionic correlations while enhancing the entropic effects. Salt adsorption at the interface is observed only at $\Gamma = 23.43$. We believe that interfacial adsorption of the minority component occurs across all parameters studied; however, in strongly selective cases, the adsorption peak is wiped out by the large difference between bulk phase concentrations.

The interfacial tension is decreased by the addition of salt, as shown in Figure 3.7(a). An increase in the effective repulsion between A and B components with the increase in Γ is reflected in the increased interfacial tension. However, this increase is relatively small compared to that observed in Figure 3.4(a); we attribute this to ion entropy dominating the behavior of salt. In the phase diagrams, we have seen that this results in screened out electrostatic interactions, effectively turning salt-containing blend into a neutral ternary blend. We see the same effects

in interfacial tension trend, where the change in normalized interfacial energy closely follows the approximate form given by Tang and Freed.[103] As a result, the normalized interfacial width shows a small decrease with increasing Γ. We find that these widths fall between the maximum and minimum widths achieved in the neutral solvent case.

At higher concentrations of salt, selectivity switching is not observed (Figure 3.6(b)). As discussed in Figure 3.5(c), entropic effects dominate in the salt-containing blends, especially when the salt concentration is not minimal. For this reason, the salt at this concentration strongly selects for the charge-dilute β-phase across all values of Γ.

This investigation has mostly focused on decoupling the effects of Γ from other effects on the selectivity of salts. We have thus assumed that the dielectric mismatch between the two phases is negligible, such as in blends of polystyrene and poly(styrene-*ran*-styrene sulfonate) (PS/P(S-SS)).[24,58] However, in salt-containing blends where the two immiscible phase have sufficiently different dielectric constants ($\Delta\epsilon_r > 2.5$), the solvation energy of the ion can significantly influence miscibility of the phases and solubility of the salts. Wang *et al* has shown that the solvation energy can effectively rescale the Flory-Huggins parameters.[22,105] In this study, we consider a simplified model of such cases, where the preferred solvation of salts by the charged polymer is reflected in χ_{AC} and χ_{BC} values ($\chi_{AC} < \chi_{BC}$). It is demonstrated in Figure 3.8 that electrostatic effects can completely alter the selectivity of the salts, inducing a selective swelling of the charge-dilute phase with the introduction of low Γ. At $\Gamma = 14.44$, the translational entropy of the mobile charges drives the salt into the charge-dilute phase to achieve a more uniform distribution of charges in the two phases. The increase in Γ to 23.43 condenses the salts back into the charge-dense phase, as expected.

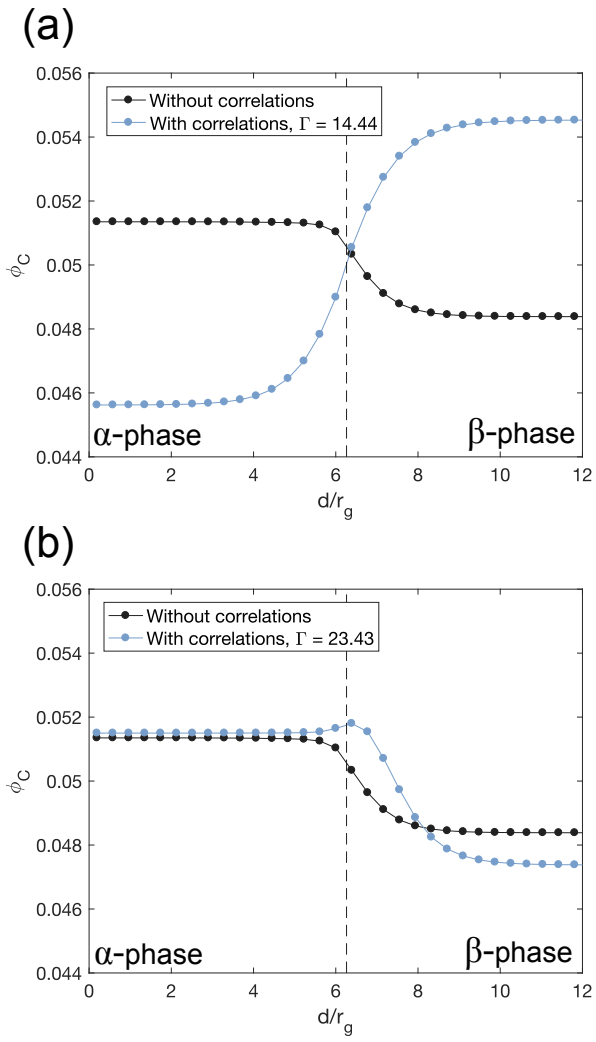

Figure 3.8. The effect of Γ on the distribution of salt that is inherently selective for the charge-dense α-phase before and after the effects of ionic correlations and translational entropy are added. Here, $f_{q,A} = 0.05, f_{q,C} = 1, \chi_{AB}N = 3.\chi_{BC} = \chi_{AB}, \chi_{AC} = 0, \Gamma = 14.44$ in (a) and $\Gamma = 23.43$ in (b). This shows that the ionic effects can significantly alter the Flory-Huggins type selectivity.

3.5. Conclusion

In this work, we have presented the equilibrium bulk and interfacial behavior of ternary charged polymer blends in strongly ionically correlated systems ($\Gamma \geq 14.44$), where A is a charged polymer with charge fraction $f_{q,A}$, B is a neutral polymer, and C is a neutral solvent

($f_{q,C} = 0$) or added salt ($f_{q,C} = 1$). It is demonstrated that an increase in Γ decreases the miscibility of blends. This is due to the ionic correlation effects, which are emphasized at higher charge fractions and can lead to the formation (in solvent-containing blends) and dissolution (in salt-containing blends) of ionic phases. For salt-containing blends, these charge effects can only be observed at low concentrations of salt, where entropic effects do not dominate. We have also shown that the inclusion of ionic correlations can lead to ionically induced selectivity in neutral, non-selective solvent and added salt, where the selectivity of the minority component can be tuned by changing the ionic correlation strength Γ. At low values of Γ, the selectivity is driven by the translational entropy of the counterions. At high values of Γ, the selectivity comes from ionic correlations, which favor the ordering of charges. These effects are further investigated by the calculation of interfacial tension and width, which deviate significantly from the trends expected in immiscible symmetric neutral blends. In salt-containing blends, the inclusion of ionic correlations allows the salt to be selective for the phase consisting of mostly neutral polymers. This has considerable advantage for designing polyelectrolytes with targeted salt selectivity. While this model can benefit from expanding to multi-component charge systems, this simple model provides an understanding of the competing mechanisms governing bulk and interfacial behavior, especially in polyelectrolyte blends with a small degree of dielectric constant mismatch.

CHAPTER 4

Phase behavior of ionomer blends with a dielectric mismatch

4.1. Abstract

We study the effects of dielectric mismatch on the miscibility of a charge-neutral polymer blend, where the charge-containing polymer has a higher dielectric constant and a very low charge fraction (below 0.1). Using a thermodynamic analysis coupled with liquid state theory that includes non-linear and many body effects (Debye-Hückel Extended Mean Spherical Approximation (DHEMSA) closure), we show that strong correlations between ions dominate the phase behavior at low dielectric mismatch ($\epsilon_A \approxeq \epsilon_B$). When the mismatch is high ($\epsilon_A >> \epsilon_B$), the miscibility of the blend is determined by solvation effects, where the preference of the ions to be solvated in a higher medium is balanced by the entropic driving force for a uniform distribution of dielectric constant throughout the system. In a binary blend with no added salt, the interplay between ionic correlations and solvation effects results in an initial decrease in miscibility followed by subsequent increase, especially for charge-rich blends. When salt is added as a third component, the effect of dielectric mismatch is significant only at low concentrations of salt. In addition, changes to the miscibility of the system due to solvation effects become dependent on the composition and dielectric constant of the blend. In regions with low charge concentration (low ϵ_r), increasing the mismatch enhances miscibility. In regions of high charge concentration (high ϵ_r), the blend becomes less miscible with increasing dielectric mismatch.

4.2. Introduction

Charge-containing polymer systems have found use in a wide range of applications from organic field-effect transistors (OFETs), actuators, fuel cell membranes, to energy storage devices.[79–83,92,106] It has been shown that charge can be a powerful tool in tuning the dielectric response, due to the multitude of complex interactions that occur in these systems, such as but not limited to Flory-Huggins interactions,[8] translational entropy of the ions, ionic correlations,[7,17,18,28,34,73,107] and solvation energy of free ions.[22,23,60,105,108] In particular, the introduction of a high dielectric constant polymer, such as poly(ethylene oxide) (PEO), into a block copolymer or a polymer blend allows for a design of attractive candidate materials, as polymers with high ϵ_r can dissolve large amounts of salt and thereby support high concentrations of charge carriers. Studies have shown that the combination of a high dielectric material with a low dielectric polymer can lead to nontrivial and unpredictable behaviors in the miscibility:[15,91,109] some theoretical studies have attributed this unusual behavior to the solvation effects, that can significantly alter the mixing thermodynamics of the blend;[22,23,60,105,108] other works have pointed to the role of ionic correlations as an important factor in determining the miscibility and phase separation in polymers that contain charge.[7,17,73,107]

Our goal in this work is to investigate the effects of dielectric mismatch on the interplay between solvation effects and ionic correlations in charge-containing polymer blends. Specifically, we want to identify regimes where ion-ion correlations dominate, solvation effects dominate, and regimes where both effects must be properly accounted for. In order to do so, we investigate electrostatic effects in a system when 1) one of the polymers contains charge and 2) there is a dielectric mismatch between the two polymers, $\epsilon_A \neq \epsilon_B$. This results in a composition-dependent dielectric constant $\epsilon_r(\phi)$ and a composition-dependent ionic correlation strength $\Gamma(\phi)$.

In order to find the effect of dielectric mismatch on mixing thermodynamics, we build upon a Flory-Huggins type model to include contributions from ionic correlations and solvation effects that arise from a dielectric mismatch.[7,8,18,28,105] Our primary system consists of a binary blend of a charged polymer (A) and a neutral polymer (B) with dielectric mismatch $\Delta\epsilon = \epsilon_A - \epsilon_B$. For the purpose of this work, we only consider cases where $\Delta\epsilon > 0$; that is, the charged polymer can always solvate ions more easily than the neutral polymer. The charge-containing polymer has a tunable charge fraction f_q along its backbone. This charge fraction is varied between 0 and 0.1 to maintain a low concentration of charge, which is later shown to play an important role in eliciting specific phenomena in strongly correlated systems. With these contributions, the total free energy of mixing can be written as:

(4.1)

$$f_{tot}(\phi_k, N_k, \chi_{kl}, f_{q,k}, a_m, \Gamma_{mn}) = f_{FH}(\phi_k, N_k, \chi_{kl}) + f_{PM}(\phi_k, f_{q,k}, a_m, \Gamma_{mn}) + f_{Born}(\phi_k, \Delta\epsilon)$$

where the Flory-Huggins contribution f_{FH}, ionic correlations and translational entropy of the ions f_{PM}, and solvation effects f_{Born} are given by the following equations:

(4.2)

$$f_{FH}(\phi_k, N_k, \chi_{kl}) = \frac{\phi_A ln\phi_A}{N_A} + \frac{\phi_B ln\phi_B}{N_B} + \chi_{AB}\phi_A\phi_B$$

(4.3)

$$f_{PM}(\phi_k, f_{q,k}, a_m, \Gamma_{mn}) = f_{q,A}\phi_A ln(f_{q,A}\phi_A) + f_{exc}(f_{q,A}\phi_A, \Gamma(\phi_A))$$

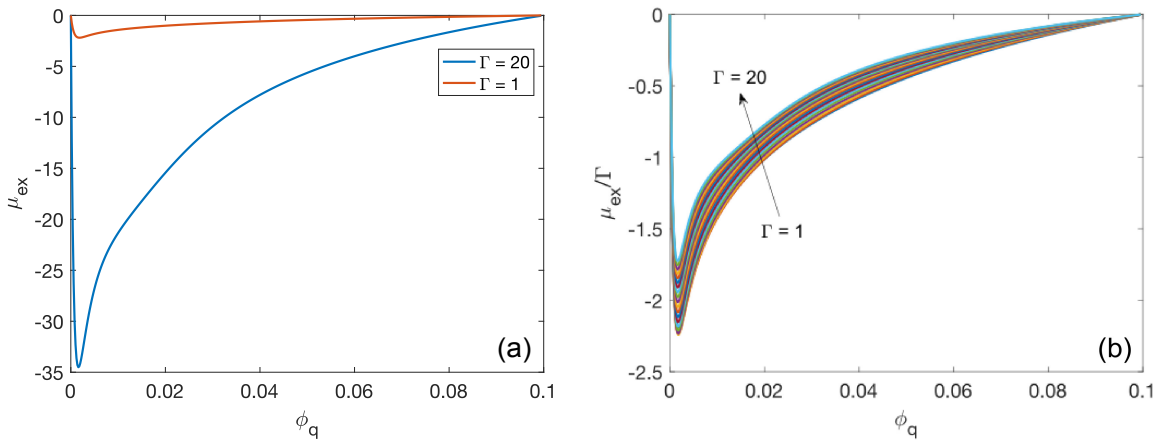

Figure 4.1. (a) Chemical potential contribution from ionic correlations as a function of charge concentration. Chemical potential is normalized by Γ (b) for ease of viewing. Note that the dip in chemical potential well is found at ϕ_q 0.002, which indicates that the effects of ionic correlations are especially dominant at low charge concentrations.

$$f_{Born}(\phi_k, \epsilon_r) = \frac{z^2 e^2}{8\pi\epsilon_0\epsilon_r(\phi_A)a_m} \tag{4.4}$$

The contribution from ionic correlations are calculated using the liquid state theory with Debye-Hückel Extended Mean Spherical Approximation (DHEMSA) closure on the Ornstein-Zernike equation.[7,18,28,110] When the dielectric mismatch between the two polymers is small, the medium can be effectively considered as homogeneous with a uniform distribution of dielectric constant. This assumption is valid for many charge-containing polymers such as polystyrene-block-poly(styrene sulfonate), where a small degree of sulfonation is not expected to appreciably change the dielectric constant. In these cases, it is important to note that effects due to ionic correlations are particularly significant at dilute concentrations of charge. Previous studies have

found a chimney-type phase segregation in systems with $\Gamma \approxeq 16$ at $f_q \approxeq 0.15$ where the composition difference between coexisting phases is very small ($\Delta\phi < 0.1$)[7,107,110] It is important to note that this is characteristic of weakly charged systems, due to a steep dip in the chemical potential found at small concentrations of charge. The chemical potential contribution from ionic correlations is plotted in Figure 4.1(a), with the normalized chemical potential plotted as a function of charge concentration in Figure 4.1(b). The dip is found at charge fraction $\phi_q = 0.002$. If the charge fraction is increased, the effect due to ionic correlations is significantly reduced, as an increased charge concentration moves the system out of the chemical potential dip. Therefore, at higher values of charge fraction, the chimney-type phase separation can no longer be accessed. It is important to make the distinction that even when the system moves out of the chemical potential dip, the effects of ionic correlations do not disappear (note that μ_{ex} scales with Γ in Figure 4.1(a)). However, this may explain why the chimney-type phase segregation is only accessible at low charge concentrations in systems with no dielectric mismatch.

However, when the dielectric constant of two polymers is large, solvation effects need to be considered in order to accurately describe the mixing thermodynamics. Furthermore, the addition of salt ions can significantly change the dielectric constant of the medium,[111] necessitating the inclusion of a composition-dependent dielectric constant of the medium, $\epsilon_r(\phi)$. In this work, the mixing rule takes the form of:[23,105]

$$\epsilon_r(\phi) = \epsilon_A\phi_A + \epsilon_B\phi_B \tag{4.5}$$

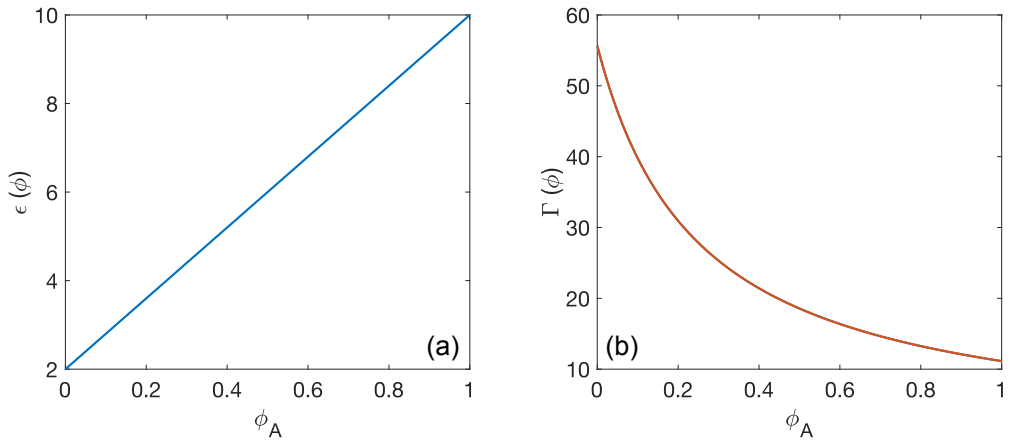

Figure 4.2. Dependence of $\Gamma(\phi_A)$ (a) and $\epsilon_r(\phi_A)$ (b) for a system where $\epsilon_A = 10$, $\epsilon_B = 2$.

Because the dielectric constant is a function of composition, both ionic correlations and solvation effects must be written as a function of composition ϕ_A:

$$\Gamma(\phi) = \frac{q_+ q_- e^2}{8\pi\epsilon_0 kTa\epsilon_r(\phi)} \tag{4.6}$$

The dependence of ϵ and Γ on the blend composition is shown in Figure 4.2. This means that, unlike the cases where a fixed concentration of salt is added into a polymer blend, charge concentration is proportional to the concentration of polymer A. As a result, forming a phase rich in polymer A may be advantageous in increasing the dielectric constant within the phase, but entropically unfavorable as it increases the amount of ions confined in the phase.

4.3. Results and discussion

4.3.1. Born Solvation and the effect of dielectric mismatch

With these factors in mind, we investigate the criticality of a charge-containing binary blend where $\Delta\epsilon$ is slowly increased. Results are summarized in Figure 4.3 for values of $\epsilon_B =$

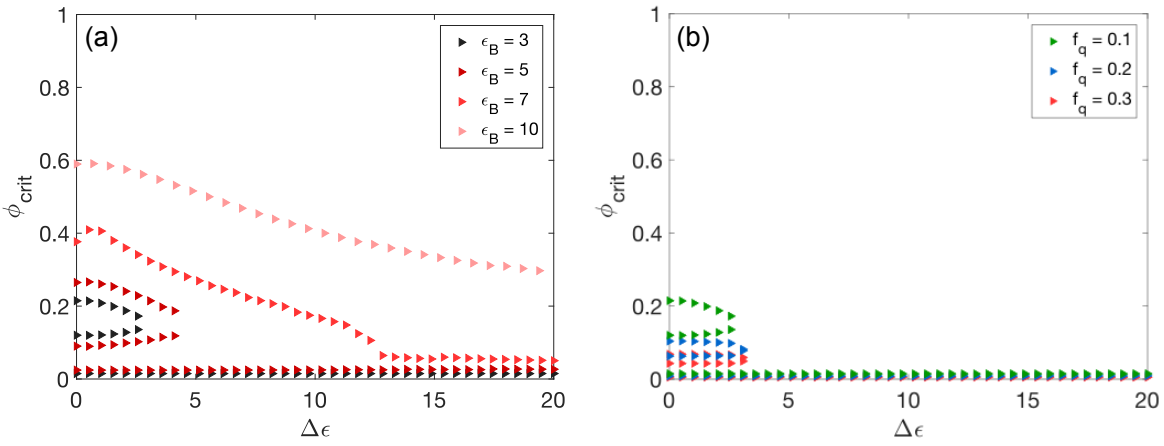

Figure 4.3. (a)Evolution of the critical point as dielectric mismatch, $\Delta\epsilon$ increases. Multiple critical points are observed for $\epsilon_B = 3, 5$ at low dielectric mismatch but only one critical point is observed for $\epsilon_B = 7, 10$. Critical points for $\Delta\epsilon < 5$ correspond to correlation-induced multiple criticality seen in Ref.[7](b) As charge fraction f_q increases, critical points due to ionic correlations disappear as the charge fraction increases, indicating the disappearance of the "chimney" type region.

$3, 5, 7, 10$ and $\Delta\epsilon = 0 - 20$. Here, ϵ_A is always larger than ϵ_B, and charge fraction f_q is kept at 0.1. As shown in Figure 4.3, the location of the critical point(s) is determined by both the absolute value of the dielectric constants ϵ_A and ϵ_B and the dielectric mismatch $\Delta\epsilon$. When ϵ_A and ϵ_B are both low, the behavior of the system is dominated by ionic correlations, whose strength Γ is inversely proportional to the dielectric constant of the system $\epsilon(\phi)$. Multiple critical points are found, and their locations correspond to the critical points previously found in highly correlated systems exhibiting a chimney.[7] When both ϵ_A and ϵ_B are high (and $\Delta\epsilon$ is small), ion entropy dominates the behavior of the system, and only one critical point is found. This critical point is located at $\phi_A \approxeq 0.6$, which is typical of weakly correlated systems.[7,17] When $\Delta\epsilon$ is large ($\epsilon_A >> \epsilon_B$), the critical point moves to a lower value of ϕ_A. In these systems, Born solvation drives the phase behavior. It is important to note that at high charge fractions

seen in Figure 4.3(b), the critical points that emerge from the chimney-type phenomena due to ionic correlations disappear. This result is consistent with our observations in Figure 4.1, where an increase in charge fraction moves the system away from the chemical potential dip. It is also consistent with a previous study,[7] where the emergence of chimney-type phase separation was seen at moderate values of Γ at low charge fraction $f_q = 0.2$. As the charge concentration is increased, the system moves away from the dip. At high values of charge concentration, the blend is strongly segregated, and coexistence is found between two almost-pure phases. This type of phase separation is driven by ionic correlations and other related electrostatic effects, but is observed to be different from a chimney-type phase separation, where the two coexisting phases are both dilute in charge.[7,110]

Having established regimes where ionic correlations or solvation effects dominate, we calculate and plot the phase boundaries in Figure 4.4, where $f_q = 0.07$. Gray lines denote the phase boundary for $\Delta\epsilon = 0$, for the selected values of ϵ_A and ϵ_B. As seen in Figures 4.4 (a),(b), and (c), when $\Delta\epsilon = 0$, the system is driven by ion-ion correlations alone when $\Delta\epsilon = 0$. The increase in ϵ_A and ϵ_B results in increased miscibility, as ionic correlation strength Γ is inversely proportional to ϵ_r: $\Gamma = \frac{q_+ q_- e^2}{8\pi\epsilon_0 kTa\epsilon_r}$. In weakly correlated charged systems, where ϵ_A and ϵ_B are high, ion entropy causes the system to become more miscible.[7]

When $\Delta\epsilon$ is increased, the blend exhibits re-entrant miscibility, where the miscibility is initially seen decrease before increasing. This behavior is found across all values of ϵ_B. The details of the trend are more obvious in Figure 4.4(c), where we plot the effect of $\Delta\epsilon$ on the phase behavior of a blend with $\epsilon_B = 7$. The switch in trend occurs at $\Delta\epsilon \approx 5$. That is, for $\Delta\epsilon < 5$, an increase in dielectric mismatch decreases miscibility, and critical χN moves to a lower value. At $\Delta\epsilon = 5$, phase separation can be found at $\chi N = 0$. For $\Delta\epsilon > 5$, increasing ϵ_A

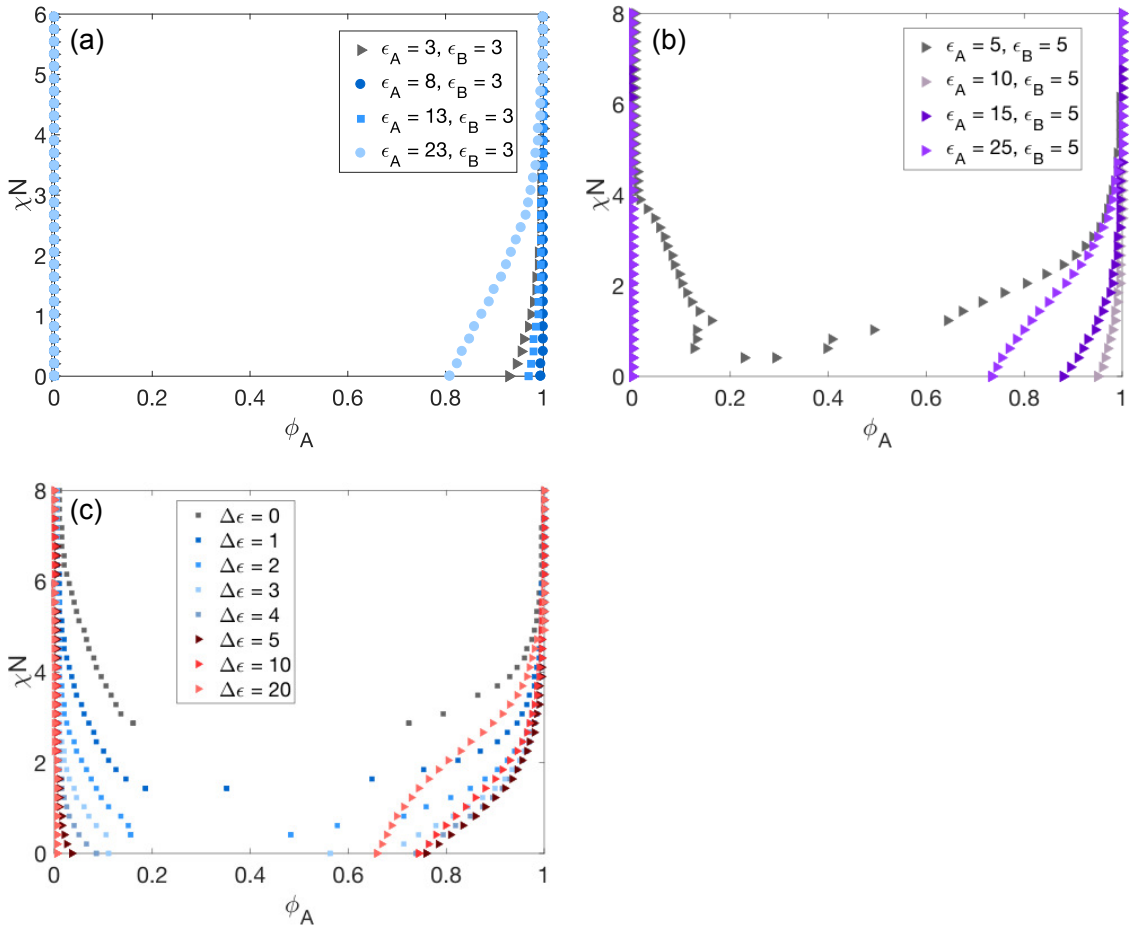

Figure 4.4. Phase diagram of binary blends where ϵ_B of the neutral polymer varies from 3 (a), 5 (b), 7 (c). ϵ_A of the charge-containing polymer is increased to increase dielectric mismatch. For all of the phase diagrams, we see that the degree of phase separation increases with small increases in dielectric constant, but decreases when the mismatch is increased further.

enhances miscibility, and the chimney becomes significantly narrower and shifts to a lower ϕ_A, especially in regions of rich ϕ_A. However, even at these values, the charge concentration is less than 0.1 by volume.

The contributions to the free energy of mixing from ionic correlations (f_{exc}) and Born solvation (f_{solv}) are compared in Figure 4.5. These curves show that re-entrant behavior arises

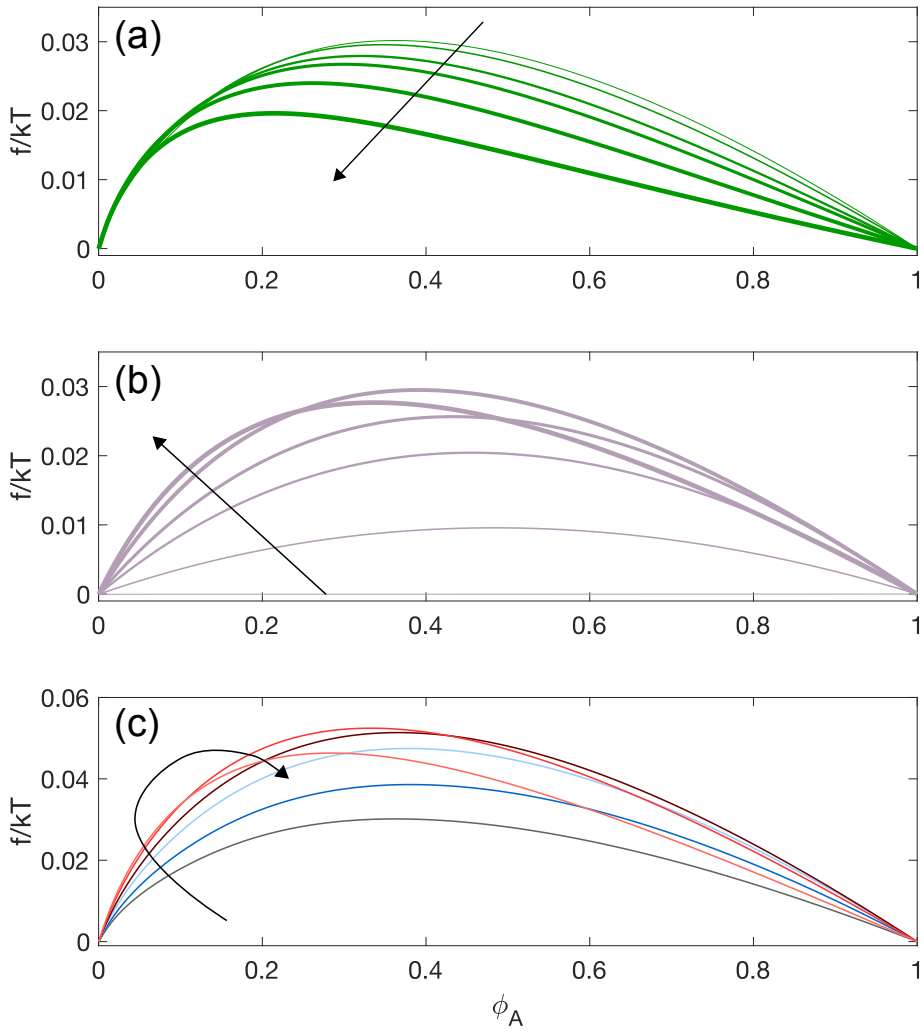

Figure 4.5. Free energy of mixing contributions from f_{exc} (a), f_{solv} (b), and $f_{exc}+f_{solv}$ (c) with increasing dielectric mismatch when $\epsilon_B = 7$. Arrows indicate increasing $\Delta\epsilon$. Free energy excess decreases with increased dielectric mismatch, but Born solvation (b) shows a non-monotonic trend. This results in an increased phase separation followed by a decrease in phase separation.

from the composition-dependent nature of solvation energy. f_{exc} (Figure 4.5(a)) decreases as ϵ_A is increased, as Γ is inversely proportional to ϵ_A. For ionic correlations, the absolute value of

ϵ_A is important, not the magnitude of $\Delta\epsilon$. For solvation effects, the increase in $\Delta\epsilon$ is significant in increasing the energy of mixing. As the mismatch increases, the ions have a stronger preference to be solvated in the higher dielectric medium. This causes phase segregation, so that a phase with a higher dielectric constant is achieved. However, as $\Delta\epsilon$ is further increased, the energy of mixing decreases; this is because while phase separation allows the system to form a phase with a higher ϵ_r, it also concentrates ions in that particular phase. It therefore becomes entropically unfavorable to obtain phase separation. This results in a subsequent change in the curvature of the free energy curve, where the energy of mixing in f_{solv} increases at low polymer content but decreases at high polymer content. This effect explains the non-monotonic trend in the free energy of mixing (Figure 4.5 (c)), where an increase in dielectric mismatch initially suppresses and subsequently enhances miscibility. It also accounts for the shift in the critical point– and chimney– of the system to a lower ϕ_A.

4.3.2. Behavior of charge-containing polymers in high dielectric media

In order to investigate systems with a large dielectric mismatch (i.e. those containing a high dielectric solvent), we extend our analysis to three component systems, where one of the components is a solvent with a high dielectric constant. For this analysis, we limit ourselves to spinodals in order to study qualitative trends. Figure 4.6 shows the effect of increasing the dielectric constant ϵ_C of the solvent in a ternary system with $\epsilon_A = 7.2, \epsilon_B = 3.2$ (a) and $\epsilon_A = 7.2, \epsilon_B = 7$ (b), which correspond to high and low dielectric mismatch cases, respectively. Polymer A is charged at $f_q = 0.1$ while polymer B is neutral.

In both cases, the increase in solvent dielectric constant increases miscibility. For a polymer blend with a higher $\Delta\epsilon$ between the two polymers ($\Delta\epsilon \approx 4$), the changes in miscibility upon

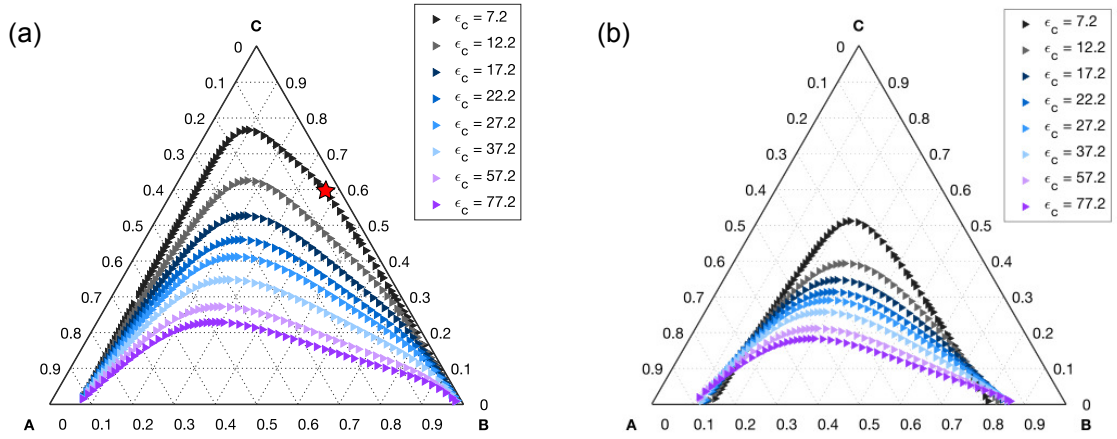

Figure 4.6. Calculated spinodals of a ternary system of charge-containing polymer A, neutral polymer B, and high dielectric solvent C, where $\epsilon_A = 7.2$ and $\epsilon_B = 3.2$ (a) and $\epsilon_B = 7$ (b). Solvent dielectric constant has a greater effect when the $\Delta\epsilon$ is greater.

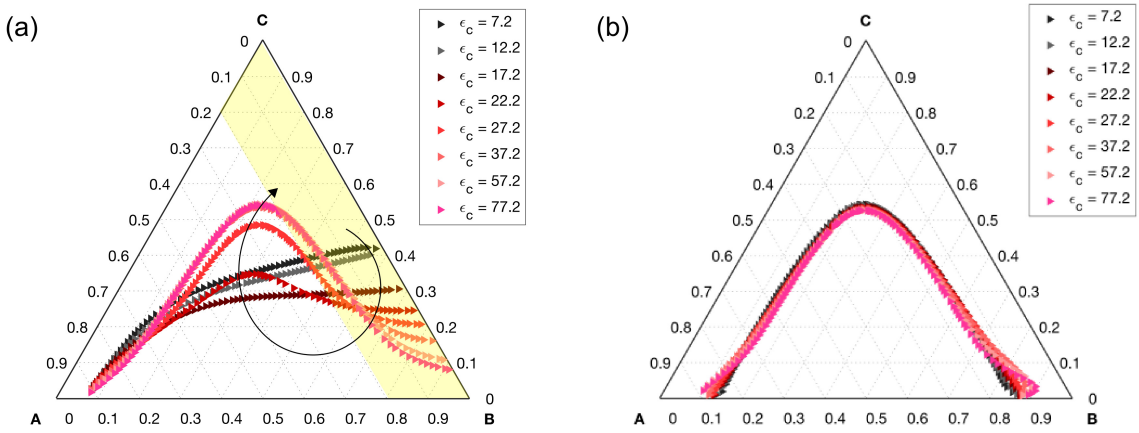

Figure 4.7. Calculated spinodals of a ternary system consisting of charge-containing polymer (A, $\epsilon_A = 7.2$), neutral polymer B ($\epsilon_B = 3.2$ in (a) and $\epsilon_B = 7$ in (b)) and salt C. Spinodals in high $\Delta\epsilon$ case (a) show that one of the coexisting phases consists of B+C with no A.

solvent addition is far more dramatic. It is important to note that the increase in solvent dielectric constant causes the disappearance of the chimney (marked with a star) in Figure 4.6(a). Even with the disappearance of the chimney, the spinodals remain wide, indicating that phase

separation occurs between two almost pure phases. This is in contrast to low dielectric mismatch case (Figure 4.6(b)), where the two coexisting phases occur at less pure concentrations of each polymer. When $\epsilon_A \cong \epsilon_B$, the dielectric constant of the solvent has a reduced effect on the overall phase behavior, as seen in the closeness of the spinodal lines. Overall, the increase in ϵ_C reduces blend miscibility. However, at dilute solvent concentrations ($\phi_C < 0.05$), increasing ϵ_C decreases the miscibility of the polymer bend. When there is little solvent, it is favorable to phase separate by incorporating the solvent into the charge dense phase (A) and increase the solvation of the ions. However, at higher concentrations of solvent $\phi_C > 0.05$, this becomes entropically unfavorable to concentrate the solvent in one phase.

Past theoretical studies have focused on the role of salt on the phase behavior of polymer blends with a dielectric mismatch,[18,105] finding that small amounts of salt can shift the phase boundaries vertically by changing the effective χN. Here, we extend the study to include the effect of salt concentration on the dielectric constant of the media.

Figure 4.7 shows the role of salt on the spinodal lines of a ternary blend with a high dielectric mismatch (Figure 4.7a) and a low dielectric mismatch (Figure 4.7(b)). Here, we treat salt as a tertiary component that can change the dielectric constant of the media using the following mixing rule: $\epsilon(\phi) = \epsilon_A\phi_A + \epsilon_B\phi_B + \epsilon_C\phi_C$.

When the dielectric mismatch in the polymer is high ($\Delta\epsilon = \epsilon_A - \epsilon_B = 4$), the increase in ϵ_C leads to a re-entrant behavior, where the miscibility is initially observed to increase and then decrease. This change is more dramatic in the charge-dilute region (low concentrations of ϕ_A), as highlighted in Figure 4.7(a). The addition of salt at $\epsilon_C \approx \epsilon_A$ causes phase separation into two phases where one of the phases is pure in B ($\phi_A = 0$). Here, salt can selectively swell into pure B phase to achieve a uniform distribution of dielectric constant across two phases. The resultant

uniform distribution of ions also makes it entropically favorable to phase separate into a phase rich in A and a phase containing B and C. As ϵ_C increases, it becomes more favorable for the salt to form its own high ϵ_r phase instead of absorbing into the B phase (as indicated by the arrow in Figure 4.7(a)). The movement of the spinodal is dramatic in the region of the diagram dominated by the low dielectric polymer as this dielectric constant drives the thermodynamics of mixing.

When the dielectric constants of the two polymer are similar (Figure 4.7(b)), increasing the dielectric constant of the salt has minimal effect, and all spinodals collapse onto a single spinodal line that is symmetric. This indicates that the salt might be forming its own phase, and that the phase behavior of the blend is unaffected by the solvation of the salt, except at very low concentrations of salt. At these concentrations ($\phi_C < 0.05$), an increase in the dielectric constant leads to decreased miscibility, which is similar to that found in the solvent-containing case (Figure 4.6).

4.3.3. Inclusion of salt in a neutral polymer blend with dielectric mismatch

In the last section of this work, we extend calculations to a salt-containing blend of neutral polymers, where the dielectric constant of the two polymers are 7.5 and 4, respectively. This allows for a comparison of our work with experimental studies of salt-doped polymer blends and block copolymers,[15,112] where the solvation energy is shown to increase effective χ and substantially decrease the miscibility of the system. Theoretical calculations have qualitatively predicted these results by calculating the phase behavior of a pseudo-binary system, where the amount of salt added is negligible and does not take up appreciable volume within the

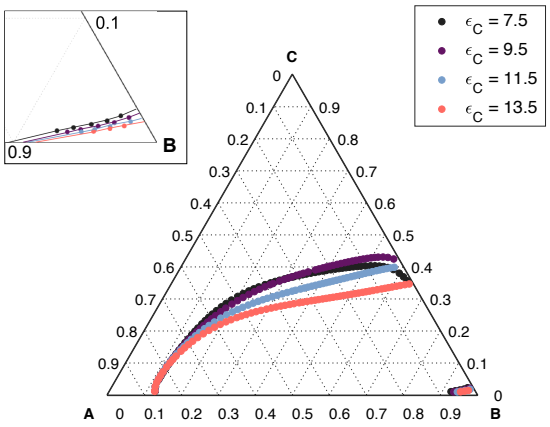

Figure 4.8. Calculated spinodals of a ternary system consisting of two neutral polymers (A, $\epsilon_A = 7.5$), neutral polymer B ($\epsilon_B = 4$ and salt with varying dielectric constant. Inset shows decreased miscibility in regions with low salt concentration.

system.[105,113] Here, we treat salt as a tertiary component, the addition of which can change the dielectric constant of the system.

Figure 4.8 shows the calculated spinodals of a salt-doped neutral polymer blend, where ϵ_r of the polymers A and B are 7.5 and 4, respectively. The dielectric contribution from the salt is varied between $\epsilon_C = 7.5$ to $\epsilon_C = 13.5$. We find that the inclusion of salt into a neutral blend with a dielectric mismatch leads to spinodal lines that grounded along the B-C axis. For this type of presumed phase segregation, it is difficult to calculate the coexistence curves; however, we believe that the shape of the spinodals is indicative of a B-C type phase separation (rather than the A-B type phase separation found in blends with charged polymers). In such a case, the two coexisting phases will contain substantially different concentrations of salt, indicating salt partitioning even in blends with dilute amounts of A. This is consistent with experimental studies of blends of polystyrene and poly(ethylene-oxide), where the inclusion of solvation effects is thought to lead to salt partitioning in these blends.

4.4. Conclusion

In this work, we show that the dielectric mismatch between charge-containing and neutral polymers has far-reaching effects on the phase behavior. In binary charge-containing blends, dielectric mismatch necessitates a composition-dependent dielectric constant $\epsilon(\phi)$ and ionic correlation strength $\Gamma(\phi)$. When ϵ_A and ϵ_B are both low, multiple criticality of the blend is dominated by ionic correlations. Very low concentrations of charge allow access to a chimney-type phase separation, where the composition difference between the two coexisting phases is small. When ϵ_A and ϵ_B are both high, the criticality can be described by ion entropy. When the dielectric mismatch is substantial ($\epsilon_A > \epsilon_B$), the competition between solvation energy and ionic correlations leads to a shift of the critical point to a lower ϕ_A and re-entrant behavior in the miscibility, where the increase in $\Delta\epsilon$ initially induces decreased miscibility followed by increased miscibility. For charge-containing blends in neutral high dielectric media, where the dielectric mismatch can be as large as 70, inclusion of media with a higher dielectric constant always leads to decreased miscibility. The solvent effect is greater for polymer blends with a greater dielectric mismatch and subdued for polymers that have negligible difference in the dielectric mismatch. On the other hand, increasing the dielectric mismatch in a polymer blend with a high dielectric mismatch by introducing salt can induce re-entrant behavior similar to one found in binary blends. In such a case, salt induces a strong segregation in blends with a symmetric composition but increases miscibility in blends with a low concentration of charged polymer. In systems with a low dielectric mismatch, the introduction of salt decreases miscibility but only at very low concentrations. For salt-doped neutral polymer blends, the dielectric

mismatch is believed to lead to a qualitatively different B-C segregation, where salt partitioning occurs in blends containing dilute concentrations of the high dielectric polymer, which is consistent with salt partitioning seen in experimental systems.[15]

We have assumed in this study that the dielectric constant of the medium is linearly dependent: $\epsilon(\phi) = \epsilon_A\phi_A + \epsilon_B\phi_B + \epsilon_C\phi_C$. In real systems, the mixing rule may deviate from this approximation; however, studies have shown that qualitative observations are still applicable across different functional forms.[23,105]

CHAPTER 5

Adsorption of polystyrene-*b*-quaternized poly(2-vinylpyridine) at oil-water interface

5.1. Abstract

Understanding the role of charge interactions in the self-assembly of ion-containing block copolymers continues to be a challenge, especially in systems such as partially quaternized polystyrene-block-poly(2-vinylpyridine) (PS-Q2VP) where multiple factors, such as ionic correlations, ion solvation, and Flory-Huggins interactions, are at play. Here, we present the results of an experiments-based approach to investigate the effect of charge interactions on the interfacial activity of PS-Q2VP diblock copolymers. We characterize interfacial activity of PS-Q2VP via a combination of pendant drop measurements and Langmuir-Blodgett measurements and demonstrate that charge interactions can be a powerful tool in controlling the interfacial adsorption and self-assembly of PS-Q2VP block copolymers, especially at liquid-liquid interfaces where the two liquid phases have a significantly large dielectric mismatch. We also perform preliminary Molecular Dynamics (MD) simulations to probe the structure of these polymer chains at the interface and within the chloroform phase. These results represent a promising model system for understanding and utilizing the role of charge interactions on the phase behavior of block ionomers using simulations and experiments. At the end of the chapter, we include a section on the interfacial tension-induced cylinder-to-sphere transition in diblock copolymers

of poly(ethylene)glycol-*bl*-poly(propylene sulfide), which was a collaborative project with Professor Evan Scott's group. While this particular section deals with a different block copolymer where the tunable parameter is oxidation of the chemical backbone, we have included this section to highlight the importance of interfacial tension in determining the micellar morphology of block copolymers. We believe that a connection can be made to micellar morphology of block ionomers, as charge can substantially change the interfacial tension– and subsequently– the micellar morphology of block ionomers of PS-*b*-Q2VP.

5.2. Introduction

Charge-containing diblock copolymers have been studied extensively for practical applications that range from fuel cells and membranes to solid polymer electrolytes for batteries.[79–83] It is understood that the property and performance of these devices are heavily dependent on the equilibrium morphology and phase behavior of the polymeric material. The morphological properties of block ionomers and ionomer blends have been explored extensively using a combination of simulations- and experiments- based approaches, with the goal of elucidating the effect of ions on the macromolecular assembly of polymer chains and the aggregation of ionic clusters.[114–117] Other attempts have explored the use of a tertiary component, in the form of small molecule plasticizers, room temperature ionic liquids (RTIL), other polymers, and salts, to induce changes in the miscibility, enhance the mechanical integrity, and to improve the performance of electrolytes within these charge-containing systems.[?,15,84–87,89–91,107] Findings have shown that the inclusion of charge can lead to non-trivial changes in the mixing thermodynamics and polymer morphology, such as the evolution of inverted phases,[14,118] ion-dependent miscibility of ion-conducting block copolymers,[106] and partitioning of salt in charge-neutral

blends.[15] Theoretical developments have been likewise remarkable, and have identified the effects of ion-ion correlations,[7,18,28,107,110] solvation energy of ions,,[22,60,105] and translational entropy of ions as significant influences on determining the mixing thermodynamics of charge-containing block copolymers and blends. Most recently, a theoretical study has shown that the relative importance of these competitive effects can be tuned in a single system by considering the dielectric mismatch $\Delta\epsilon_r$ between the polymeric components, where a system with a low dielectric mismatch $\Delta\epsilon$ is dominated by ion-ion correlations while a system exhibiting a high dielectric mismatch $\Delta\epsilon$ is governed by ion solvation.[119] However, an experimental confirmation of these interconnected effects remains a challenge, due to the fact that a single experimental system only allows us to access a very small range of behaviors predicted by theories. For example, block copolymers and blends of polystyrene (PS) and poly(ethylene-oxide) (PEO) are popular for use as solid polymer electrolytes,[15] but the dielectric mismatch between PS and PEO is non-negligible, and many experimental results have been explained using solvation energy. At the other extreme, systems containing polystyrene (PS) and sulfonated polystyrene (SPS) have a small dielectric mismatch, but the regions where inverted morphologies are expected are not accessible due to the glass transition temperature (T_g). In this work, quaternized block copolymers of poly(styrene)-block-poly(2-vinylpyridine) (PS-*b*-P2VP) is used for experimental confirmation of charge effects. PS-PVP block copolymers (both P2VP and P4VP version) have been extensively studied in literature. The two blocks can be easily and controllably synthesized. Furthermore, the PVP block can be selectively quaternized, allowing us to controllably change the charge fraction along the backbone without relying on pH-dependent dissociation. Previous research on PS-PVP has shown that the micellar self-assembly of these block copolymers is dependent on the quaternizing agent,[120] the selection of solvent or ionic liquid,[121–123]

and the block length and hydrophilicity of each block.[124] Several works to date have employed modification of the PVP block to charge into the backbone, noting that this makes the block copolymer extremely sensitive to water, unlike the unmodified versions.[118] This work aims to take research in this area further, by demonstrating the effect of charge fraction on the self-assembly of PS-*b*-QVP in the bulk and at the oil-water interface, and correlating our findings to theoretical analysis. To date, this is the only work that looks at the self-assembly of these block copolymers as a function of charge fraction. Furthermore, the similarity between PS and PVP monomers makes this work extremely conducive to comparison with theoretical models.

5.3. Methods

5.3.1. Materials

The block copolymer used for this study was a diblock copolymer of polystyrene-*block*-poly(2-vinylpyridine) (PS-P2VP) with molecular weight of 20210 (g/mol) for the PS block and 4220 (g/mol) for the P2VP block and an overall polydispersity index of 1.06. The degree of polymerization is 194 for the PS block, and 40 for the P2VP block. These polymers were synthesized via anionic polymerization by Professor Kenneth R. Shull. The molecular weights and polydispersity of the precursor PS block and the final diblock copolymer were confirmed via GPC to ensure that no degradation occurred between synthesis and quaternization.

5.3.1.1. Quaternized PS-b-P2VP. PS_{194}-*b*-$P2VP_{40}$ were quaternized at various quaternization ratios. Quaternized diblock copolymers are noted by PS-*b*-QVPx*yy*, where *yy* is the mole percent of P2VP block that has been quaternized. First, PS_{194}-*b*-$P2VP_{40}$ were dissolved in DMF (Sigma-Aldrich) at 7 weight %. Ethyl bromide (EtBr, Sigma-Aldrich) of calculated amounts were added to achieve target quaternization ratios. The reaction, shown in Figure 5.1, was left

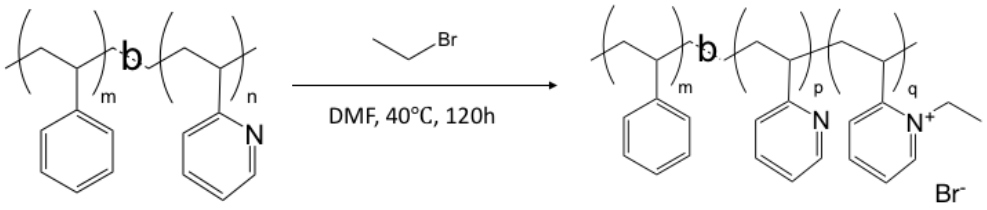

Figure 5.1. Quaternization of PS_{194}-*b*-$P2VP_{40}$ using EtBr.

Polymer	Molecular Weight (kg/mol)			f_q	$W_{QVP}/W_{PS\text{-}b\text{-}QVP}$
	Diblock	PS	QVP		
PS-*b*-QVPx0	24.43	20.21	4.22	0	0.173
PS-*b*-QVPx4	24.46	20.21	4.25	0.04	0.174
PS-*b*-QVPx5	24.47	20.21	4.26	0.05	0.174
PS-*b*-QVPx11	24.54	20.21	4.33	0.11	0.176
PS-*b*-QVPx37	24.86	20.21	4.65	0.37	0.187
PS-*b*-QVPx39	24.87	20.21	4.66	0.39	0.187

Table 5.1. Quaternized versions of PS_{194}-*b*-$P2VP_{40}$. Only PS-*b*-QVPx0, 4, 11, and 37 are used for this study.

to proceed at $40°$C for 120 hours and precipitated out into cold Diethyl Ether (Fisher Scientific) at 1:10 volume ratio. The precipitates were decanted and dried in the vacuum oven at 762 Torr for 8 hours, and dialyzed against deionized water for 4 days, with the external solution replaced every 24 h. Purified product was dried and characterized via H^1-NMR, with spectra obtained from a Bruker Avance III 500 MHz system, Ag500. NMR spectra for samples prior to and after quaternization are shown in Figure 5.2. Degree of quaternization can be determined by the area of peaks at 9.2 ppm, which correspond to the shifts phenolic H in the QVP block due to quaternization. The top spectrum corresponds to 37.4% quaternization of the P2VP block.

Samples quaternized are summarized in Table 5.1.

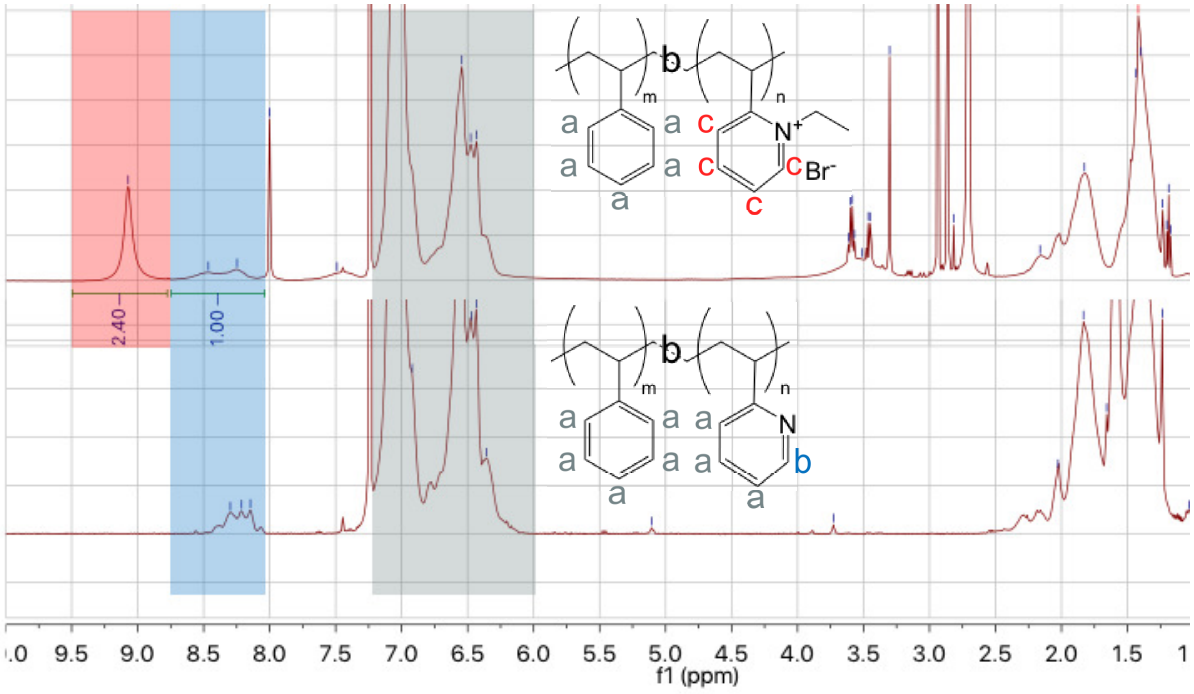

Figure 5.2. H^1-NMR spectra of PS-*b*-QVPx0 (bottom) and PS-*b*-QVPx37 (top).

5.3.2. Interfacial Measurements

5.3.2.1. Drop Shape Apparatus. Interfacial tension γ of PS-*b*-QVP samples at the chloroform-water interface was measured at room temperature using the bubble drop method, with chloroform (HPLC grade, Fisher, as received) as the embedding phase and Milli-Q water (resistance of 18.2 MΩcm) as the bubble phase. Polymer solutions were prepared at 2 mg/mL in chloroform. Experiments were run inside a glass cuvette (12.5 mm by 22.5 mm by 48 mm) filled with approximately 10 mL of chloroform. By using a U-shaped needle, a bubble of water of approximately 4 μL was created, as shown in Figure 5.3. A Kruss DSA100 drop shape analyzer was utilized to give γ. The water bubble was left to equilibrate with the chloroform phase for 15 minutes to obtain the baseline interfacial tension of $\approx 32.8 mN/m$, which corresponds

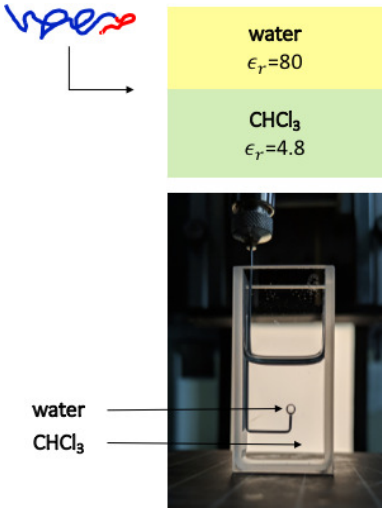

Figure 5.3. Schematic and photograph of the set-up. The two liquid phases have dielectric constants of 80 and 4.8 respectively, which will affect the interfacial adsorption of the block ionomer.

to the interfacial tension between water and chloroform at room temperature. At 15 minutes, $\approx 0.35mL$ of the polymer solution were injected into the embedding phase.

Between runs, the cuvette was thoroughly washed with acetone, ethanol, dichloroethane, and chloroform. Syringe and needle were washed with acetone, ethanol, and Milli-Q water.

5.3.2.2. Langmuir-Blodgett trough. The surface pressure of PS-*b*-QVP samples at the air-water interface was measured at room temperature using a Langmuir-Blodgett (LB) trough (Nima Technology, model 116). Surface pressure Π was monitored using a tensiometer attached to a Wilhemy plate. In a typical experiment, 50 μL of a 1 mg/mL block copolymer solution (in $CHCl_3$) was spread on a pure water (Milli-Q, 18.2MΩ resistivity) surface at different locations. After twenty minutes to allow for equilibration, the LB trough with total surface area of 235 cm^2 was compressed at a speed of $70cm^2/min$. The film was subsequently expanded at the same rate, but it was found that the polymer film had collapsed and did not re-expand to cover the entire surface area. For this reason, only expansion isotherms are shown in this chapter.

5.4. Results and Discussion

Interfacial tension, as measured by Drop Shape Apparatus, is critical to determining the interfacial behavior of block ionomers. Prior to presenting that particular data, we present first the surface pressure isotherm as determined from Langmuir-Blodgett trough. This is done to calculate the surface coverage at a target interfacial tension, and also to compare intermolecular interactions at a single-layer level. In this work, this measurement is not fully utilized to its potential, and only crude preliminary data are shown. However, it must be noted that this measurement can be further utilized to create monolayers of the block ionomer, which will be helpful in revealing intermolecular interactions and resulting confirmations.

5.4.1. Surface pressure isotherm

Surface pressure (Π) isotherms were measured using Langmuir-Blodgett (LB) trough for PS-*b*-QVP samples. Here, the surface pressure comes from the interactions between block ionomer molecules. The full surface pressure isotherm is shown in Figure 5.4. The surface pressure Π is related to the interfacial tension of the block copolymer samples measured using DSA:

$$\Pi(A) = \gamma_0 - \gamma(A) \tag{5.1}$$

where the interfacial tension with the polymer film depends on the area per molecule A. With this, note that the surface pressure isotherm becomes inversely proportional to the interfacial tension γ.

The surface pressure isotherm for the samples with varying quaternization ratio is shown in Figure 5.4. At the maximum area, $A = 235\ cm^2$, the average surface area per molecule varies between $19.07\ nm^2/molecule$ for PS-*b*-QVPx0 and $19.41\ nm^2/molecule$ for PS-*b*-QVPx37.

A zoomed-in version of the top figure (Figure 5.4 bottom) shows that there is a non-monotonic trend in the interfacial behavior of the four polymers with different charge ratios. At the same surface coverage, the surface pressure initially increases with 4% charge, and then subsequently decreases with increasing charge. This indicates that the initial increase in charge increases the interaction between the molecules at the interface, but a further increase in charge does not appreciably change the interactions between the charged molecules.

5.4.2. Interfacial tension measurements

Interfacial tension was measured by extracting the bubble profile in time increments and fitting it to the Laplace equation as described in Figure 5.5. It is to be noted that the Laplace equation describes a balance between the surface tension γ, which tries to keep the spherical shape of the bubble, and the density difference, which tries to pull the bubble in an upward direction.[125] A deformation of the bubble, as shown in Figure 5.5, is indicative of changes in the interfacial tension, and is tracked by extracting the bubble profile and fitting R_0, the radius of curvature at the apex, and B_0, the shape parameter, to calculate the interfacial tension γ.

The interfacial tension measurements show that an increase in charge fraction is correlated with a significant drop in the interfacial tension at the oil-water interface. This is due to increased interfacial adsorption of the polymers at the oil-water interface with increasing charge. As with the surface isotherm, the difference is significant from 0% to 4% charge, but is non-monotonic and smaller in magnitude with subsequent increases in charge.

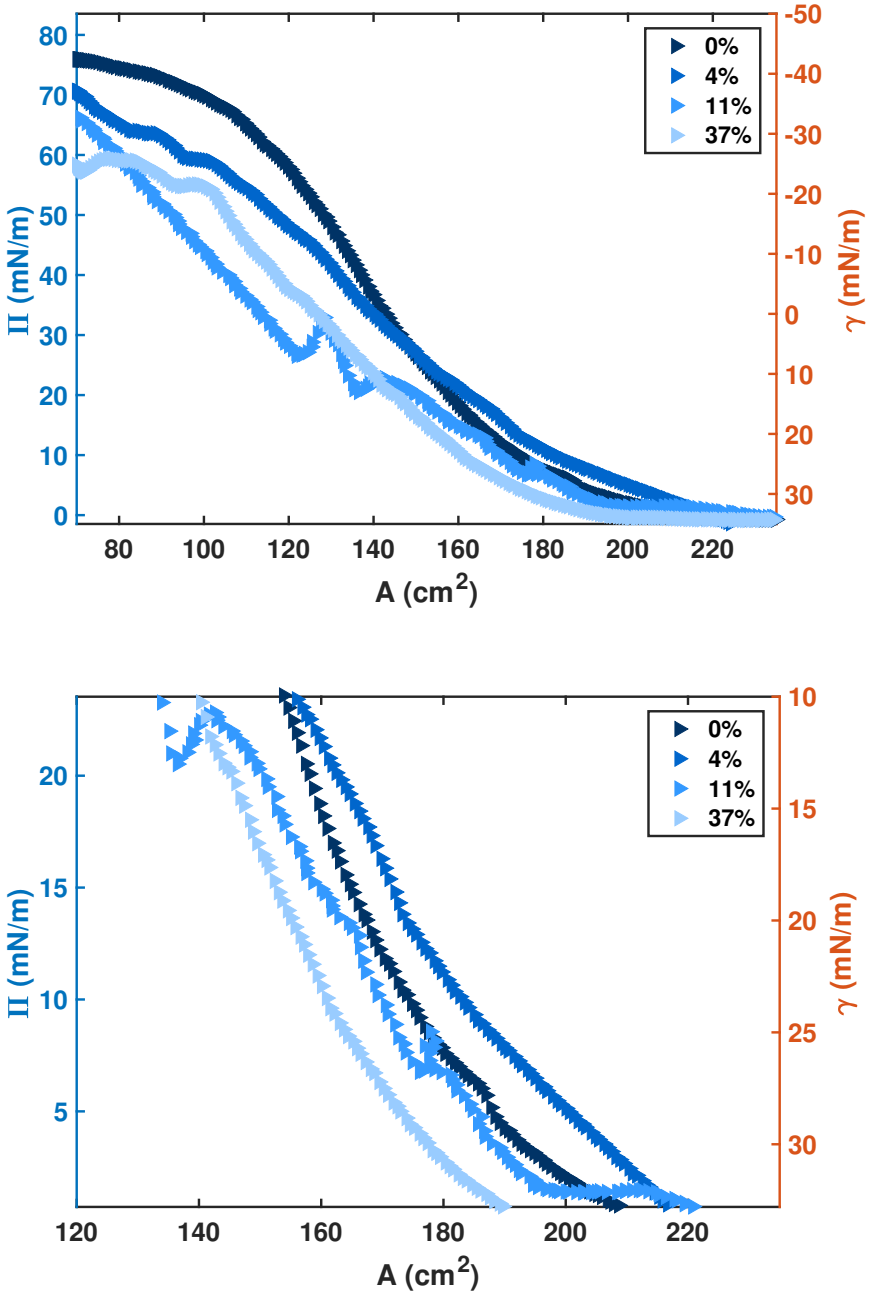

Figure 5.4. Surface pressure isotherm of PS-*b*-QVP from LB trough. Top figure shows the full isotherm, and bottom shows a zoomed-in version. Curves are very similar to one another, but exhibits a non-monotonic trend with increasing charge.

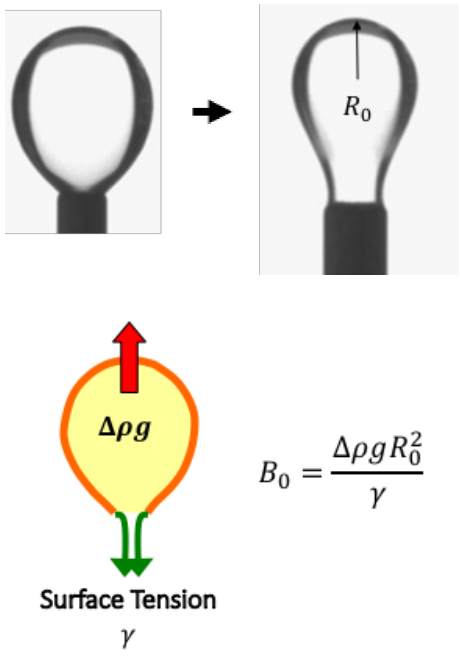

Figure 5.5. Schematic for calculating the interfacial tension. Bubble deformation is indicative of changes in the surface tension. The surface tension is calculated by fitting the bubble profile and determining the shape parameter B_0 and radius of curvature R_0.

When the interfacial tension measurements in Figure 5.6 are compared with the surface pressure isotherm, we find that the qualitative trends are consistent across the two surface measurements. By comparing the area of the LB trough at interfacial tensions γ obtained by DSA, we can also calculate the density of PS-*b*-QVP molecules at the interface corresponding to those interfacial tensions. This information is found in Table 5.2.

From the information in Table 5.2, we can see that the amount of adsorbed molecules increases with increasing charge. The primary reason for adsorption of molecules is to decrease the incompatibility between the two liquid phases, chloroform and water. Increased charge fraction in our block ionomer allows it to compatibilize both water and chloroform phases by associating with water via the charge-carrying ends and associating with chloroform via the

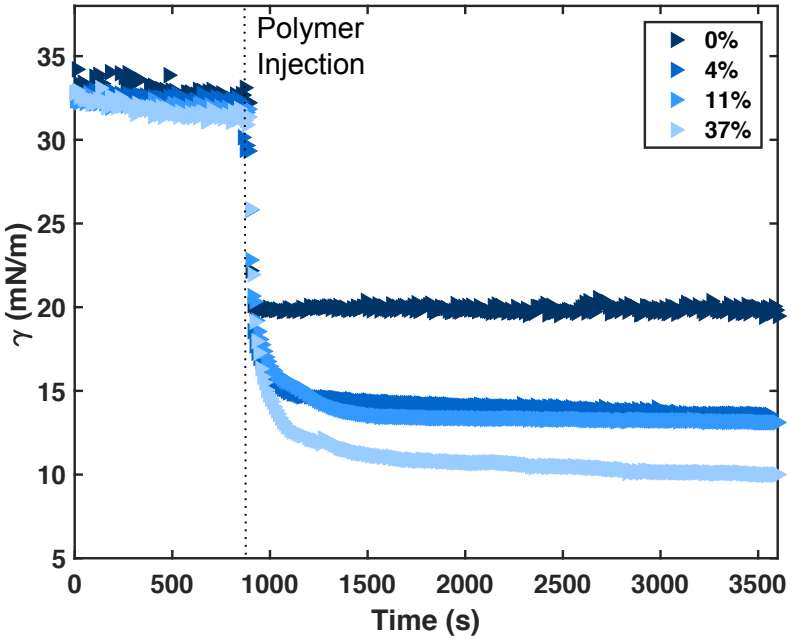

Figure 5.6. Interfacial tension of PS-*b*-QVP at chloroform-water interface. Polymer is injected at 900 seconds. A substantial drop in interfacial tension is seen for all samples.

Polymer	Interfacial Tension γ (mN/m)	Film Area (cm^2)	Area/molecule $(nm^2/molecule)$
PS-*b*-QVPx0	20	167	13.55
PS-*b*-QVPx4	13.5	163	13.25
PS-*b*-QVPx11	13	150	12.23
PS-*b*-QVPx37	10	140	11.56

Table 5.2. Interfacial tension and area per molecule of PS-*b*-QVP samples used for this study. The film area and area per molecule information are calculated from LB trough measurements at interfacial tensions corresponding to DSA-measured interfacial tensions at equilibrium and full polymer adsorption.

hydrophobic PS block. This argument follows that an increase in interfacial adsorption is correlated with the increase in hydrophilicity due to charge.

However, there are other factors that need to be considered. For example, the energetic gain from reducing the liquid-liquid incompatibility needs to offset the entropic decrease that comes from pinning the block ionomers at the interface. In addition, the polymers have to "unfurl" the strongly-correlated charge-carrying cores to dip them into the water phase. In chloroform, the dielectric constant is $\epsilon_r = 4.8$, which means that the energy of coupling between the ions is as large as $\approx 20kT$. Of course, there are other entropic and enthalpic advantages for the block ionomer to move to the interface. One, as discussed, is the decrease in incompatibility between two liquid phases. In addition, allowing the charge-carrying parts of the chain into the higher dielectric water phase will lower the solvation energy and increase the entropy of the ions, which can now move across the medium. The competition between these driving factors must be properly investigated in order to understand the non-monotonic trends in interfacial adsorption. For this, we turn to Molecular Dynamics simulations of interfacial adsorption, and find that an increase in charge in these block ionomers leads to a structural transition of the micelles.

5.4.3. Molecular Dynamics studies

Preliminary molecular dynamics simulations were run by Dr. Felipe Jiménez-Ángeles in order to investigate the structure of PS-*b*-QVP at chloroform-water interface. The simulation setup and model are shown in Figure 5.7.

From the simulations run for an uncharged block copolymer (PS-*b*-QVPx0), we see that the polymer takes on a jellyfish-like conformation at the interface, with the PVP block aggregated near the water phase and the PS blocks extended into the chloroform phase (Figure 5.8).

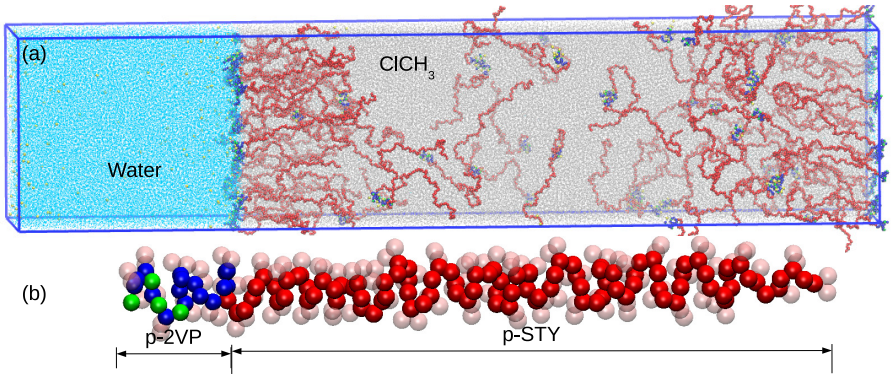

Figure 5.7. Simulation setup and models. (a) Water-chloroform ($CHCl_3$) interface with an amphiphilic copolymer. (b) Coarse-grain model of the polystyrene-poly-2-vinylpyridine copolymer constituted by 50 styrene monomers and 10 2-vinylpyridine monomers. The backbone atoms of polystyrene are colored in red; the backbone atoms of poly-2-vinylpyridine are in blue; the hanging aromatic rings are in pale pink, and the quaternized groups are in green. Figures courtesy of Dr. Felipe Jiménez-Ángeles.

The PVP cores are formed by aggregation of multiple PVP molecules, ranging from 3 nm (6 molecules) to 8 nm (15 molecules).

When the PVP block is quaternized at 40% (PS-*b*-QVPx40), the degree of adsorption increases, where the molecules adsorb in a rod-like fashion, as seen in Figure 5.9. Here, there is a significant increase in the adsorption, as the charge-containing QVP block is attracted to one another and to the water phase. The electrostatic interaction between the QVP cores lead to a rod-like arrangement of aggregated QVP cores at the interface ranging from 3 nm (5 or fewer molecules) to 11 nm (15 molecules).

In the bulk chloroform phase, simulations show structural differences in the two samples. While the neutral sample (PS-*b*-QVPx0) shows spherical micelles with PS corona and PVP core, the charged sample (PS-*b*-QVPx40) shows a helical morphology. How much of a role does the equilibrium conformation in the bulk play on the interfacial behavior of these polymers? This is a question that will need to be addressed by further investigations.

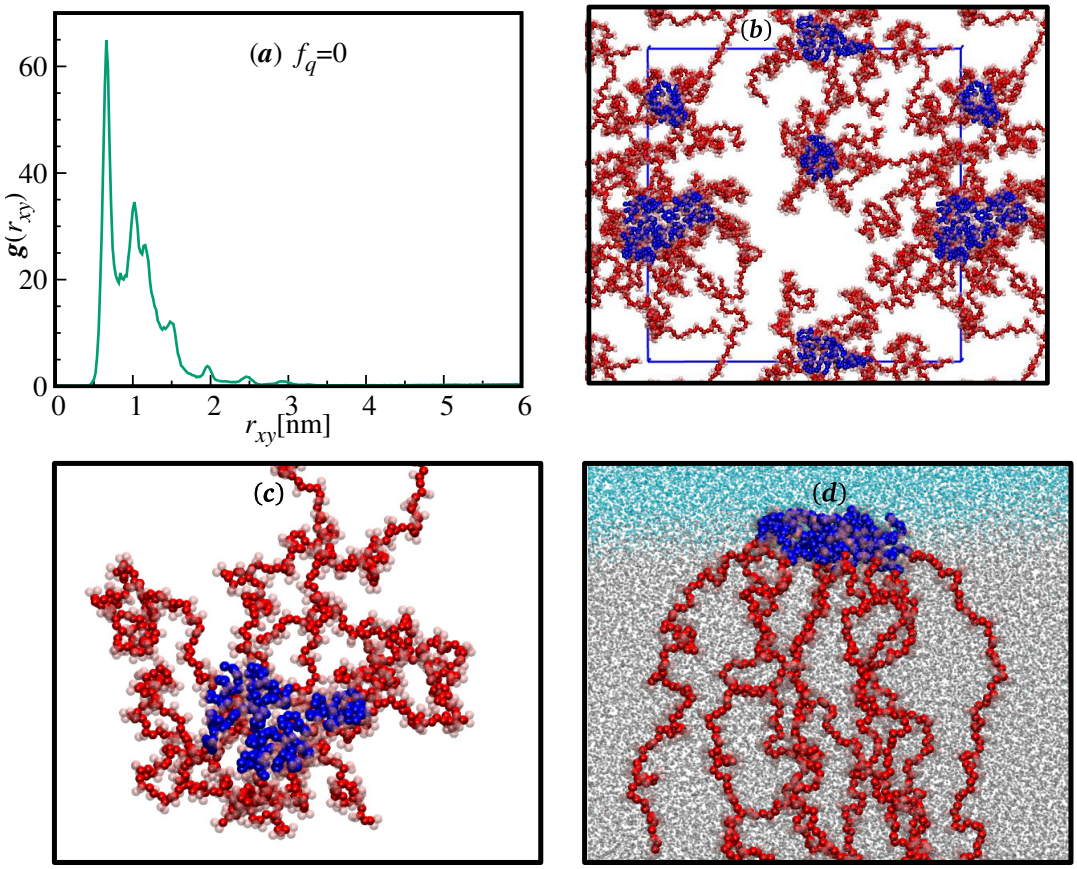

Figure 5.8. Structure of the uncharged copolymer ($f_q = 0$) at the water-chloroform interface. (a) Radial distribution function $g(r_{xy})$ between the segments of 2-vinylpyridine at the interface; r_{xy} between two segments is the center-center separation distance on the $x - y$-plane. (b) Snapshot of the copolymers at the interface from the top. (c) Top and (d) side views of the largest aggregate at the interface. $\Gamma = 0.0562$ molecs./nm^2, $\gamma = 20.5$ mN/m. Largest aggregate is about 8 nm (15 molecules), small are of 3 nm (6 molecules). Figures courtesy of Dr. Felipe Jiménez-Ángeles.

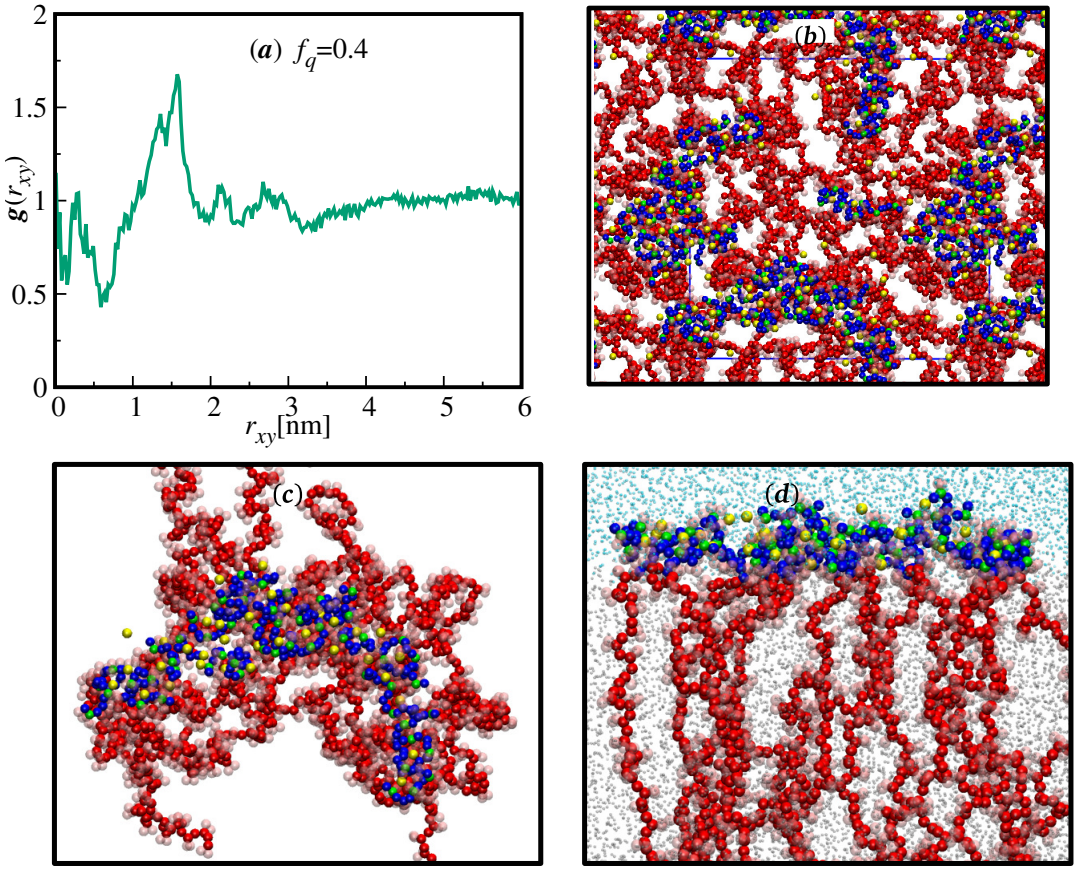

Figure 5.9. Structure of the charged copolymer ($f_q = 0.4$) at the water-chloroform interface. (a) Radial distribution function $g(r_{xy})$ between the segments of 2-vinylpyridine at the interface. (b) Snapshot of the copolymers at the interface from the top. (c) Top and (d) side views of the largest aggregate at the interface. $\Gamma = 0.173$ molecs./nm^2, $\gamma = 8.05$ mN/m. Largest aggregate is about 11 nm (15 molecules), small are of less than 3 nm (5 or fewer molecules). Figures courtesy of Dr. Felipe Jiménez-Ángeles.

5.4.4. The role of interfacial tension on micellar morphology

Of particular interest is the role of interfacial tension on the micellar morphology of diblock copolymers. Previous research in amphiphilic block copolymer micelles has shown that cylinder-to-sphere morphological transition can be driven by interfacial tension.[126–128]

Recently, co-workers in Professor Evan Scott's group have shown that cylinder-to-sphere transition of self-assembled filomicelle (FM) scaffolds of diblock copolymers of poly(ethylene glycol)-*bl*-poly(propylene sulfide) (PEG-*bl*-PPS) can be induced via photo-oxidation or physiological oxidation for drug delivery applications. The details of the synthesis and experiments are found in a recent publication of Karabin *et al*.[129] It is believed that this oxidation-induced transition is due to substantial changes in the interfacial tension between the two incompatible blocks. Modeling and experimental work supporting this argument are reproduced here.

In this work, using a thermodynamic model and interfacial measurements obtained via drop shape apparatus, we show that the transition in PEG-PPS can be understood by the reduction of interfacial energy upon oxidation of the sulfide group which is balanced by the chain stretching of core and corona blocks.

The thermodynamic analysis of PEG-PPS in solution follows the framework outlined in theoretical work by Zhulina *et al*[128] and Lund *et al*.[127] In this model, the total free energy of a block copolymer micelle is written as a sum of three components: the interfacial energy between core and solvent, F_{int}; the elastic energy of stretching chains in the core, F_{core}; and the energy associated with the chains in the corona, F_{corona}.[126] Using the approach given by Lund *et al*[127] and Zhulina *et al*[128] each contribution can be broken down for cylindrical and spherical morphologies:

$$F_{int} = \frac{A_j \gamma}{P k_B T} \begin{cases} A_j = 4\pi R_c^2 & \text{Spheres} \\ A_j = 2\pi R_c L & \text{Cylinders} \end{cases} \tag{5.2}$$

Here, γ is the interfacial tension, R_c the core radius, P the aggregation number assuming a compact core: $P = 4\pi R_c^3 N_{avo}/(3V_{PPS})$ and $P = \pi R_c^2 L N_{avo}/V_{PPS}$ for spheres and cylinders, respectively. V_{PPS} is the molar volume of PPS block and N_{avo} is Avogadro's number.

$$F_{core} = k_j \frac{R_c^2}{R_{ee}^2} \begin{cases} k_j = \frac{\pi^2}{16} & \text{Spheres} \\ k_j = \frac{3\pi^2}{80} & \text{Cylinders} \end{cases} \tag{5.3}$$

where $R_{ee} = N_{PPS}^{1/2} l_{PPS}$ is the unperturbed end-to-end radius of gyration of PPS, the core-forming block.

$$F_{corona} \begin{cases} \frac{\nu C_F R_c}{\sqrt{s}} \ln\left(1 + \frac{l_{PEG} C_H N_{PEG} (s/l_{PEG}^2)^{(\nu-1)/2\nu}}{\nu R_c}\right) & \text{Spheres} \\ \frac{2C_F R_C}{\sqrt{s}} \left[\left(1 + \frac{(1+\nu) l_{PEG} C_H N_{PEG} (s/l_{PEG}^2)^{(\nu-1)/2\nu)}}{2\nu R_c}\right)^{\nu/(\nu+1)} - 1\right] & \text{Cylinders} \end{cases} \tag{5.4}$$

The total free energy of a micelle, $F_{micelle} = F_{int} + F_{core} + F_{corona}$, is minimized with respect to the core radius, R_c. The calculations were performed with all molecular parameters fixed. This included the compositions and molecular weights known from characterizations, while radii of gyration and segment lengths were estimated from previous works.[127] Numerical prefactor parameters, C_F and C_H were taken from works by Zhulina and Lund.[127,128] The equilibrium core radius R_c corresponding to free energy minima for spherical and cylindrical micelles is shown in Figure 5.10. The micelle free energy calculated at the equilibrium core radius is shown in Figure 5.10.

At high interfacial tension, cylindrical micelles are favored. Cylindrical micelles have a smaller core radius at the same interfacial energy, which reduces the elastic energy of the chains

in the core. At lower interfacial tension, the system can accommodate a larger interfacial area, which leads to the formation of spherical micelles that minimize the interchain repulsion in the corona. From the thermodynamic model, we predict the transition to occur at $\gamma \cong 8$ mN/m.

Experimentally measured values of the interfacial tension are shown in Figure 5.11 for PEG-PPS micelles prior to and post oxidation in phosphate-buffered saline solution (PBS). Interfacial tension measurements were collected using drop shape apparatus (DSA) following procedure outlined in a previous paper.[130] We show that the oxidation of the PPS block leads to a substantial decrease in the interfacial tension. The final interfacial tension ($\gamma \cong 5mN/m$) of the oxidized polymer is below our calculated transition point; the decrease in γ can trigger the transition from cylinders to spheres in PEG-PPS micelles as the PPS block is oxidized.

This model provides a qualitatively satisfying confirmation of interfacial tension-driven cylinder-to-sphere transition in PEG-PPS. However, a quantitative comparison is not straightforward for a few reasons. First, the measured interfacial tension in DSA represents the energy between PPS and PEG blocks across the chloroform-water interface (Figure **??**). This interface contains a lower concentration of polymer than the model interface between the core and the corona block. Second, the thermodynamic model relies on numerical prefactors and long chain statistics, which is not necessarily applicable in the present system of only 44 PPS and 45 PEG repeat units. Further theoretical work would be necessary to more appropriately capture the description of the present system, but this is beyond the scope of the paper.

5.5. Conclusion

In this chapter, we have investigated the effect of charge on the interfacial activity of diblock copolymers of PS-*b*-Q2VP. We have shown that the initial increase in charge, from 0% of the

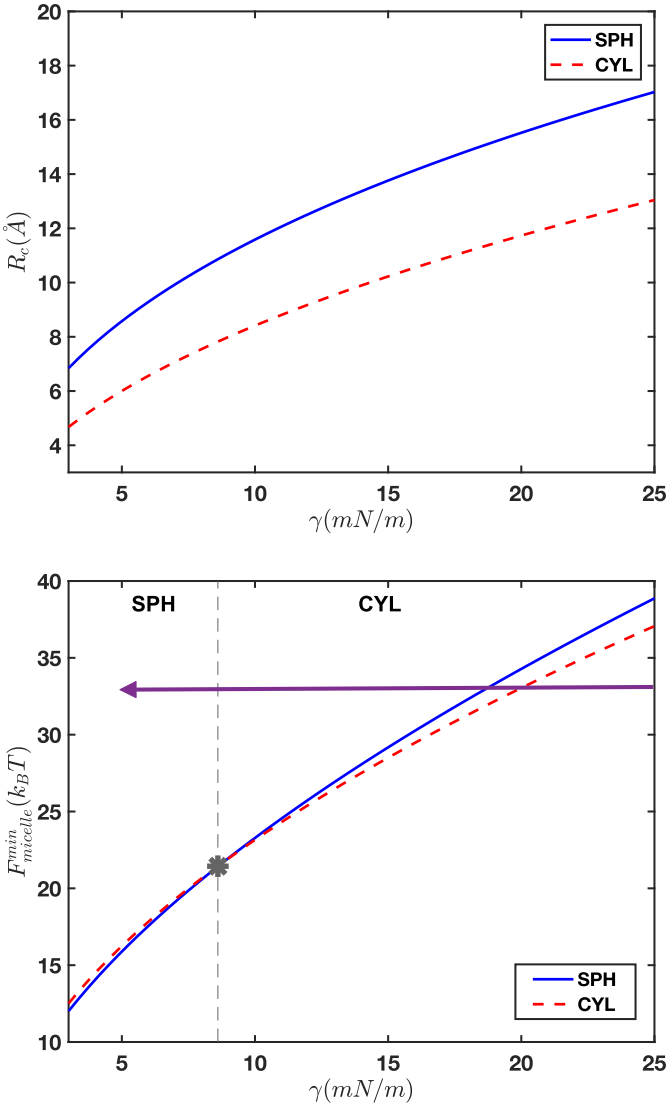

Figure 5.10. Equilibrium micelle core radii corresponding to the free energy minima for spherical and cylindrical micelles (left) and total free energy of micelles calculated at the equilibrium core radii (right) Star represents the interfacial tension at which cylinder-to-sphere transition occurs ($\gamma \approxeq 8$). Above this interfacial tension, PEG-PPS micelles prefer a cylindrical morphology; below this energy, the polymer forms spherical micelles. As PEG-PPS is oxidized, it moves across the morphological map as indicated by purple arrow.

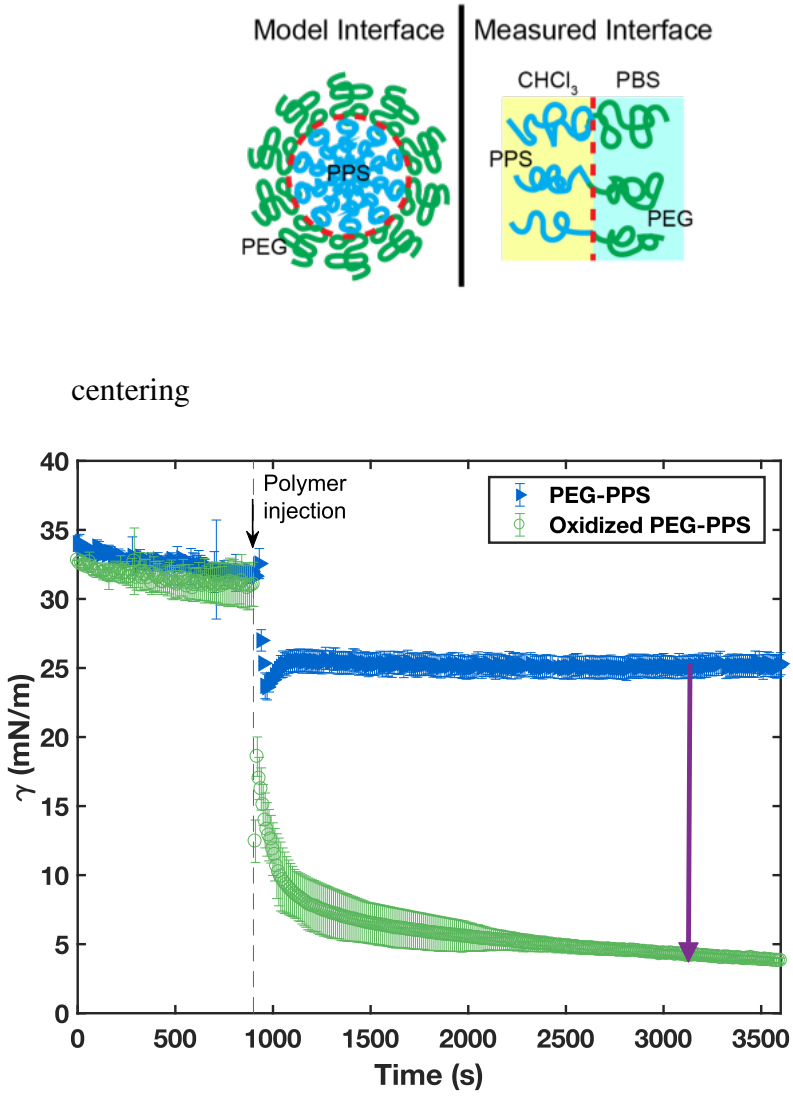

Figure 5.11. Interfacial tension measurements with 2mg/mL of PEG-PPS injected into the chloroform embedding phase at 900 seconds. Oxidizing PEG-PPS reduces the interfacial tension as indicated by purple arrow. This drop in interfacial tension corresponds to the movement across the morphological map in Figure 5.10.

PVP block to 4%, has a substantial importance. As shown in the surface-pressure isotherm, the surface pressure increases with this initial charge, and subsequently decreases. The ”charging” of this amphiphilic molecule increases the attraction between molecules at water-oil interface,

but a further increase in charge does not appreciably increase or decrease the interaction between chains, hinting that charge interactions are a complex phenomenon that does not scale linearly. When these diblock copolymers are placed at oil-water interface, an increase in charge leads to a significant adsorption of the polymers at the interface, and orders into a qualitatively different conformation. While this can be said to be due the increased hydrophilicity of the PVP block with charge, MD simulations show that the adsorption behavior cannot be attributed to hydrophilicity alone. An increase in the solvation of the counterions is shown to lead to changes in the morphology of the charged molecules in the oil and at the interface.

CHAPTER 6

Morphology of block ionomer melts

6.1. Abstract

In this chapter, we focus on future directions that can sprout from discussions in this thesis, and some preliminary results. Thus far, we have investigated the role of electrostatic interactions in ionomer blends with two or three components. In Chapter 5, we discussed interfacial activity and micellization of diblock copolymers of PS-*b*-QVP. In these systems, the dielectric constants of the two liquid phases, and the resulting differences in solvation energy, control the micellar structure within chloroform phase and at the interface. In this chapter, we discuss the effect of charge on the equilibrium morphology in the melt, where there are no liquid phases. This is of interest for water filtration membrane and solid polymer electrolyte applications, as the equilibrium nanodomain size and morphology within these polymeric materials can dictate the performance of these applications. For us, the interest lies in being able to answer a fundamental question: how do electrostatic interactions change in a system with and without solvent? Can we decouple the effects of ionic correlations from the consequences of ion solvation? In contrast to the interfacial studies, the melt study has the potential to probe equilibrium behaviors at low dielectric mismatch $\Delta\epsilon$, where ionic correlations are believed to dominate. This can provide experimental confirmation for electrostatic effects that have only been theorized but never observed.

6.2. Preliminary work

The polymers were quaternized and characterized as outlined in Chapter 5. The equilibrium morphology was characterized using Grazing Incidence Small Angle X-Ray Scattering (GISAXS).

6.2.1. Grazing Incidence Small Angle X-Ray Scattering (GISAXS)

Grazing Incidence Small Angle X-Ray Scattering (GISAXS) measurements were performed at Sector 5-ID-E of the Advanced Photon Source at Argonne National Laboratory. GISAXS samples were prepared by spin-coating the prepared polymer solutions (of 5 mg/mL) onto Si substrates. The fabricated films were estimated to be approximately 200 nm thick from the blue color of the film. Samples were annealed in solvent chambers containing solvents of Ethanol and THF at various concentrations for three days prior to imaging. Sample alignments were performed using an avalanche photodiode detector. X-ray scattering patterns of the spin-coated films was collected using a 2-D detector (PILATUS 1M pixel array detector) with an X-ray energy of 10.915 keV, and a sample-to-detector distance of 2.165 m. A silver behenate standard is used as reference. Typical incident angles for polymer thin films on silicon substrates are varied between 0.08° to 0.14°, which is between the critical angles for total reflection of the film and the substrate. For the samples shown in this chapter, the incident angles are kept at 0.12°.

At a photon energy of 10.915 keV, the critical angle of the film is $\approx 0.10^\circ$. Under these conditions, the beam will penetrate the sample but reflect off of the substrate, fully illuminating the sample volume along the footprint of the beam.

GISAXS patterns were processed with a beamline MATLAB program, which accounts for both the sample-to-detector distance and detector resolution, and produces intensity maps in the inline image plane ($q_y - q_z$). In the GISAXS scattering geometry, q_y is the scattering vector parallel to the sample surface and perpendicular to the scattering plane, and q_z is the component perpendicular to the sample surface.

6.2.2. GISAXS characterization

Samples of PS-*b*-QVPx0, 4, 11, 37 under five solvent annealing conditions (THF:Ethanol 0:100, 25:75, 50:50, 75:25, 100:0 by volume) were analyzed. Ethanol represents a selective solvent for the QVP block, while THF is a good solvent for both blocks. Shown in Figures 6.1,6.2,6.3,6.5 are GISAXS diffraction patterns from the five different annealing conditions.

From the diffraction patterns, we first note that the films are not very well ordered, as indicated by the lack of higher order peaks, especially in PS-*b*-QVPx0 and PS-*b*-QVPx37. However, it is worth noting that the solvent quality changes for block copolymer films containing different charge ratios. Specifically, when the solvent conditions are changed from 100% THF to 75% THF (25% Ethanol), the degree of order in films of PS-*b*-QVPx0 and PS-*b*-QVPx04 decreases, while PS-*b*-QVPx11 and PS-*b*-QVPx37 become more ordered. However, if the amount of Ethanol is further increased, all of the samples become less ordered, presumably because of the amount of PS in the system (and its immiscibility in Ethanol). This shows that even small degrees of charge ratio can significantly alter the mixing thermodynamics of the diblock copolymer. However, further investigations are necessary in order to determine the effect of quaternization on solvent solubility of the diblock copolymers.

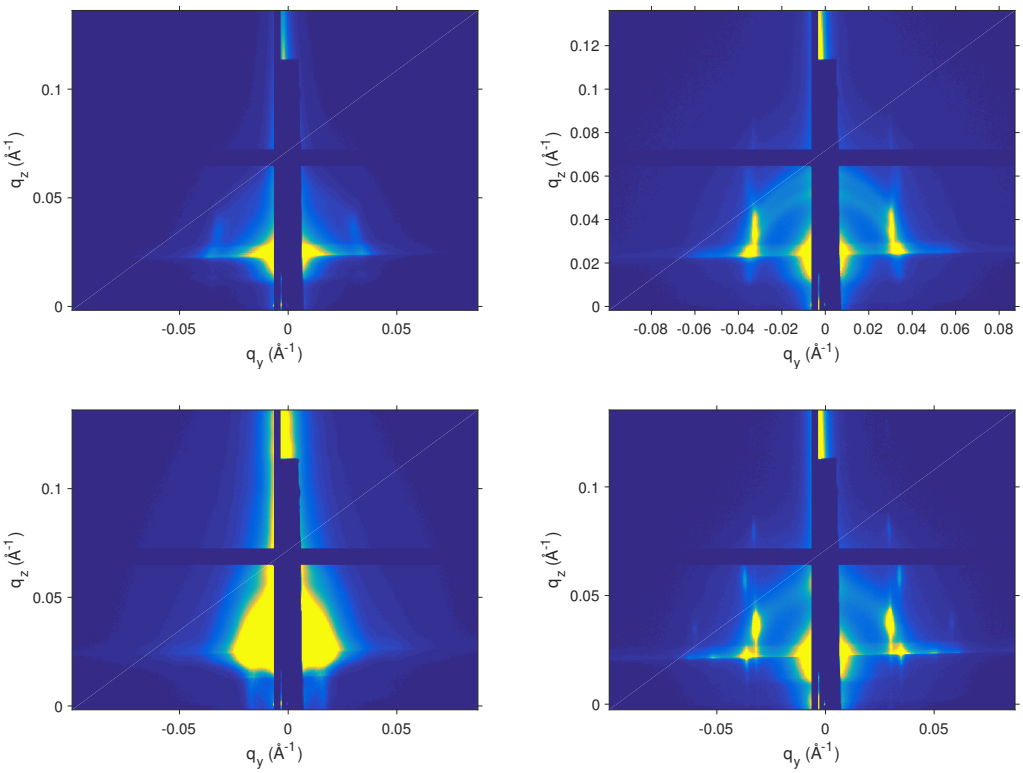

Figure 6.1. QVPx0, 4, 11, 37 at THF:Ethanol 100:0 in a clockwise direction.

In this section, only a selection of patterns are analyzed. First, we begin by looking at films solvent annealed in 100% of THF, the linecuts of which are shown in Figure 6.6. For this series of linecuts, the linecuts are taken by integrating between $q_z = 0.01$ and $q_z = 0.1$ as a function of q_y. It is clearly seen that with increase in charge, from 0% to 11%, the peaks become more defined. Furthermore, higher order peaks begin to develop for 11%, indicating an increased degree of order with increasing charge. At 37%, the peaks become more difficult to define; this can be attributed to the changes in the solvent miscibility as described above. From Figure 6.2, which shows the only ordered film for 37%, it can be determined that the 37% takes on a BCC morphology under equilibrium solvent conditions.

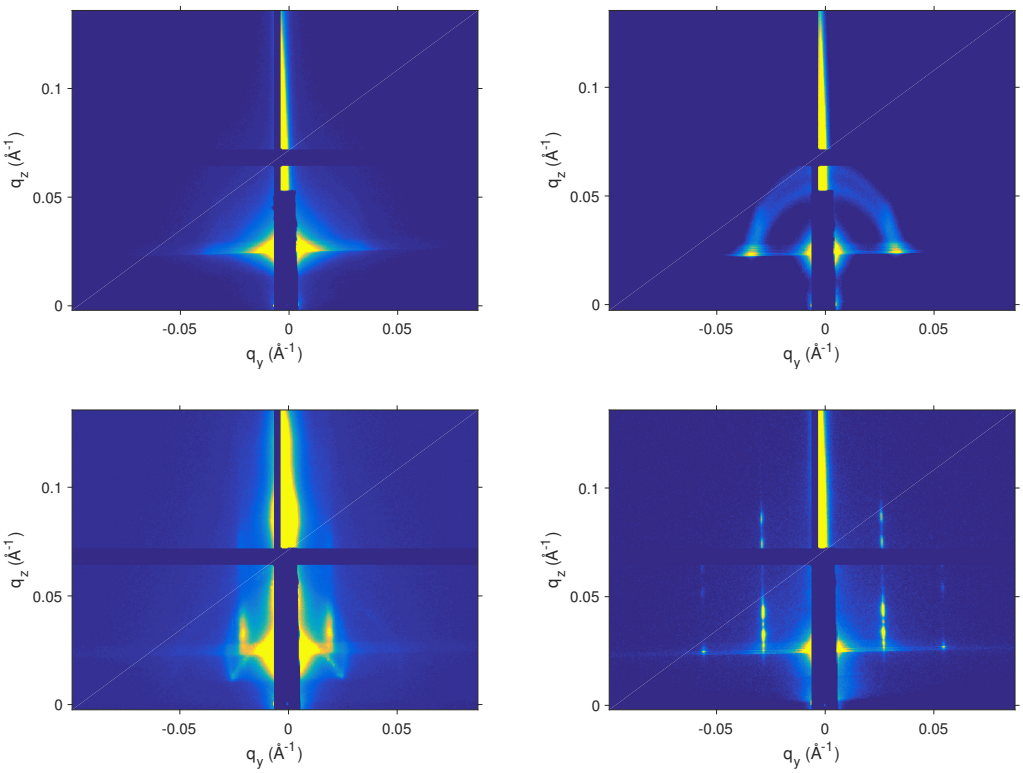

Figure 6.2. QVPx0, 4, 11, 37 at THF:Ethanol 75:25 in a clockwise direction.

It is difficult to assign peaks for samples of PS-*b*-QVPx0 and 4, as these lack higher order peaks. However, from the higher order peaks present in patterns of PS-*b*-QVPx11, we can assign the peaks to body-centered cubic (BCC) spheres, with [110] plane parallel to the substrate.

The lattice parameters in GIXGUI correspond to $a = 244, b = 345, c = 300$ and $\alpha = \beta = \gamma = 90°$. For cubic cells, it is expected that $a = b = c$. However, the mapping of BCC spheres due to [110] being parallel to the substrate, as well as due to a distortion in the $z-$direction of the film due to swelling or drying of the film, may change the lattice parameters. The simulated peaks for the lattice parameters given are superimposed on the diffraction pattern in Figure 6.6, and seen to match very closely.

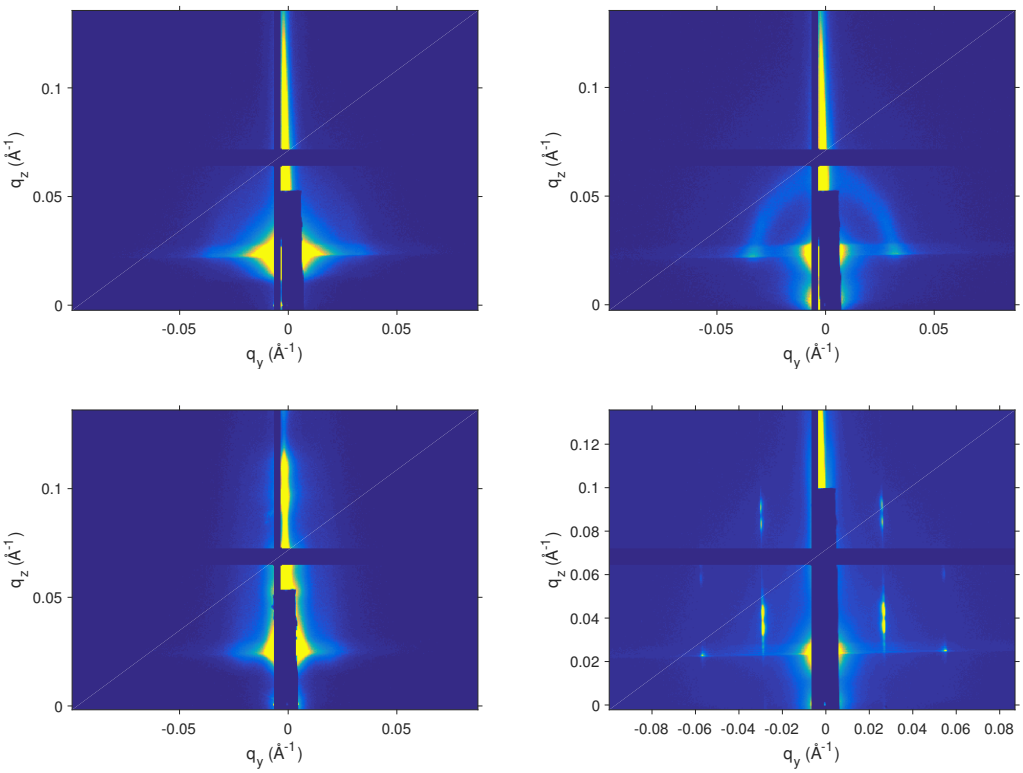

Figure 6.3. QVPx0, 4, 11, 37 at THF:Ethanol 50:50 in a clockwise direction.

However, TEM images of I_2 stained film (courtesy of Dr. Hiroaki Sai, Stupp Group) of PS-*b*-QVPx11 solvent-annealed in 100% THF show regions where the imaged area differs decidedly from BCC spheres. It has been hypothesized that there might be regions within PS-*b*-QVPx11 that form closely packed spheres or hexagonally packed inverted cylinders. This information is not easy to extract from the GISAXS images, as the diffraction pattern shown in the GISAXS is representative of the averaged-out morphology; that is, if the majority of the film forms BCC spheres, the diffraction pattern will be most representative of that particular morphology. As only a very small area of the sample shows this unconfirmed morphology, it is unlikely that this will be distinguishable using GISAXS. Further studies will have to be done

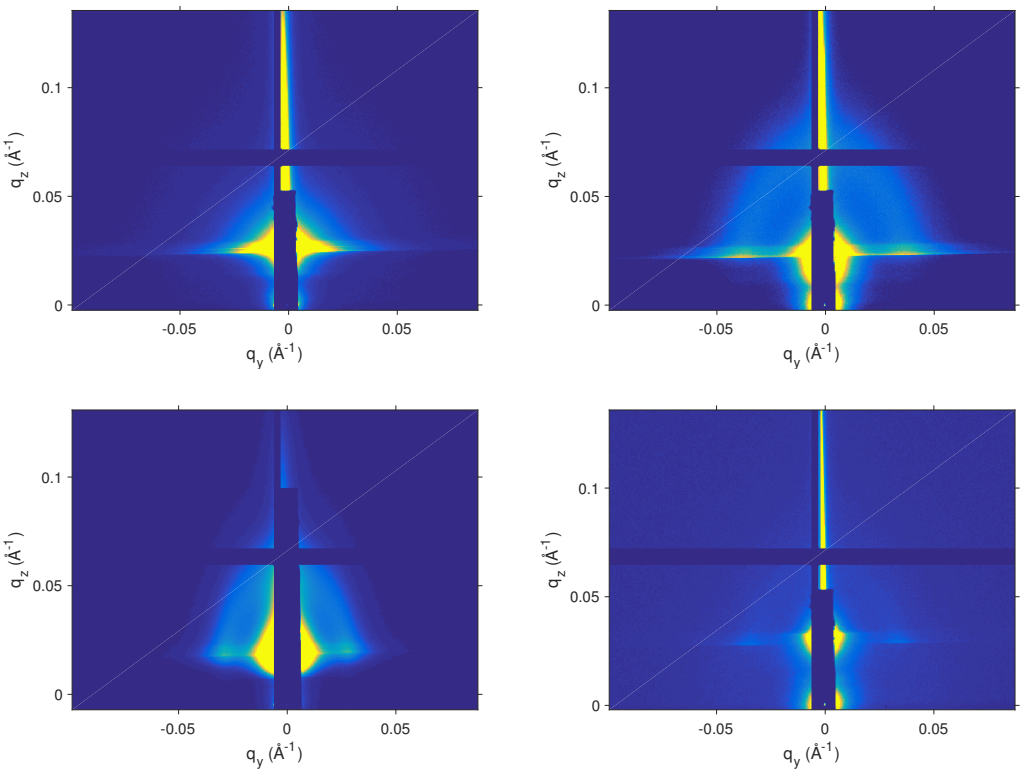

Figure 6.4. QVPx0, 4, 11, 37 at THF:Ethanol 25:75 in a clockwise direction.

in order to 1) confirm the morphology of this region and 2) identify conditions that lead to the formation of this particular morphology.

Next, we analyze a single sample, PS-*b*-QVPx11, annealed under the five different solvent conditions. The linecut is shown in Figure 6.8.

We find that the sample is not very well ordered in solvent conditions with a large amount of solvent (THF:EtOH 0:100, THF:EtOH 25:75), but exhibit order in solvent conditions with a higher concentration of THF. We believe that in THF:EtOH 50:50 and THF:EtOH 25:75, film is ordered in hexagonally packed cylinders, with the cylinders lying down parallel to the substrate. In THF:EtOH 100:0, the film is organized in BCC spheres with the [110] plane parallel to the

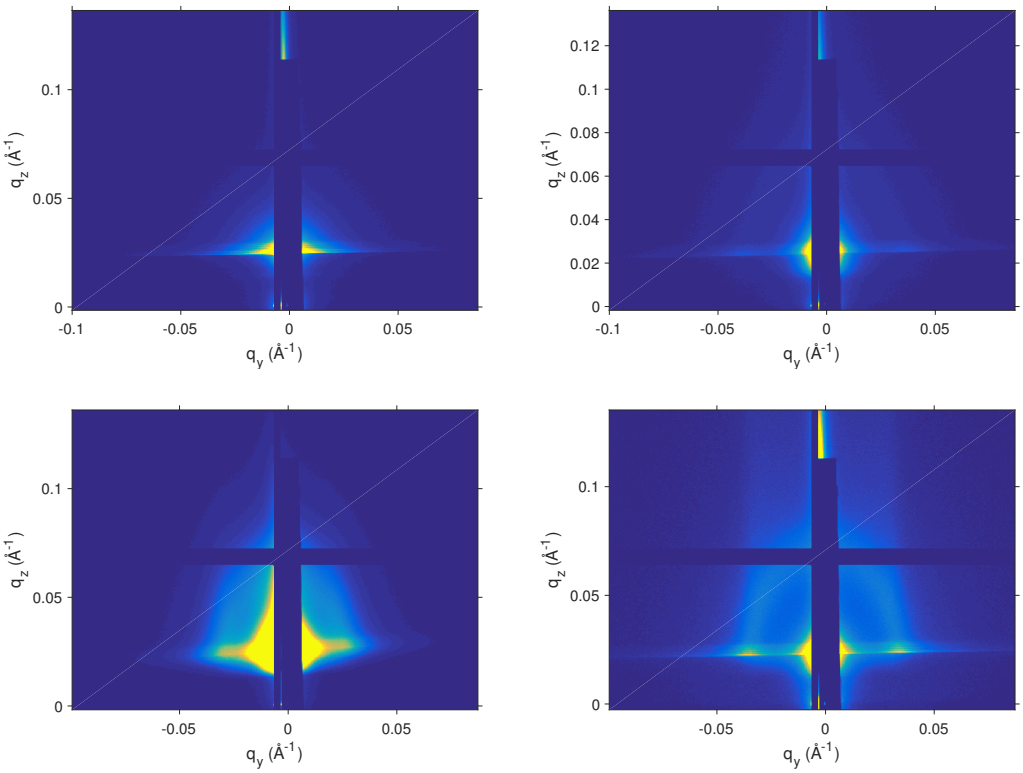

Figure 6.5. QVPx0, 4, 11, 37 at THF:Ethanol 0:100 in a clockwise direction.

substrate. This shows that when charge is introduced, the block copolymers become sensitive to different solvent conditions. At charge fraction of 11%, the film forms BCC spheres in 100% THF, but forms cylinders when solvent-annealed in 25% Ethanol. This is presumably due to the charge-containing block being more selective for the polar solvent; however, further investigations are needed in order to verify this observation.

6.3. Future work

The equilibrium morphology of ionomer block copolymers has an incredible potential. Some of the directions in which this can be headed are:

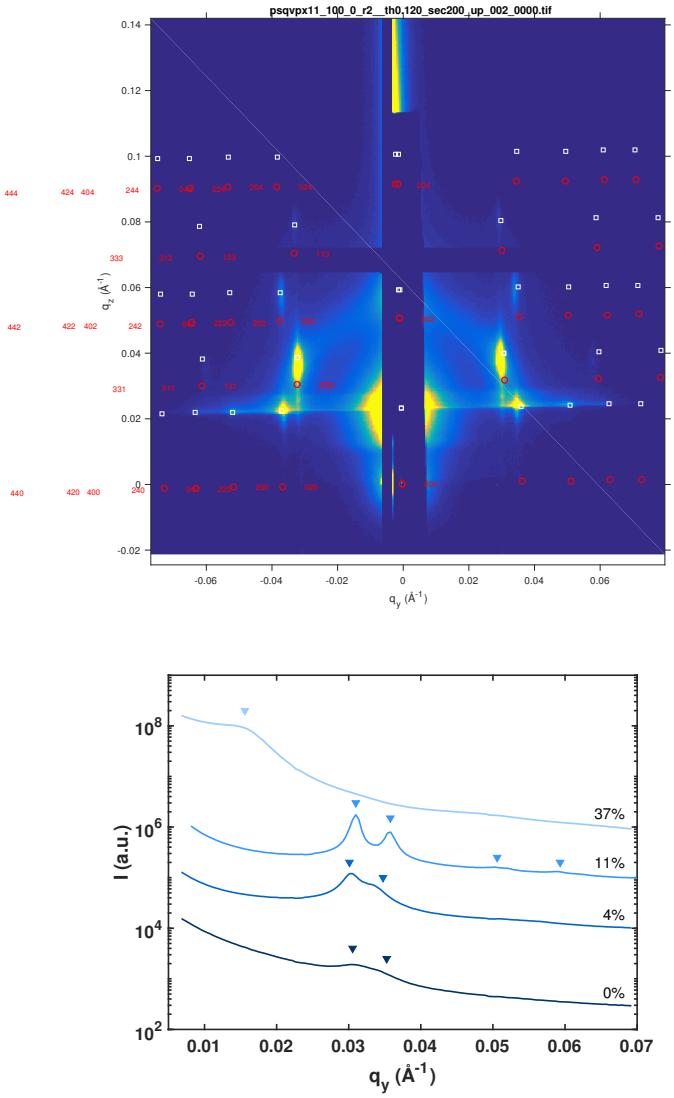

Figure 6.6. Top shows the formulated peaks for BCC spheres with [110] plane parallel to the substrate and lattice parameters of $a = 244, b = 234, c = 300\mathring{A}$. Bottom shows linecuts for PS-*b*-QVP samples solvent-annealed in 100% THF.

- Verification of block copolymer morphology using transmission electron microscope (TEM), Small-Angle X-Ray Scattering (SAXS)
- Expansion of the system to PS-*b*-QVP with varying block lengths
- Exploring solvent-selectivity in PS-*b*-QVP melts

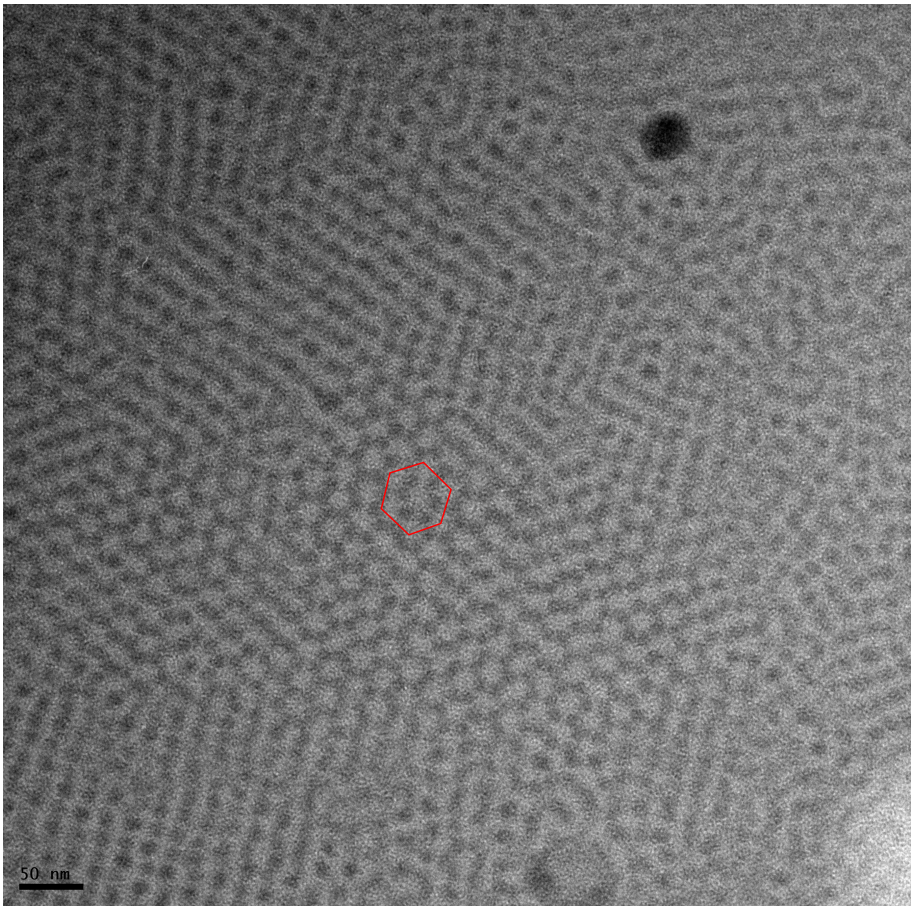

Figure 6.7. TEM image of PS-*b*-QVPx11, annealed under 100% THF and stained with I_2. Image courtesy of Dr. Hiroaki Sai. Red hexagon outlines the region with unconfirmed morphology.

- Studying the effect of block and polymer architecture on electrostatic interactions

As explored earlier in this Chapter, the identification of morphological structures is especially challenging, due to the lack of higher order peaks in diffraction patterns and the coexistence between different morphologies as shown in Figure 6.7. Conducting TEM on samples of PS-*b*-QVP with varying charge ratios can assist in visually identifying the coexisting morphologies in the melt. Cross-referencing with SAXS will be useful, as SAXS can probe bulk morphologies

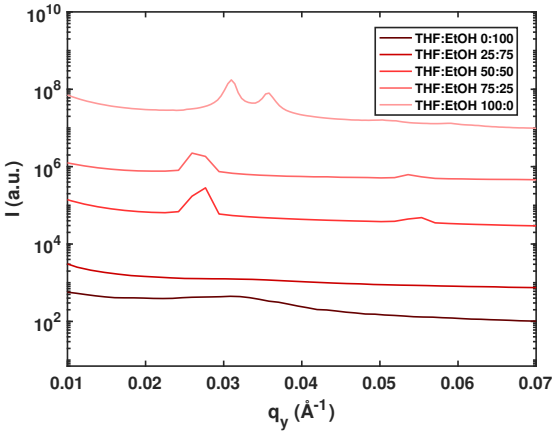

Figure 6.8. Linecuts of PS-*b*-QVPx11, solvent-annealed under five different solvent conditions.

in the absence of confinement effects, unlike GISAXS which characterizes anisotropic ordering in thin films of polymers.

Another way to overcome the lack of higher order peaks is to move to block copolymers with a longer PVP block. This will increase the segregation strength χN between the two blocks. Furthermore, having a longer PVP block would allow for a wider range of charge fraction (quaternization ratios). In addition, block volume asymmetry will have to be explored in order to completely map out the phase diagram of PS-*b*-QVP.

The solvent-selectivity in these melts are also of interest. We've seen that melts with varying charge fraction ratios respond differently to solvent annealing conditions. For this thesis, the analysis has been limited to a qualitative assessment of the polarity of solvents; Ethanol (relative polarity of 0.654) has a higher polarity than THF (relative polarity of 0.207),[131] and therefore is a selective solvent for the charge-containing parts. However, a quantitative analysis, with a focus on relating the polarity and dielectric constant of a solvent with its ability to associate

or order the ionomer block copolymer may be extremely useful for future experiments using charged block copolymers.

References

[1] Michael Rubinstein and Ralph H Colby. *Polymer physics*, volume 23. Oxford university press New York, 2003.

[2] Mark W Matsen. Effect of architecture on the phase behavior of ab-type block copolymer melts. *Macromolecules*, 45(4):2161–2165, 2012.

[3] Frank S. Bates and Glenn H. Fredrickson. Block copolymers-designer soft materials. *Physics Today*, 52(2):32–38, 2 1999.

[4] C Huang, M Olvera de La Cruz, and BW Swift. Phase separation of ternary mixtures: symmetric polymer blends. *Macromolecules*, 28(24):7996–8005, 1995.

[5] C Huang and M Olvera de la Cruz. Adsorption of a minority component in polymer blend interfaces. *Physical Review E*, 53(1):812, 1996.

[6] Ching-I Huang. *Studies of phase separation dynamics and interfaces in ternary systems*. PhD thesis, Northwestern University, Evanston, Illinois, 6 1996.

[7] Ha-Kyung Kwon, Jos W Zwanikken, Kenneth R Shull, and Monica Olvera de la Cruz. Theoretical analysis of multiple phase coexistence in polyelectrolyte blends. *Macromolecules*, 48(16):6008–6015, 2015.

[8] Paul J Flory. Thermodynamics of high polymer solutions. *The Journal of Chemical Physics*, 9(8):660–660, 1941.

[9] MW Matsen and Frank S Bates. Unifying weak-and strong-segregation block copolymer theories. *Macromolecules*, 29(4):1091–1098, 1996.

[10] Frank S Bates. Polymer-polymer phase behavior. *Science*, 251(4996):898–905, 1991.

[11] Stefan Walheim, Marcus Ramstein, and Ullrich Steiner. Morphologies in ternary polymer blends after spin-coating. *Langmuir*, 15(14):4828–4836, 1999.

[12] Kenneth R Shull, Edward J Kramer, Georges Hadziioannou, and Wing Tang. Segregation of block copolymers to interfaces between immiscible homopolymers. *Macromolecules*, 23(22):4780–4787, 1990.

[13] Masha Lifschitz and Karl F Freed. Interfacial behavior of compressible polymer blends. *The Journal of chemical physics*, 98(11):8994–9013, 1993.

[14] Moon Jeong Park and Nitash P Balsara. Phase behavior of symmetric sulfonated block copolymers. *Macromolecules*, 41(10):3678–3687, 2008.

[15] Shuyi Xie and Timothy P Lodge. Phase behavior of binary polymer blends doped with salt. *Macromolecules*, 2017.

[16] Moon Jeong Park and Sung Yeon Kim. Ion transport in sulfonated polymers. *Journal of Polymer Science Part B: Polymer Physics*, 51(7):481–493, 2013.

[17] Charles E Sing, Jos W Zwanikken, and Monica Olvera de la Cruz. Interfacial behavior in polyelectrolyte blends: Hybrid liquid-state integral equation and self-consistent field theory study. *Physical review letters*, 111(16):168303, 2013.

[18] Charles E Sing, Jos W Zwanikken, and Monica Olvera de la Cruz. Electrostatic control of block copolymer morphology. *Nature materials*, 13(7):694–698, 2014.

[19] EJW Verwey and KF Niessen. Xl. the electrical double layer at the interface of two liquids. *The London, Edinburgh, and Dublin Philosophical Magazine and Journal of Science*, 28(189):435–446, 1939.

[20] Markus Bier, Jos Zwanikken, and René van Roij. Liquid-liquid interfacial tension of electrolyte solutions. *Physical review letters*, 101(4):046104, 2008.

[21] Yan Levin. Polarizable ions at interfaces. *Physical review letters*, 102(14):147803, 2009.

[22] Zhen-Gang Wang. Fluctuation in electrolyte solutions: The self energy. *Physical Review E*, 81(2):021501, 2010.

[23] Artem M. Rumyantsev and Elena Yu. Kramarenko. Two regions of microphase separation in ion-containing polymer solutions. *Soft Matter*, 13:6831–6844, 2017.

[24] Nancy C Zhou, Wesley R Burghardt, and Karen I Winey. Blend miscibility of sulfonated polystyrene ionomers with polystyrene: Effect of counterion valency and neutralization level. *Macromolecules*, 40(17):6401–6405, 2007.

[25] Kevin J Henderson, Tian C Zhou, Kathryn J Otim, and Kenneth R Shull. Ionically cross-linked triblock copolymer hydrogels with high strength. *Macromolecules*, 43(14):6193–6201, 2010.

[26] L S Ornstein and F Zernike. Accidental deviations of density and opalescence at the critical point of a single substance. In *Proc. Akad. Sci.(Amsterdam)*, volume 17, page 793, 1914.

[27] Jean-Pierre Hansen and IR McDonald. *Theory of Simple Liquids*. Academic Press, 2006.

[28] Jos W Zwanikken, Prateek K Jha, and Monica Olvera de la Cruz. A practical integral equation for the structure and thermodynamics of hard sphere coulomb fluids. *The Journal of chemical physics*, 135(6):064106, 2011.

[29] J Th G Overbeek and MJ Voorn. Phase separation in polyelectrolyte solutions. theory of complex coacervation. *Journal of Cellular and Comparative Physiology*, 49(S1):7–26, 1957.

[30] Jian Qin, Dimitrios Priftis, Robert Farina, Sarah L Perry, Lorraine Leon, Jonathan Whitmer, Kyle Hoffmann, Matthew Tirrell, and Juan J de Pablo. Interfacial tension of polyelectrolyte complex coacervate phases. *ACS Macro Letters*, 3(6):565–568, 2014.

[31] Dimitrios Priftis, Xiaoxing Xia, Khatcher O Margossian, Sarah L Perry, Lorraine Leon, Jian Qin, Juan J de Pablo, and Matthew Tirrell. Ternary, tunable polyelectrolyte complex fluids driven by complex coacervation. *Macromolecules*, 47(9):3076–3085, 2014.

[32] David Mecerreyes. Polymeric ionic liquids: Broadening the properties and applications of polyelectrolytes. *Progress in Polymer Science*, 36(12):1629–1648, 2011.

[33] Hiroyuki Ohno. *Electrochemical aspects of ionic liquids*. John Wiley & Sons, 2011.

[34] Charles E Sing, Jos W Zwanikken, and Monica Olvera de la Cruz. Theory of melt polyelectrolyte blends and block copolymers: Phase behavior, surface tension, and microphase periodicity. *The Journal of Chemical Physics*, 142(3):034902, 2015.

[35] AJ Staverman. The entropy of liquid mixtures: Ii. deviations from raoult's law in mixtures containing large, flexible molecules. *Recueil des Travaux Chimiques des Pays-Bas*, 60(9):640–649, 1941.

[36] Maurice L Huggins. Thermodynamic properties of solutions of high polymers: the empirical constant in the activity equation. *Annals of the New York Academy of Sciences*, 44(4):431–443, 1943.

[37] RT Farouki and S Hamaguchi. Thermodynamics of strongly-coupled yukawa systems near the one-component-plasma limit. ii. molecular dynamics simulations. *The Journal of chemical physics*, 101(11):9885–9893, 1994.

[38] OS Vaulina and SA Khrapak. Scaling law for the fluid-solid phase transition in yukawa systems (dusty plasmas). *Journal of Experimental and Theoretical Physics*, 90(2):287–289, 2000.

[39] Eduardo Waisman and Joel L Lebowitz. Mean spherical model integral equation for charged hard spheres i. method of solution. *The Journal of Chemical Physics*, 56(6):3086–3093, 1972.

[40] Tohru Morita. Theory of classical fluids: Hyper-netted chain approximation. iii: A new integral equation for the pair distribution function. *Progress of Theoretical Physics*, 23(5):829–845, 1960.

[41] Loup Verlet and Jean-Jacques Weis. Equilibrium theory of simple liquids. *Physical Review A*, 5(2):939, 1972.

[42] Glenn Fredrickson. *The equilibrium theory of inhomogeneous polymers (international series of monographs on physics)*. Oxford University Press, 2013.

[43] Charles E Sing, Jos W Zwanikken, and Monica Olvera de la Cruz. Ion correlation-induced phase separation in polyelectrolyte blends. *ACS Macro Letters*, 2(11):1042–1046, 2013.

[44] Sam F Edwards. The statistical mechanics of polymers with excluded volume. *Proceedings of the Physical Society*, 85(4):613, 1965.

[45] Kenneth R Shull. Mean-field theory of block copolymers: bulk melts, surfaces, and thin films. *Macromolecules*, 25(8):2122–2133, 1992.

[46] Michel Armand and J-M Tarascon. Building better batteries. *Nature*, 451(7179):652–657, 2008.

[47] EJ Plichta, M Hendrickson, R Thompson, G Au, WK Behl, MC Smart, BV Ratnakumar, and S Surampudi. Development of low temperature li-ion electrolytes for nasa and dod applications. *Journal of power sources*, 94(2):160–162, 2001.

[48] Dominica HC Wong, Jacob L Thelen, Yanbao Fu, Didier Devaux, Ashish A Pandya, Vincent S Battaglia, Nitash P Balsara, and Joseph M DeSimone. Nonflammable perfluoropolyether-based electrolytes for lithium batteries. *Proceedings of the National Academy of Sciences*, 111(9):3327–3331, 2014.

[49] Laetitia Dubau, Luis Castanheira, Frédéric Maillard, Marian Chatenet, Olivier Lottin, Gaël Maranzana, Jérôme Dillet, Adrien Lamibrac, Jean-Christophe Perrin, Eddy Moukheiber, et al. A review of pem fuel cell durability: materials degradation, local heterogeneities of aging and possible mitigation strategies. *Wiley Interdisciplinary Reviews: Energy and Environment*, 3(6):540–560, 2014.

[50] Ludwik Leibler. Theory of microphase separation in block copolymers. *Macromolecules*, 13(6):1602–1617, 1980.

[51] Ayan Ghosh, Chunsheng Wang, and Peter Kofinas. Block copolymer solid battery electrolyte with high li-ion transference number. *Journal of the Electrochemical Society*, 157(7):A846–A849, 2010.

[52] Sebnem Inceoglu, Adriana A Rojas, Didier Devaux, X Chelsea Chen, Greg M Stone, and Nitash P Balsara. Morphology–conductivity relationship of single-ion-conducting block copolymer electrolytes for lithium batteries. *ACS Macro Letters*, 3(6):510–514, 2014.

[53] Shuang Yang, Aleksey Vishnyakov, and Alexander V Neimark. Self-assembly in block polyelectrolytes. *The Journal of chemical physics*, 134(5):054104, 2011.

[54] Klaus-Dieter Kreuer and Giuseppe Portale. A critical revision of the nano-morphology of proton conducting ionomers and polyelectrolytes for fuel cell applications. *Advanced Functional Materials*, 23(43):5390–5397, 2013.

[55] Nicholas P Young, Didier Devaux, Rachna Khurana, Geoffrey W Coates, and Nitash P Balsara. Investigating polypropylene-poly (ethylene oxide)-polypropylene triblock copolymers as solid polymer electrolytes for lithium batteries. *Solid State Ionics*, 263:87–94, 2014.

[56] Scott A Eastman, Sangcheol Kim, Kirt A Page, Brandon W Rowe, Shuhui Kang, Christopher L Soles, and Kevin G Yager. Effect of confinement on structure, water solubility, and water transport in nafion thin films. *Macromolecules*, 45(19):7920–7930, 2012.

[57] William Kung, Francisco J Solis, and Monica Olvera de la Cruz. Thermodynamics of ion solvation and differential adsorption at liquid-liquid interfaces and membranes. *arXiv preprint arXiv:0710.0369*, 2007.

[58] Nancy C Zhou, Chen Xu, Wesley R Burghardt, Russell J Composto, and Karen I Winey. Phase behavior of polystyrene and poly (styrene-r an-styrenesulfonate) blends. *Macromolecules*, 39(6):2373–2379, 2006.

[59] AV Kyrylyuk and JGEM Fraaije. Microphase separation of weakly charged block polyelectrolyte solutions: Donnan theory for dynamic polymer morphologies. *The Journal of chemical physics*, 121(6):2806–2812, 2004.

[60] Issei Nakamura and Zhen-Gang Wang. Thermodynamics of salt-doped block copolymers, 2014.

[61] Jasmine N Hunt, Kathleen E Feldman, Nathaniel A Lynd, Joanna Deek, Luis M Campos, Jason M Spruell, Blanca M Hernandez, Edward J Kramer, and Craig J Hawker. Tunable, high modulus hydrogels driven by ionic coacervation. *Advanced Materials*, 23(20):2327–2331, 2011.

[62] Jasper Van der Gucht, Evan Spruijt, Marc Lemmers, and Martien A Cohen Stuart. Polyelectrolyte complexes: bulk phases and colloidal systems. *Journal of colloid and interface science*, 361(2):407–422, 2011.

[63] Jared F Mike and Jodie L Lutkenhaus. Recent advances in conjugated polymer energy storage. *Journal of Polymer Science Part B: Polymer Physics*, 51(7):468–480, 2013.

[64] Christoph Keplinger, Jeong-Yun Sun, Choon Chiang Foo, Philipp Rothemund, George M Whitesides, and Zhigang Suo. Stretchable, transparent, ionic conductors. *Science*, 341(6149):984–987, 2013.

[65] Sumit Kewalramani, Jos W Zwanikken, Robert J Macfarlane, Cheuk-Yui Leung, Monica Olvera de la Cruz, Chad A Mirkin, and Michael J Bedzyk. Counterion distribution surrounding spherical nucleic acid–au nanoparticle conjugates probed by small-angle x-ray scattering. *ACS nano*, 7(12):11301–11309, 2013.

[66] Klaus Schmidt-Rohr and Qiang Chen. Parallel cylindrical water nanochannels in nafion fuel-cell membranes. *Nature materials*, 7(1):75–83, 2008.

[67] Evan Spruijt, Joris Sprakel, Martien A Cohen Stuart, and Jasper van der Gucht. Interfacial tension between a complex coacervate phase and its coexisting aqueous phase. *Soft Matter*, 6(1):172–178, 2010.

[68] Evan Spruijt, Adrie H Westphal, Jan Willem Borst, Martien A Cohen Stuart, and Jasper van der Gucht. Binodal compositions of polyelectrolyte complexes. *Macromolecules*, 43(15):6476–6484, 2010.

[69] G Orkoulas, Sanat K Kumar, and Athanassios Z Panagiotopoulos. Monte carlo study of coulombic criticality in polyelectrolytes. *Physical review letters*, 90(4):048303, 2003.

[70] Hai Tang, Igal Szleifer, and Sanat K Kumar. Critical temperature shifts in thin polymer blend films. *The Journal of chemical physics*, 100(7):5367–5371, 1994.

[71] Erik Luijten, Michael E Fisher, and Athanassios Z Panagiotopoulos. Universality class of criticality in the restricted primitive model electrolyte. *Physical review letters*, 88(18):185701, 2002.

[72] Michael E Fisher and Yan Levin. Criticality in ionic fluids: Debye-hückel theory, bjerrum, and beyond. *Physical review letters*, 71(23):3826, 1993.

[73] Charles E Sing, Jos W Zwanikken, and Monica Olvera de la Cruz. Effect of ion–ion correlations on polyelectrolyte gel collapse and reentrant swelling. *Macromolecules*, 46(12):5053–5065, 2013.

[74] NP Balsara, AA Lefebvre, JH Lee, CC Lin, and B Hammouda. Search for a model polymer blend. *AIChE journal*, 44(11):2515–2519, 1998.

[75] Stephen J Paddison, David W Reagor, and Thomas A Zawodzinski Jr. High frequency dielectric studies of hydrated nafion®. *Journal of Electroanalytical Chemistry*, 459(1):91–97, 1998.

[76] Masanori Hara and Adi Eisenberg. Miscibility enhancement via ion-dipole interactions. 2. lcst behavior in polystyrene ionomer/poly (alkylene oxide) systems. *Macromolecules*, 20(9):2160–2164, 1987.

[77] Alicia M Castagna, Wenqin Wang, Karen I Winey, and James Runt. Structure and dynamics of zinc-neutralized sulfonated polystyrene ionomers. *Macromolecules*, 44(8):2791–2798, 2011.

[78] C Francisco Buitrago, Dan S Bolintineanu, Michelle E Seitz, Kathleen L Opper, Kenneth B Wagener, Mark J Stevens, Amalie L Frischknecht, and Karen I Winey. Direct comparisons of x-ray scattering and atomistic molecular dynamics simulations for precise acid copolymers and ionomers. *Macromolecules*, 48(4):1210–1220, 2015.

[79] Zhigang Xue, Dan He, and Xiaolin Xie. Poly (ethylene oxide)-based electrolytes for lithium-ion batteries. *Journal of Materials Chemistry A*, 3(38):19218–19253, 2015.

[80] Yugang Sun. Lithium ion conducting membranes for lithium-air batteries. *Nano Energy*, 2(5):801–816, 2013.

[81] MM Noor, MH Buraidah, MA Careem, SR Majid, and AK Arof. An optimized poly (vinylidene fluoride-hexafluoropropylene)–nai gel polymer electrolyte and its application in natural dye sensitized solar cells. *Electrochimica Acta*, 121:159–167, 2014.

[82] Vijay Kumar Thakur, Guoqiang Ding, Jan Ma, Pooi See Lee, and Xuehong Lu. Hybrid materials and polymer electrolytes for electrochromic device applications. *Advanced Materials*, 24(30):4071–4096, 2012.

[83] P Varshney, M Deepa, SA Agnihotry, and KC Ho. Photo-polymerized films of lithium ion conducting solid polymer electrolyte for electrochromic windows (ecws). *Solar energy materials and solar cells*, 79(4):449–458, 2003.

[84] Mauricio Echeverri, Cosette Hamad, and Thein Kyu. Highly conductive, completely amorphous polymer electrolyte membranes fabricated through photo-polymerization of poly (ethylene glycol diacrylate) in mixtures of solid plasticizer and lithium salt. *Solid State Ionics*, 254:92–100, 2014.

[85] Jayaraman Theerthagiri, Raja Arumugam Senthil, Jagannathan Madhavan, Mohd Arof, Abdul Kariem, et al. Studies of solvent effect on the conductivity of 2-mercaptopyridine-doped solid polymer blend electrolytes and its application in dye-sensitized solar cells. *Journal of Applied Polymer Science*, 132(35), 2015.

[86] Ruixuan He and Thein Kyu. Effect of plasticization on ionic conductivity enhancement in relation to glass transition temperature of crosslinked polymer electrolyte membranes. *Macromolecules*, 49(15):5637–5648, 2016.

[87] Giovanni Battista Appetecchi, Guk-Tae Kim, Maria Montanino, F Alessandrini, and S Passerini. Room temperature lithium polymer batteries based on ionic liquids. *Journal of Power Sources*, 196(16):6703–6709, 2011.

[88] Joon-Ho Shin, Wesley A Henderson, Cosimo Tizzani, Stefano Passerini, Sang-Sik Jeong, and Ki-Won Kim. Characterization of solvent-free polymer electrolytes consisting of ternary peo–litfsi–pyr14 tfsi. *Journal of The Electrochemical Society*, 153(9):A1649–A1654, 2006.

[89] Luciano T Costa, Bing Sun, Fabian Jeschull, and Daniel Brandell. Polymer-ionic liquid ternary systems for li-battery electrolytes: Molecular dynamics studies of litfsi in a emim-tfsi and peo blend. *The Journal of chemical physics*, 143(2):024904, 2015.

[90] JY Song, YY Wang, and CC Wan. Review of gel-type polymer electrolytes for lithium-ion batteries. *Journal of Power Sources*, 77(2):183–197, 1999.

[91] Chun-Yi Chiu, Hsien-Wei Chen, Shiao-Wei Kuo, Chih-Feng Huang, and Feng-Chin Chang. Investigating the effect of miscibility on the ionic conductivity of liclo4/peo/pcl ternary blends. *Macromolecules*, 37(22):8424–8430, 2004.

[92] Dominica HC Wong, Alessandra Vitale, Didier Devaux, Austria Taylor, Ashish A Pandya, Daniel T Hallinan, Jacob L Thelen, Sue J Mecham, Simon F Lux, Alexander M Lapides, et al. Phase behavior and electrochemical characterization of blends of perfluoropolyether, poly (ethylene glycol), and a lithium salt. *Chemistry of Materials*, 27(2):597–603, 2015.

[93] Honghao Li, Aykut Erbas, Jos Zwanikken, and Monica Olvera de la Cruz. Ionic conductivity in polyelectrolyte hydrogels. *Macromolecules*, 2016.

[94] Robert Ferris, Angus Hucknall, Byung Seok Kwon, Tao Chen, Ashutosh Chilkoti, and Stefan Zauscher. Field-induced nanolithography for patterning of non-fouling polymer brush surfaces. *Small*, 7(21):3032–3037, 2011.

[95] Debra J Audus, Jeffrey D Gopez, Daniel V Krogstad, Nathaniel A Lynd, Edward J Kramer, Craig J Hawker, and Glenn H Fredrickson. Phase behavior of electrostatically complexed polyelectrolyte gels using an embedded fluctuation model. *Soft matter*, 11(6):1214–1225, 2015.

[96] E Yu Kramarenko, I Ya Erukhimovich, and AR Khokhlov. The influence of ion pair formation on the phase behavior of polyelectrolyte solutions. *Macromolecular theory and simulations*, 11(5):462–471, 2002.

[97] M Olvera de la Cruz. Theory of microphase separation in block copolymer solutions. *The Journal of Chemical Physics*, 90(3):1995–2002, 1989.

[98] Eugene Helfand and Yukiko Tagami. Theory of the interface between immiscible polymers. *The Journal of Chemical Physics*, 57(4):1812–1813, 1972.

[99] Michelle D Lefebvre, Monica Olvera de La Cruz, and Kenneth R Shull. Phase segregation in gradient copolymer melts. *Macromolecules*, 37(3):1118–1123, 2004.

[100] Michelle D Lefebvre and Kenneth R Shull. Homopolymer solubilization and nanoparticle encapsulation in diblock copolymer micelles. *Macromolecules*, 39(9):3450–3457, 2006.

[101] Jacob L Thelen, Sebnem Inceoglu, Naveen R Venkatesan, Nikolaus G Mackay, and Nitash P Balsara. Relationship between ion dissociation, melt morphology, and electrochemical performance of lithium and magnesium single-ion conducting block copolymers. *Macromolecules*, 49(23):9139–9147, 2016.

[102] Eugene Helfand and Yukiko Tagami. Theory of the interface between immiscible polymers. *Journal of Polymer Science Part B: Polymer Letters*, 9(10):741–746, 1971.

[103] Hai Tang and Karl F Freed. Interfacial studies of incompressible binary blends. *The Journal of chemical physics*, 94(9):6307–6322, 1991.

[104] Kenneth R Shull, Anne M Mayes, and Thomas P Russell. Segment distributions in lamellar diblock copolymers. *Macromolecules*, 26(15):3929–3936, 1993.

[105] Zhen-Gang Wang. Effects of ion solvation on the miscibility of binary polymer blends. *The Journal of Physical Chemistry B*, 112(50):16205–16213, 2008.

[106] Adriana A Rojas, Sebnem Inceoglu, Nikolaus G Mackay, Jacob L Thelen, Didier Devaux, Gregory M Stone, and Nitash P Balsara. Effect of lithium-ion concentration on morphology and ion transport in single-ion-conducting block copolymer electrolytes. *Macromolecules*, 48(18):6589–6595, 2015.

[107] Ha-Kyung Kwon, Victor A Pryamitsyn, Jos W Zwanikken, Ken Shull, and Monica Olvera de la Cruz. Solubility and interfacial segregation of salts in ternary polyelectrolyte blends. *Soft Matter*, 2017.

[108] Issei Nakamura, An-Chang Shi, and Zhen-Gang Wang. Ion solvation in liquid mixtures: Effects of solvent reorganization. *Physical review letters*, 109(25):257802, 2012.

[109] S Ramesh, AH Yahaya, and AK Arof. Miscibility studies of pvc blends (pvc/pmma and pvc/peo) based polymer electrolytes. *Solid State Ionics*, 148(3-4):483–486, 2002.

[110] Victor A Pryamitsyn, Ha-Kyung Kwon, Jos W Zwanikken, and Monica Olvera de La Cruz. Anomalous phase behavior of ionic polymer blends and ionic copolymers. *Macromolecules*, 50(13):5194–5207, 2017.

[111] JB Hasted, DM Ritson, and CH Collie. Dielectric properties of aqueous ionic solutions. parts i and ii. *The Journal of Chemical Physics*, 16(1):1–21, 1948.

[112] Alexander A Teran and Nitash P Balsara. Thermodynamics of block copolymers with and without salt. *The Journal of Physical Chemistry B*, 118(1):4–17, 2013.

[113] Chun-Lai Ren, Issei Nakamura, and Zhen-Gang Wang. Effects of ion-induced cross-linking on the phase behavior in salt-doped polymer blends. *Macromolecules*, 49(1):425–431, 2015.

[114] Boran Ma, Trung Dac Nguyen, Victor A Pryamitsyn, and Monica Olvera de la Cruz. Ionic correlations in random ionomers. *ACS nano*, 2018.

[115] Dan S Bolintineanu, Mark J Stevens, and Amalie L Frischknecht. Atomistic simulations predict a surprising variety of morphologies in precise ionomers. *ACS Macro Letters*, 2(3):206–210, 2013.

[116] Lisa M Hall, Michelle E Seitz, Karen I Winey, Kathleen L Opper, Kenneth B Wagener, Mark J Stevens, and Amalie L Frischknecht. Ionic aggregate structure in ionomer melts: effect of molecular architecture on aggregates and the ionomer peak. *Journal of the American Chemical Society*, 134(1):574–587, 2011.

[117] L Robert Middleton and Karen I Winey. Nanoscale aggregation in acid-and ion-containing polymers. *Annual review of chemical and biomolecular engineering*, 8:499–523, 2017.

[118] Lixin Song and Yeng Ming Lam. Nanopattern formation using a chemically modified ps-p4vp diblock copolymer. *Nanotechnology*, 18(7):075304, 2007.

[119] Ha-Kyung Kwon and Monica Olvera de la Cruz. Criticality in charge-containing polymer blends with dielectric mismatch. *Journal of Chemical Physics*, Submitted.

[120] Jiayi Zhu, Adi Eisenberg, and R Bruce Lennox. Interfacial behavior of block polyelectrolytes. 1. evidence for novel surface micelle formation. *Journal of the American Chemical Society*, 113(15):5583–5588, 1991.

[121] Haiyun Lu, Dong Hyun Lee, and Thomas P Russell. Temperature tunable micellization of polystyrene-block-poly (2-vinylpyridine) at si- ionic liquid interface. *Langmuir*, 26(22):17126–17132, 2010.

[122] Sivashankar Krishnamoorthy, Raphaël Pugin, Juergen Brugger, Harry Heinzelmann, Arno C Hoogerwerf, and Christian Hinderling. Block copolymer micelles as switchable templates for nanofabrication. *Langmuir*, 22(8):3450–3452, 2006.

[123] Byeong-Hyeok Sohn, Seong-Il Yoo, Byung-Wook Seo, Sang-Hyun Yun, and Sang-Min Park. Nanopatterns by free-standing monolayer films of diblock copolymer micelles with in situ core- corona inversion. *Journal of the American Chemical Society*, 123(50):12734–12735, 2001.

[124] Iryna I Perepichka, Qing Lu, Antonella Badia, and C Geraldine Bazuin. Understanding and controlling morphology formation in langmuir–blodgett block copolymer films using ps-p4vp and ps-p4vp/pdp. *Langmuir*, 29(14):4502–4519, 2013.

[125] Arthur W Adamson, Alice Petry Gast, et al. Physical chemistry of surfaces. 1967.

[126] AN Semenov. Contribution to the theory of microphase layering in block-copolymer melts. *Zh. Eksp. Teor. Fiz*, 88(4):1242–1256, 1985.

[127] Reidar Lund, Vitaliy Pipich, Lutz Willner, Aurel Radulescu, Juan Colmenero, and Dieter Richter. Structural and thermodynamic aspects of the cylinder-to-sphere transition in amphiphilic diblock copolymer micelles. *Soft Matter*, 7(4):1491–1500, 2011.

[128] Ekaterina B Zhulina, Mireile Adam, Isaac LaRue, Sergei S Sheiko, and Michael Rubinstein. Diblock copolymer micelles in a dilute solution. *Macromolecules*, 38(12):5330–5351, 2005.

[129] Nicholas B Karabin, Sean Allen, Ha-Kyung Kwon, Sharan Bobbala, Emre Firlar, Tolou Shokuhfar, Kenneth R Shull, and Evan A Scott. Sustained micellar delivery via inducible transitions in nanostructure morphology. *Nature communications*, 9(1):624, 2018.

[130] Daniel Carvajal, Evan J Laprade, Kevin J Henderson, and Kenneth R Shull. Mechanics of pendant drops and axisymmetric membranes. *Soft Matter*, 7(22):10508–10519, 2011.

[131] Christian Reichardt and Thomas Welton. *Solvents and solvent effects in organic chemistry*. John Wiley & Sons, 2011.